SOLID-STATE NMR STUDIES OF ION DYNAMICS IN PROTON-CONDUCTING POLYMERS AND COMPOSITES

SOLID-STATE NMR STUDIES OF ION DYNAMICS IN PROTON-CONDUCTING POLYMERS AND COMPOSITES

By

GANG YE, M. SC., B. ENG.

A Thesis
Submitted to the School of Graduate Studies
in Partial Fulfilment of the Requirements
for the Degree
Doctor of Philosophy

McMaster University

Doctor of Philosophy (2008) Department of Chemistry

McMaster University

Hamilton, Ontario

TITLE: Solid-State NMR Studies of Ion Dynamics in Proton-Conducting Polymers and Composites

AUTHOR: Gang Ye, M. Sc., B. Eng.

SUPERVISOR: Professor G. R. Goward

NUMBER OF PAGES: xiv, 249

ABSTRACT

High resolution solid state ^{1}H NMR is used to investigate proton mobility of Nafion, Sulfonated Polyether Ether Ketones(S-PEEK) and their composites, which provides better understanding of their proton conductivities. Proton exchange between sulfonic acid groups and water was observed in these materials. The proton mobility is dependent on both the temperature and the water content. Variable temperature experiments were used to determine the activation energy for proton transportation which generally increases with decrease in hydration level.

The preparation of Nafion/SiO_2 composites can cause large difference in proton diffusion coefficients and proton conductivities in dried states. This indicates that the amount of dopants needs to be optimized to minimize the blocking of proton diffusion pathways by dopant particles. Detailed information on the control of surface hydroxyl groups in Nafion/SiO_2 is obtained through the combination of ^{29}Si and ^{1}H NMR.

Although hydrated Nafion/ZrP composites show reduced proton activation energy, they present lower proton conductivity at 35 ^{o}C than unmodified Nafion. For composites dried at 160 ^{o}C, both the conversion of monohydrogen phosphate into pyrophosphate and the protonation of monohydrogen phosphate have been observed, which could be one of reasons for the decreased proton conductivity after rehydration.

Under high humidification, a single or multiple sulfonic acid proton environments was observed in S-PEEKs, which explains the small proton conductivity difference between some of S-PEEKs. However, the observed conductivity difference for S-PEEKs cast from different solvents was attributed to distinct mobilities of polymer chains. In the crosslinked S-PEEK, not all the crosslinkers of ethylene glycol are fully crosslinked. Proton exchange between residual sulfonic acid and hydroxyls of the crosslinker was observed, which is the primary reason that the crosslinked S-PEEK, with very low residual degree of sulfonation (13 %), still shows proton conductivity comparable to those of S-PEEKs.

ACKNOWLEDGEMENTS

On the journey to accomplish my doctoral studies, I was accompanied by a wonderful group of people who supported me in multiple ways, for which I would like to express thanks.

Firstly, I highly appreciate my supervisor, Dr. Gillian R. Goward, for her guidance during the course of my doctoral work at McMaster University. This work would not have been possible without her support and encouragement. Her research insight as well as her patience and kindness have been invaluable to me. I would also like to extend my gratitude to my research committee members, Dr. Peter Kruse and Dr. Giuseppe Melacini, for their thoughtful suggestions which helped my research substantially.

I would like to thank the staff of the department of chemistry at McMaster University for their support and help during my Ph.D. studies. Special thanks go to Dr. Bob Berno and Dr. Steve Kornic for keeping the NMR spectrometers working under excellent condition.

I would also like to thank the Goward group: Lindsay, Jason, Linda, Mark, Janzen, Casey, Kristen, Becky, Blythe, Agata, Vijay and Sonia. Thanks for their kind help and the joyful time they shared with me.

Finally, I would like to thank my family: my parents and my wife, for their love, support and encouragement.

Table of Contents

Chapter 1 Introduction

Chapter 2 Experimental techniques

Chapter 3 Comparative studies of Nafion and S-PEEK by solid state NMR

Chapter 4 Proton dynamics of Nafion/SiO_2 composites

Chapter 5 Solid state NMR spectroscopic characterization of zirconium phosphate

Chapter 6 Solid state NMR spectroscopic characterization of Nafion/ZrP composites

Chapter 7 Proton dynamics of S-PEEKs

List of Figures

List of Tables

Chapter 1 Introduction

With the increasing environmental concern for pollutants caused by the combustion of fossil fuels to produce electricity and power vehicles, more and more attention is given to the development of fuel cells which generate electricity by an electrochemical reaction of oxygen with fuels such as hydrogen. Compared with traditional electricity production technology fuel cells release little to no pollutants into the atmosphere. [1] Moreover, the fuel cells have electrical efficiencies much higher than internal combustion engines with an added bonus of them operating very quietly. Fuel cells can be applied from systems as small as portable electronic devices to large scale industrial manufacturing. All these features of fuel cells make their application very attractive. [2] In this chapter, an introduction to fuel cells and more specifically, the polymer electrolyte membrane fuel cell, is presented. The current research for polymer electrolyte membranes based on several types of polymers, as well as polymer composites, is reviewed. At the end of the chapter, the research goals of this thesis are outlined.

1.1 Fuel cells

The invention of the fuel cell can be dated back to the middle of the 19th century. Sir William Grove produced the first fuel cell in 1839. In 1889 Charles Langer and Ludwig Mond introduced the term “fuel cell” for their device used to produce electricity by air and industrial coal gas. Unfortunately projects on fuel cell technology dropped because of platinum catalyst poisoning and many other problems.[3] Until 1932, modern fuel cell technology was revived again by Francis T. Bacon, an English engineer associated with Cambridge University. At the end of the 1950's Bacon had developed a 5 kW fuel cell. [4] The first application of the fuel cell was in the U.S. space program in the 1960's and the first fuel cell powered van was built by General Motors in the mid-1960s. From then on the application of fuel cells started its entrepreneurial phase. In 1993 the first passenger car was demonstrated by Energy Partners. [5] Following that, many car manufacturers had built their fuel cell-powered vehicles by the end of the last century, which became the birth of a new industry.

1.1.1 The basic principles of fuel cells

A typical fuel cell consists of an anode, cathode, electrolyte and catalyst. As can be seen from the schematic of a hydrogen/oxygen fuel cell in Figure 1-1, an external circuit is connected with the anode and the cathode which are separated by the electrolyte. The hydrogen is oxidized on the anode by the following reaction:

$$H_2 \rightarrow 2\,H^+ + 2e^- \qquad (1\text{-}1)$$

The electrons will reach the cathode through the external circuit and the hydrogen ions will reach the cathode by diffusing through the electrolyte. In the meantime, the oxygen is reduced on the cathode as follows:

$$O_2 + 4e^- \rightarrow 2\,O^{2-} \tag{1-2}$$

The oxygen ions can then recombine with the hydrogen ions to form water. The overall reaction is given as follows:

$$2\,H^+ + O^{2-} \rightarrow H_2O \tag{1-3}$$

Taking into account the energy produced in this process, the overall reaction is as follows:

$$H_2 + 1/2\,O_2 \rightarrow H_2O + \text{Electrical energy} + \text{Heat} \tag{1-4}$$

When a continuous supply of fuel and oxygen is available, a current is obtained in the external circuit.

In equation (1-4) the electrical energy is determined by the change in the Gibbs free energy of the reaction. Theoretically, the Gibbs free energy is completely converted into electrical energy: [6]

$$\Delta G = - n F E \tag{1-5}$$

Where E is the theoretical potential, n is the number of moles of electrons transferred in the reaction, and F is the Faraday constant. The efficiency for a fuel cell can therefore be calculated as follows:

$$\eta = n F E / -\Delta H = \Delta G / \Delta H = 1 - T\,\Delta S / \Delta H \tag{1-6}$$

Where ΔH and ΔS are the changes of reaction enthalpy and entropy, respectively, T is reaction temperature. For a hydrogen/oxygen fuel cell, the Gibbs free energy is $\Delta G =$

-237 kJ/mol. [2] The heat generated in the reaction is ΔH = -286 kJ/mol. Therefore, the theoretical efficiency is 0.83. In practice, the efficiency of a fuel cell is lower than this value because of the electrolyte resistance and the electrode overpotentials caused by the finite reaction rate at the electrodes. [7]

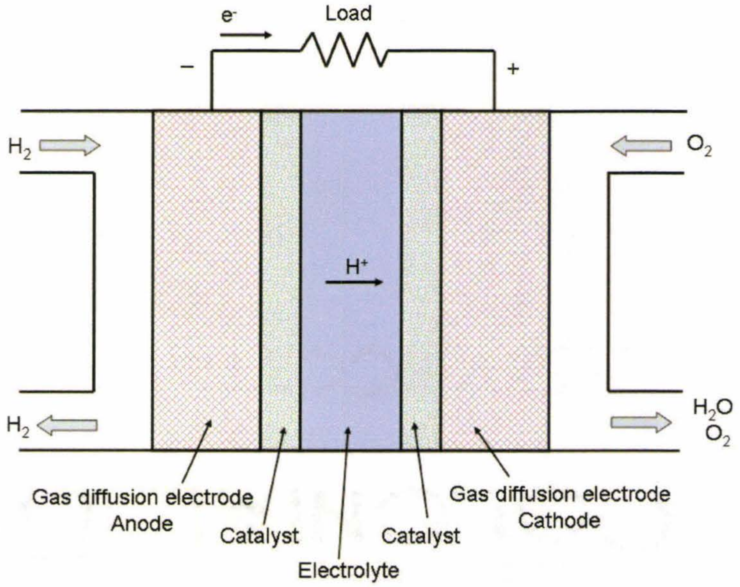

Figure 1-1. Scheme of hydrogen/oxygen fuel cell

1.1.2 Polymer electrolyte membrane fuel cells

Fuel cells are often classified by the electrolyte used in the cell. The typical fuel cell includes polymer electrolyte membrane fuel cells (PEMFC), direct methanol fuel cells (DMFC), molten carbonate fuel cells (MCFC) and solid oxide fuel cells (SOFC). Their features are shown in Table 1-1. [8] Detailed information for the PEMFC is given in the following section.

Table 1-1. Comparison of different types of fuel cells [8]

Fuel cells	MCFC	SOFC	PEMFC	DMFC
Electrolyte	LiK/LiNa carbonate	ZrO_2, CeO_2	solid organic polymer	
Mobile ion	CO_3^{2-}	O^{2-}	H^+	
Anode reaction	$H_2+CO_3^{2-}\rightarrow H_2O+CO_2+2e^-$	$H_2+O^{2-}\rightarrow H_2O+2e^-$	$H_2\rightarrow 2H^++2e^-$	$CH_3OH+H_2O\rightarrow CO_2+6H^++6e^-$
Cathode reaction	$1/2\ O_2+CO_2+2e^-\rightarrow CO_3^{2-}$	$1/2\ O_2+2e^-\rightarrow O^{2-}$	$1/2\ O_2+2H^++2e^-\rightarrow H_2O$	$3/2\ O_2+6H^++6e^-\rightarrow 3H_2O$
Overall reaction	$H_2 + 1/2\ O_2 \rightarrow H_2O$			$CH_3OH+3/2\ O_2\rightarrow CO_2+2H_2O$
Operating temperature	600 ~ 800 °C	600 ~ 1000 °C	60 ~ 120 °C	
Applications	power for stationary systems		transportation, portable power, energy storage systems	

In PEMFC a solid polymer membrane is used as a proton exchange membrane. It is therefore often called a proton exchange membrane fuel cell. The idea of using an ion exchange membrane as an electrolyte was first introduced by Willard Grubb at General Electric in 1959. [9] The hydrogen fuelled PEMFC normally operates at temperatures around 60 °C to 120 °C. PEMFC has a high power to weight ratio as well as fast startup times varying from seconds to minutes. This makes it particularly suitable for automotive applications. However, the noble-metal catalyst, for instance platinum, which is usually dispersed on gas diffusion electrodes to catalyze the reactions (1-1) and (1-2), can be easily poisoned by the trace of carbon monoxide in the hydrogen fuel. [10, 11] This leads to added costs for removal of CO from the fuel.

Water management is also very important for the performance of PEMFC as the ionic conductivity of the proton exchange membrane is closely correlated to the level of humidification. Both humidifying the hydrogen gas and hydrating the membrane have been shown to be effective means to control water content in the fuel cell.[12, 13] It is clear however, that the role of water in the ionic conductivity limits the operating temperatures of PEMFC to below 100 °C and above 0 °C. How this limitation is overcome is discussed in the studies of polymer composites in Chapter 4 and Chapter 6. A significant barrier to the PEMFC powered car is hydrogen storage. [14] Due to the low energy density of hydrogen, the hydrogen stored in a PEMFC powered car is not enough to travel the same distance as an internal combustion engine powered car.

Overall, the major obstacles for PEMFC to be used in vehicles are high cost, adequate and safe storage of hydrogen, and diminished PEMFC performance when working at low hydration levels seen at temperatures higher than 100 °C.

1.2 Motivations of this research

This research will focus on the investigation of the polymer electrolyte which is one of the key components in the PEMFC. The conductivities for many polymer electrolytes have been reported. Although the conductivities are usually strongly dependent on water content in these materials, the water content does not adequately explain the conductivity difference between different materials. Many efforts have also been taken to study polymer electrolytes using small angle X-ray scattering (SAXS) and small angle neutron scattering (SANS). These techniques provide valuable structural information for these materials which is helpful for understanding their conductivities. However, neither SAXS nor SANS can probe the dynamics of proton motion in the polymer electrolytes which is even more important for interpreting the conductivity difference of these materials. Another crucial technique, solid state nuclear magnetic resonance (SS-NMR) which has been widely used in exploring the local structure of materials, can be utilized to study proton dynamics of polymer electrolytes. This provides very useful information for understanding the conductivity differences of these materials on a molecular level which is a strong motivation for this research. In the following sections, a review regarding the studies of polymer electrolytes will be given, and then the goal of this research will be presented.

1.3 Polymer electrolyte membranes for PEMFC

1.3.1 General requirements

In PEMFC the polymer electrolyte membrane (PEM) is the heart of the fuel cell. According to the structure of fuel cell shown in Figure 1-1, the PEM must exhibit high ionic conductivity but extremely low electronic conductivity which otherwise causes a short circuit of the fuel cell. [15] Furthermore, the PEM must prevent either gas from passing to the other side of the fuel cell, known as gas crossover, which lowers the efficiency of fuel cell. In addition, the PEM must be chemically and thermally stable in both the reducing environment at the anode and the oxidative environment at the cathode.

Since the invention of PEMFCs in 1959, various PEMs have been developed to improve the overall performance of PEMs. One of the most outstanding PEMs is the perfluoronated ionomer Nafion® shown in Figure 1-2. Both perfluorinated ionomer PEMs and non-fluorinated ionomer PEMs are introduced separately in the following subsections.

1.3.2 Perfluorinated ionomers

The motivation of developing Nafion for PEMFC comes from the degradation of the polystyrene sulfonate (PSS) polymer which was used as a PEM in fuel cells on the Gemini spacecraft. It was found that the HO_2 radicals attack the PSS PEM, which deteriorates the performance of the PEMFC and reduces its lifetime. The use of Nafion, developed by Dupont in 1968, significantly improved both the performance and the lifetime of PEMFC and was first used in the Biosatellite spacecraft in 1969. [16]

Compared with PSS, Nafion possesses higher proton conductivity (up to 0.07 S/cm at room temperature) and is far more stable both chemically and thermally due to its poly tetrafluroethylene (PTFE) based structure. Encouraged by the excellent performance of Nafion, other companies such as Dow and Aciplex developed their own perfluorinated ionomers (shown in Figure 1-2). The main difference between these ionomers is that they have different side chain lengths. Ascribing to the structural similarity, they all have similar properties including very good chemical stability, and high proton conductivity. A major drawback however, is the high cost associated with the perfluorinated backbone.

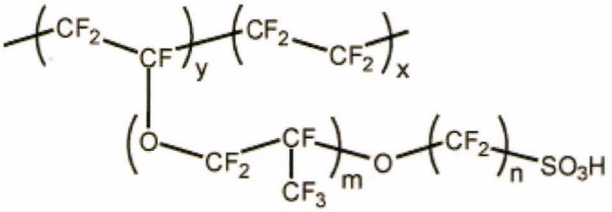

Figure 1-2. Chemical structure of Nafion and other perfluorinated ionomers. For Nafion: x=5-13.5; y=1000; m≥1, n=2; Dow membrane: x=3.6-10, m=0, n=2; Aciplex membrane: x=1.5-14; m=0, 3; n=2-5;

At the present time, Nafion has received the most attention compared to any other PEMs. Over the last few decades, many researchers have used various techniques to understand the nature of Nafion. The common Nafion products used for fuel cell applications are Nafion117, Nafion115 and Nafion112. These products have the same equivalent weight (EW):1100 g/mol, but different thickness, 0.007 in., 0.005 in., and

0.002 in., respectively. The EW represents the mass of dry PEM per mole of sulfonic acid groups. It is inversely proportional to the ion-exchange capacity (IEC) by the equation of IEC=1000/EW. As reported in the literature, [17, 18] the proton conductivity of Nafion strongly depends on its hydration states. When it works in low humidity environments, the conductivity drops dramatically. Several models have been proposed to understand the morphology of Nafion which contributes to conductivity changes of Nafion before and after hydration.

(a) Cluster network model by Gierke *et al.* Using SAXS and wide-angle X-ray diffraction (WAXD), Gierke and co-workers studied the morphology of Nafion in the unhydrolyzed and hydrolyzed form. [19, 20, 21] They proposed that the morphology of hydrated Nafion can be described by a cluster-network model in which the ionic clusters are approximately spherical and are interconnected by narrow channels, as shown in Figure 1-3. With this model, Gierke and co-workers further calculated the cluster diameter, the number of ion-exchange sites per cluster and water per exchange site. These values exhibited a linear increase with increased water content. Therefore, it was proposed that the growth of clusters does not only occur by an expansion of the dehydrated clusters but also with a continuous reorganization of exchange sites which leads to fewer but larger clusters in fully hydrated samples. The proposed model has been used frequently in literature to interpret characteristics of Nafion.

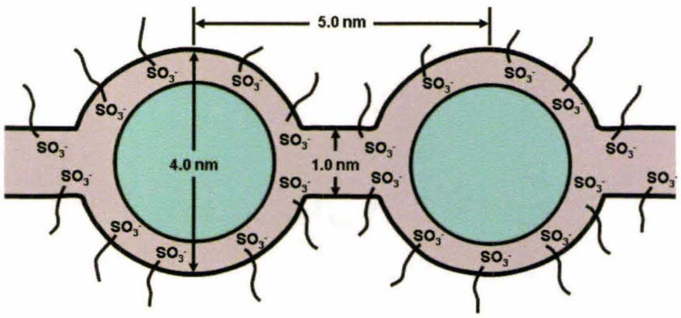

Figure 1-3. Schematic representation of cluster-network model

(resketched from ref. [21])

(b) Depleted-zone core-shell model by Fujimura *et al.* Fujimural and co-workers characterized Nafion with variable equivalent weights by using SAXS and WAXD. [22, 23] The SAXS scattering profiles of swelling samples were simulated to propose a core-shell model shown in Figure 1-4(a). In this model, the ionic cluster is considered an ion-rich core which is surrounded by ion-poor shells consisting of fluorocarbon chains containing nonclustered ions. Moreover, the core-shell particles are dispersed in the matrix of the intermediate ionic phase. The authors also found that although the simulation of the scattering profile can be interpreted by another two-phase model (shown in Figure 1-4(b)) where the ionic clusters are directly dispersed in the matrix of the intermediate ionic phase, the membrane deformation behaviour and swelling behaviour clearly supports the core-shell model in which the short-range order distance causes the ionic scattering maximum.

The intraparticle core-shell model is similar to the one proposed by MacKnight and co-workers. [24, 25] Although it works well in explaining some results, a key assumption of this model - that the clusters are homogeneously distributed - conflicts with Roche *et al.*'s results [26] which clearly indicates an inhomogeneous distribution of clusters. In addition, the core-shell model does not show a view of long range structure of ionic clusters which may be useful for understanding the long range properties such as ionic conductivities.

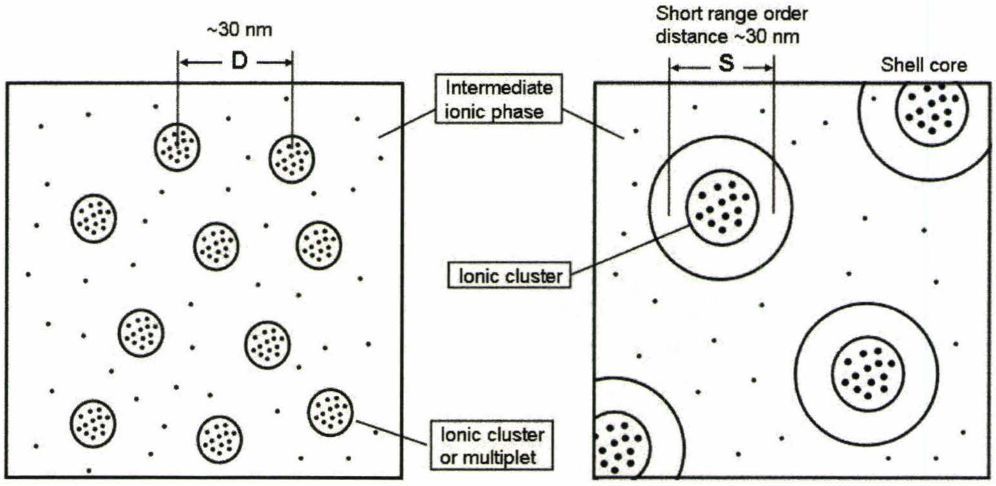

(b) (a)

Figure 1-4. Models proposed by Fujimural *et al.* (resketched from ref. [23]). The dots indicate ionic sites. The crystalline region is omitted in the diagram for simplicity. (a) core-shell model, for which the scattering peak is from intraparticle interference. (b) two-phase model, for which the scattering peak is from the interparticle interference.

(c) Local-order model by Gebel *et al.* Using SAXS and small angle neutron scattering (SANS), Gebel and co-workers investigated a series of perfluorinated ionomers with variable equivalent weight. [27, 28, 29] The authors presented a schematic description of the swelling and dissolution process, as shown in Figure 1-5. [30] In this scheme, the dry membrane has isolated spherical ionic clusters with diameters close to 15 Å and an inter-cluster distance of about 27 Å. This explains the very low ionic conductivity of samples with low water content. When water content increases, the ionic clusters are hydrated first. With further increases in water content, the percolation of swollen ionic clusters occurs. The volume of the connecting channels in this structure must not significantly contribute to the scattering intensity since the structure is still well described by the local order model. After that, an inversion of the structure happens if water content continuously increases. At this point the membrane becomes a connected network of rod-like polymer aggregates which can further swell and change into solution.

(d) Other models There are also some other models including a rod-like model by Rubatat, [31] a sandwich-like mode proposed by Haubold, [32] and so on. These models have given the structure of Nafion an approximate description for specific aspects of the structure. Nevertheless, a more overall description was presented by Kreuer based on their SAXS and pulse-field gradient (PFG) NMR data. [33] In their microstructure, the hydrated Nafion has wide and well-connected water channels. Both the separation of -SO_3H/-SO_3H and the hydrophobic/hydrophilic interface are small. This description provides further information for both short and long range properties, which is very helpful for understanding the excellent proton conductivity of Nafion in the hydrated states. However, a deeper understanding of the proton conductivity of Nafion still needs further investigation regarding the proton dynamics of Nafion. This information will be presented in the subsequent chapters of this thesis.

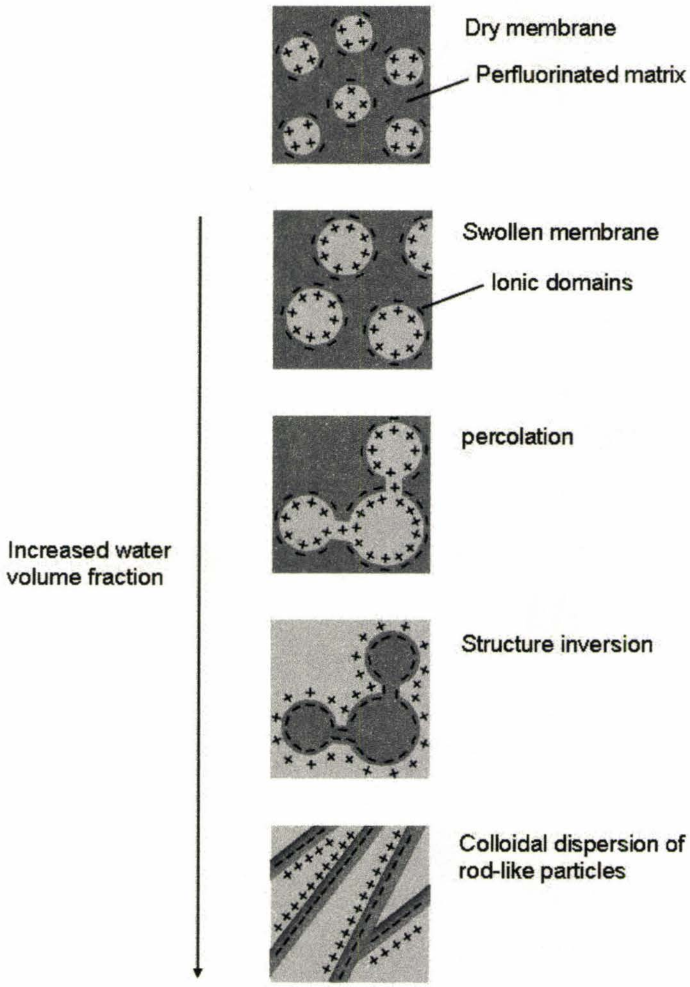

Figure 1-5. Schematic description of the swelling and dissolution process of Nafion (resketched from ref. [30])

1.3.3 Nonfluorinated ionomers

The development of PEMs based on nonfluorinated ionomers has also been given much attention since these hydrocarbon polymers have many advantages over the perfluorinated polymers. For example, they are much cheaper and can be easily recycled by conventional methods. Furthermore, they have reduced gas diffusion effects not seen in the prefluourinated counterparts. Some hydrocarbon polymers show high water content over a wide temperature range, which may be used for enhancing the operating temperature of PEMFC. Typically, the proton conductivity of hydrocarbon polymers can be achieved by chemical modification such as sulfonation reaction which attaches sulfonic acid groups to the polymer backbone. The popular hydrocarbon polymers in PEMFC research include sulfonated polyether ether ketone (S-PEEK), sulfonated polybenzimidazole (S-PBI) and a variety of polymer membrane composites. Descriptions of each are presented in detail below.

1.3.3.1 Sulfonated polyether ether ketones (S-PEEK)

PEEK belongs to the family of polyether ketone polymers. It is a thermoplastic polymer with a glass transition temperature of 143 ^{o}C. It does not dissolve in organic solvents except strong acids. Thus, the sulfonated PEEK (S-PEEK, shown in Figure 1-6) is prepared by simply dissolving the PEEK in concentrated sulfuric acid. The degree of sulfonation (DS), which is a ratio of the sulfonated unit to the total unit, is usually controlled by sulfonation time. The properties of S-PEEK have been investigated by many groups. [34, 35, 36, 37] It was reported that the water uptake of S-PEEK increases with increasing DS, which contributes to the increased proton conductivity. It was also reported that although the S-PEEK presents proton conductivity comparable with Nafion at high relative humidity, the proton conductivity of S-PEEK depends on the relative humidity more strongly than that of Nafion. [34, 36] Significant contributions to the correlation of the conductivity in S-PEEK to structural and dynamic properties observed in SS-NMR experiments is presented in this thesis.

Using SAXS, Yang and co-workers studied S-PEEK with variable degrees of sulfonation. [38] The authors proposed that both the cluster size and the number of sulfonic acid group in each cluster are small due to the high rigidity of the S-PEEK polymer chain. They found that the number of ionic clusters increases with increasing degree of sulfonation, resulting in shorter distances between ionic clusters. This adequately explains the dependence of conductivity on degree of sulfonation. Zhao and co-workers investigated the block S-PEEK and random S-PEEK (by sulfonation of PEEK) using SAXS. [39, 40] They found that the block S-PEEK polymer has larger ionic cluster size and larger proton transport channels. This interprets the enhanced proton conductivity of block S-PEEK very well. In spite of the above structural information, no specific models have been proposed for S-PEEK to understand the morphology changes during hydration. Similar to the studies of Nafion, information regarding proton dynamics was also absent for S-PEEK in these studies.

Kaliaguine and co-workers studied the influence of casting solvents such as Dimethylacetamide (DMAc), N-methyl-2-pyrrolidone (NMP), and dimethylformamide (DMF), on the conductivity of resulting S-PEEK membranes. [41, 42] They found that DMF strongly decreases the proton conductivity of S-PEEK due to the formation of strong hydrogen bonds between DMF and the sulfonic acid proton of S-PEEK. However, although this interprets the conductivity difference of S-PEEK membranes with residual casting solvents (which should have been removed before conductivity measurements), it does not disclose the real difference of S-PEEK membranes prepared by different casting solvents. Using WAXD, dynamic mechanical analysis (DMA) and modulated differential scanning calorimetry (MDSC), Kaliaguine and co-workers reported that the hydrophilic/hydrophobic phase separation is promoted by thermal treatment. Samples that experienced a sequence of heating-cooling cycles showed higher proton conductivity than untreated samples. This was attributed to irreversible microstructural modifications that support proton conduction. [43] Kaliaguine and co-workers also prepared crosslinked S-PEEK by using ethylene glycol to make the resulting membrane less susceptible to swelling. [44, 45] The crosslinked S-PEEK membrane is more rigid than the non-crosslinked S-PEEK and comparable to Nafion in mechanical strength as well as conductivity. However, this crosslinked polymer is not well characterized, in terms of equivalent weight, residual degree of sulfonation, and interactions of crosslinkers and sulfonic acid groups. This information is necessary to understand the high conductivity of crosslinked S-PEEK and will be addressed in this thesis.

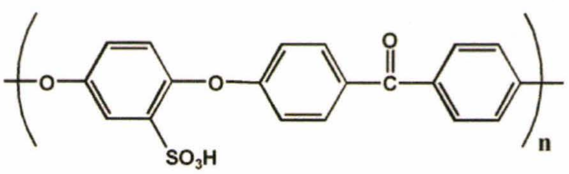

Sulfonated polyether ether ketone (S-PEEK)

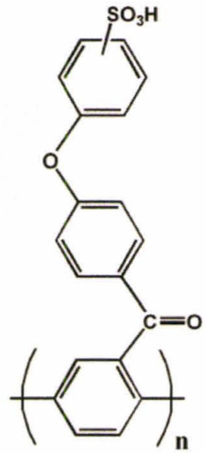

Sulfonated poly (4-phenoxybenzoyl-1,4-phenylene) (S-PPBP)

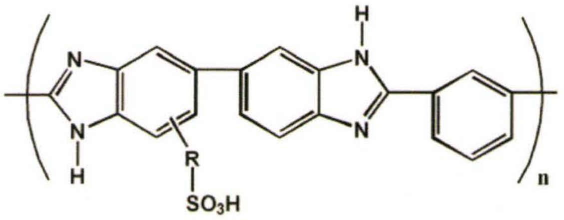

Sulfonated polybenzimidazole (S-PBI)

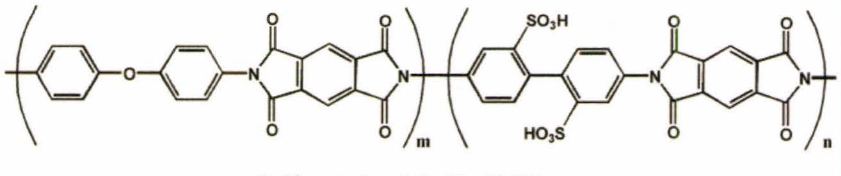

Sulfonated polyimide (S-PI)

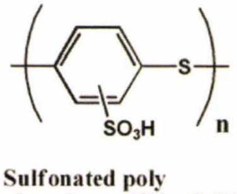

Sulfonated poly phenylenesulfide (S-PPS)

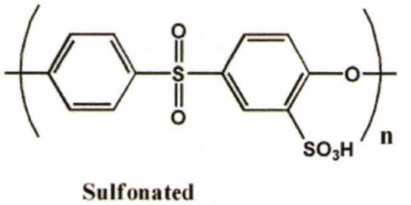

Sulfonated polyethersulfone (S-PES)

Figure 1-6. Structures of sulfonated polymers for application in PEMFC

1.3.3.2 Sulfonated polybenzimidazole (S-PBI)

Polybenzimidazole (PBI) is a polymer with a very high glass transition temperature of 425 ~ 435 °C, which has excellent thermal and mechanical stability. Similar to PEEK, sulfonic acid groups can be introduced to PBI (shown in Figure 1-6) to increase proton conductivity. [46, 47, 48] Glipa studied the benzylsulfonated PBI with variable degree of sulfonation. [46] It was reported that the proton conductivity of the resulting membrane increases with increasing degree of sulfonation from 10^{-4} S/cm for non-sulfonated PBI to $>10^{-2}$ S/cm for a sample with 75% degree of sulfonation. However, the shrinkage of S-PBI membrane was observed once sorbed water was removed. Bae and co-workers investigated PBI sulfonated by butanesultone (BS). [49] It was found that the PBI-BS showed lower conductivity than Nafion117 below 80 °C. At temperatures higher than 80 °C, PBI-BS did not show significant loss of conductivity, which indicates that PBI-BS can be used in PEMFCs with high operating temperatures. Using DSC, the authors found that the sulfonic acid groups in S-PBI have a stronger interaction with the adsorbed water than those in Nafion. This explains the retention of the absorbed water at enhanced temperatures for S-PBI.

1.3.3.3 Sulfonated polyimide (S-PI)

Polyimides (PI) (shown in Figure 1-6) are thermoplastic polymers as well. They demonstrate good mechanical and thermal properties, which in turn makes them good candidates for sulfonated PEMs. S-PI is considered to be a new type of ion exchange membrane with advantages including indifference to external conditions and conductivities not as strongly correlated to water content. [50] Ye and co-workers synthesized and characterized a series of sulfonated PI. [51] They reported that the conductivity dramatically increased with increasing temperatures from 120 °C to 160 °C where the relative humidity is decreasing. This indicates a more significant effect of temperature than the relative humidity at high temperatures.

Using SAXS and SANS, Cornet and co-workers investigated the structure of S-PI.[50] A disc-like hydrophobic domains spaced by a continuous ionic phase, instead of ionic domains dispersed in the polymer matrix which are essentially spherical ionic domains, is proposed for the structure of S-PI.

1.3.3.4 Other sulfonated nonfluorinated ionomers

There are also many other polymers such as polyethersulphone (PES), [52] poly (4-phenoxybenzoyl-1, 4-phenylene) (PPBP) [53] and polyphenylenesulfide (PPS), [54] which are sulfonated (as shown in Figure 1-6) for PEMFC applications. Similar to the above introduced non-perfluorinated ionomers, the conductivities of these sulfonated polymers were investigated but information on their structure and morphology is seldom reported and still needed for understanding their distinct conductivities.

1.4 Polymer electrolyte membrane composites

It is known that operating PEMFC at temperatures above 130 °C has many advantages such as fast reaction kinetics and much higher allowable concentration of CO for platinum catalyst. Nevertheless, almost all investigated PEMs so far show decreased conductivity with increasing temperature due to water loss. Since a higher operating temperature is so attractive, many strategies have been used to develop the desired PEMs. Among them, adding dopants to the matrix of the ionomer seems to be very promising. The dopants are usually insoluble inorganic solids which not only improve proton conductivity at high temperature through self-humidification but also improved mechanical strength and thermal stability of the membrane. A further advantage of introducing inorganic solid dopants is the suppression of fuel crossover. Oxide based composites, layered phosphate composites, and heteropolyacid composites are all discussed in detail below. It is generally thought that the inorganic dopants in the polymer matrix decrease the chemical potential of the water inside the polymer, by which an additional pathway for proton conduction is created. [55] In addition, the proton hydrogen-bonding sites provided by the dopants help water retention and proton transportation.

1.4.1 Oxides based composites

Oxides such as SiO_2, TiO_2, ZrO_2, Al_2O_3 and WO_3 have been used to prepare membrane composites. A direct way to make these polymer/oxides composites is to mix their powder with the polymer solution and then recast the mixture to form the membrane. Nafion/SiO_2, [56, 57] Nafion/Al_2O_3, [58] S-PEEK/SiO_2 [59] and S-PEEK/WO_3 [60] have been investigated. Improved water uptake was observed for some composites. [56] With 3% SiO_2 loading, the Nafion/SiO_2 composites show 41% water content which is much higher than the 18% of unmodified Nafion. However, usually this method is not able to produce very small particle sizes for the dopants in the polymer matrix, although it does allow for very accurate control of loading of dopants.

An alternative way to load SiO_2, TiO_2 and ZrO_2 in polymers is to hydrolyze silanes and metal oxides in solutions of polymer. Using anomalous small angle X-ray scattering (ASAXS) which is an element-specific technique, Prado and co-workers studied the morphology and distribution of ZrO_2 in S-PEEK/ZrO_2 composites. [61] The ZrO_2 particles were found to be smaller than 13 Å, however, the conductivity of the composites with 13.5% ZrO_2 is 3 orders of magnitude lower than that of pure S-PEEK. This was attributed to the binding of the sulfonic acid groups to the ZrO_2 species. By hydrolyzing the precursors of dopants in the S-PEEK solution, Nunes and co-workers prepared S-PEEK/TiO_2, S-PEEK/ZrO_2 and S-PEEK/SiO_2 composites. [62] However, although TiO_2 and ZrO_2 are homogeneously dispersed in S-PEEK, large SiO_2 particles were observed in S-PEEK and since the higher interface interaction between the polymer and the dopants would modify the polymer to a greater extent, smaller particle size of dopants is desired.

Mauritz *et al.* developed a sol-gel method to form SiO_2 in Nafion *in-situ.* [63, 64] In the sol-gel method, the tetraethylorthosilicate (TEOS) permeates into the previously swollen Nafion membrane, hydrolyzes with the catalysis of sulfonic acid from Nafion and then condense to form SiO_2. Since the whole process occurs in a polymer matrix instead of a polymer solution, the particle size of SiO_2 is very small due to the small channels in Nafion. This was supported by SAXS, [65] FT-IR [66] and dielectric relaxation measurements [67] where it was shown that the nano-phase separated morphology of Nafion works as a template for the *in-situ* formation of SiO_2. The resulting composites showed higher water uptake than the original Nafion which is believed to be due to water absorption on the surface of the SiO_2.

Baradie and co-workers reported the conductivity of various Nafion/SiO_2 composites. [68] When the composites have a Si/SO_3H ratio of 5, the measured conductivity at 80 °C and 100% relative humidity is 9.9×10^{-2} S cm^{-1} which is slightly higher than that of the original Nafion, 7.4×10^{-2} S cm^{-1}. Recently, the performance of Nafion/SiO_2 composites in an H_2/O_2 PEMFC at temperatures above 100 °C has been investigated by Adjemian and co-workers. [69, 70] A PEMFC based on the Nafion/SiO_2 composite with 10 % SiO_2 content delivered current densities four times higher than that of the unmodified Nafion. They also found that the performance can be further enhanced by decreasing the equivalent weight and thickness of the membrane. However, information on how the SiO_2 changes the proton dynamics of the original Nafion was not reported in these studies. This information is important not only for understanding the conductivity of the composites but also for guiding the preparation of the composites, which will be addressed in this thesis.

1.4.2 Layered phosphate based composites

Polymer composites with layered phosphates have been studied by many groups. Those phosphates can be expressed by $M^{IV}(RPO_3)_2$, where M is a tetravalent metal such as Zr, Ti, Ce, or Sn; R is an inorganic or organic group such as -H, -OH, or $-CH_2OH$. These compounds differ from the previous metal oxide dopants in that they are good proton conductors whose hydroxyl protons are direct participants in proton conductivity. [71] Similar to polymer oxide composites, these polymer phosphate composites can be prepared by either recasting a mixture of polymer and phosphates or forming the phosphates *in-situ* in the polymer.

At present, one of the most popular phosphates in this field is the zirconium phosphates (ZrP). There are two types of crystallized ZrP; α-ZrP and γ-ZrP. [72] Clearfield reported that the conductance of ZrP increases with a decrease in the structural order, [73] thus, making amorphous ZrP the preferred phase for PEM doping. Parado *et al.* prepared S-PEEK/ZrP composites by recasting a mixture of S-PEEK solution with ZrP precipitates. [61] They found that although the ZrP particle size is very large - up to 185 Å - the conductivity of the composites is only slightly lower than that of unmodified Nafion. By continuously treating the Nafion in a Zirconium solution followed by addition of phosphoric acid, Costamagna and co-workers were able to form ZrP in Nafion *in-situ.* [74, 75] The ZrP particle size was found to be about 11 nm which is in a good agreement with Chalkova. [76] Although at 80 °C the Ohmic resistance of fuel cell based on Nafion/ZrP composites is slightly higher than that of the unmodified Nafion the ZrP composite fuel cells showed improved electrochemical performance. Current densities of 1000 mA/cm^2 at 0.45 V and 130 °C were measured and are 4 times higher than that of fuel cell with unmodified Nafion under the same conditions. Moreover, at this temperature the composites showed thermal stability not seen in unmodified Nafion where degradation was observed.

Using the same techniques for preparation of Nafion/ZrP composites, Bauer *et al.* investigated the structure of the composites, as well as the dependence of the composite conductivity on the % ZrP. [77, 78] Diffraction data indicated that a monolayered structure of ZrP is present rather than a multi-layered structure seen in other Nafion composites. This could result in very strong ionic interactions between the filler and the hydrophilic clusters of Nafion. When the relative humidity is lower than 90% at 125 °C or 150 °C, the Nafion/ZrP composites with 24 % ZrP loading exhibited higher proton conductivity than the unmodified Nafion, but those with ZrP loading lower than 15% did not. They suggest that this is due to changes in the ionic interactions between the sulfonic acid group of the Nafion and the phosphoric acid group of ZrP rather than the additional water adsorbed on the surface of ZrP. This is somewhat consistent with Alberti, [79] who proposed that the improved conductivity is due to a modification of the polymer microstructure rather than the conductivity of ZrP. A further study of interactions between Nafion and ZrP will be presented in this thesis to help better understand the conductivity of Nafion/ZrP composites.

Another layered phosphate which has further enhanced proton conductivity is sulfophenylenphosphonates (SPP). It has a general form $M(HPO_4)_{2-x}(O_3PC_6H_4SO_3H)_x$, where M is the tetravalent ion and x=0.4~1.35. [80] Zirconium phosphate SPP and titanium phosphate SPP have been studied. [81, 82] Their conductivity can be up to 0.1 S/cm at 100 °C and 90 % relative humidity. [83] However, due to the insolubility of these compounds, the corresponding polymer composites can only be prepared by recasting the mixture of polymer solution and these compounds. Using the above method, Alberti [82] prepared sulfonated polyether ketone (S-PEK)/$Zr(HPO_4)_{0.7}(SPP)_{1.3}$ composites. The composites with 20% $Zr(HPO_4)_{0.7}(SPP)_{1.3}$ loading showed conductivities 10 times higher than that of pure S-PEK at temperatures of 80-110 °C and 90% relative humidity. Similarly, Krishnan prepared S-PEEK/$Zr(HPO_4)_{0.65}(SPP)_{1.35}$ composites with 10-50 wt. % of $Zr(HPO_4)_{0.65}(SPP)_{1.35}$.[84] They found that the composite with 10% dopant loading consistently showed conductivity lower than that of pure S-PEEK. However, when the loading of the dopant is 50%, a three-fold increase in conductivity was obtained. This may suggest that a critical concentration of dopant is needed to create conduction pathways in the S-PEEK composites.

1.4.3 Heteropolyacids based composites

The typical heteropolyacids include phosphomolybdic acid $H_3PMo_{12}O_{40}\cdot nH_2O$ (PMA), phosphotungstic acid $H_3PW_{12}O_{40}\cdot nH_2O$ (PTA) and silicotungstic acid $H_4SiW_{12}O_{40}\cdot nH_2O$ (STA). Heteropolyacids are strongly acidic and show high conductivity when hydrated. [85] The polymer/heteropolyacids composites are prepared by recasting the polymer solution containing heteropolyacids. [86, 87] Tazi prepared Nafion/PMA composites by recasting a Nafion solution with PMA. [88] The composite showed 95% water uptake which is much higher than 27% of the unmodified Nafion. Moreover, better electrochemical performance was observed for the composite PEM fuel cell. At 80 °C the current density at 0.6V increased from 640 mA/cm^2 for a fuel cell with unmodified Nafion to 940 mA/cm^2 for a fuel cell with a Nafion/PMA composite. Using the same method, S-PEEK composites containing PMA or PTA were prepared. [89] The S-PEEK composites also exhibited higher water uptake and higher conductivity than pure S-PEEK.

1.4.4 Other composites

There are many other compounds used to prepare polymer composites as well. Acids such as H_3PO_4, H_2SO_4, HCl etc. have been doped into membranes for preparation of composites. [90] The strong acids react with basic sites such as the ether, amide, or imide groups of polymers, which establishes hydrogen bonds and leads to increased acid dissociation. As a result, the proton conductivity of the polymer composites can be enhanced. Although high acid content usually gives high conductivity, the mechanical properties are worsened because of too much acid. This makes polymers with high glass transition temperature, such as PBI, desirable. High proton conductivities of PBI membranes doped with H_3PO_4 and H_2SO_4 were reported to be 2×10^{-3} S cm^{-1} and 6×10^{-2} S cm^{-1}, respectively. [91] The fuel cell with H_3PO_4 doped PBI exhibits higher performance than that with pure Nafion117. [92] Solid acids such as $CsHSO_4$ have been used as dopants as well. [93] The conductivity of polyvinylidene fluoride / $CsHSO_4$ composites is up to 1×10^{-2} S cm^{-1} at 160 °C and 80% relative humidity. BPO_4 was also used to prepare composites [94] where the room temperature conductivity of S-PEEK/BPO_4 with 60% BPO_4 and 80% degree of sulfonation was found to be 5 times higher than that of the unmodified S-PEEK.

1.5 Summary for current status of PEM research

Investigation of PEMs has been mainly focused on Nafion which shows a strong dependence of proton conductivity on water content. The existence of ionic clusters is observed in SAXS and SANS studies and attributed to the conductivity differences under different relative humidity conditions. Models have been proposed to understand the morphologies of Nafion at low and high hydration level. The swelling of ionic aggregates and polymer reorganization during the hydration process are proposed in both the cluster network model and the local order model, which adequately explains increased proton conductivity with increasing water content.

The studies of non-perfluorinated PEMs have been performed for different polymers such as S-PEEK, S-PBI, S-PI and so on. Proton conductivities for these materials increase with increasing degree of sulfonation. Similar to Nafion, they display a strong dependence of conductivity on water content as well. However, structural information is absent for most of these hydrocarbon PEMs. Therefore, there are currently no models proposed to interpret their conductivity differences.

As alternatives with improved conductivities, the PEM composites are mainly based on oxides, phosphates, and heteropolyacids. The water uptake of the composites is usually improved by the addition of dopants. Although the conductivities of the composites at relatively low temperature (below 80 °C) are generally lower than those of unmodified PEMs, at temperatures above 100 °C, composites show elevated conductivities than their pure counterparts. Moreover, the composites show greater stability during fuel cell operation. Some structural studies have been performed to understand these composites as well. However, the morphology information is too limited to interpret the conductivities of the composites as the interaction of dopants and PEMs is even more complicated and can not be observed from SAXS and SANS studies.

1.6 The goal of this research

As reviewed above, the dynamic information of proton transport is absent from the literature. This information is crucial when trying to understand and enhance proton conductivity. In this research, SS-NMR is used to explore the link between local proton mobility at the molecular level and long range proton conductivity at the macroscopic level (see introduction in Chapter 2). This technique was chosen for the investigation of proton dynamics of PEMs and PEM composites. The PEMs specific to this thesis are Nafion and S-PEEK which represent the typical perfluorinated and non-perfluorinated PEMs, respectively. Their composites will be based on SiO_2 and

$Zr(HPO_4)_2$ since these composites have displayed improved proton conductivity at high operating temperatures.

These PEMs and PEM composites will be studied by variable temperature NMR experiments which investigate the dependence of proton mobility on temperature. A Back-to-Back (BaBa) NMR experiment will be used to distinguish rigid protons from mobile protons by contrasting with standard ^{1}H MAS NMR experiments. This information is very useful to understand proton conductivity under different conditions. Moreover, for samples with multiple mobile proton sites, 2D exchange spectroscopy (EXSY) NMR experiments will be used to study exchange between proton sites which are involved in conductivity. In addition, other experiments such as ^{13}C, ^{29}Si, ^{31}P NMR and their proton correlation NMR experiments will be used to provide some structural information for these PEMs and PEM composites. With the combination of impedance spectroscopy data, the information of proton dynamics and structures of PEMs and PEM composites will allow a better understanding of their proton conductivity at the molecular level.

1.7 Outline of thesis

The first chapter introduces the current status of research regarding proton exchange membranes with the goals of this thesis outlined. The techniques used in this research, including SS-NMR, pulse field gradient NMR and impedance spectroscopy, are introduced in the second chapter. The third chapter presents studies of Nafion compared with those of S-PEEK. This comparison highlights the clear differences in the nature of hydrogen bonding in the two polymers. Studies of Nafion/SiO_2 composites are presented and discussed in Chapter 4. The differences in the proton diffusion coefficients and proton conductivities between the pure and the composite are discussed with consideration of the SS- NMR results.

The studies of ZrP are presented in Chapter 5 with the investigation of Nafion/ZrP composites presented in Chapter 6. The characterization of ZrP and the investigation of the interaction of ZrP with the acidic protons of H_2SO_4 in Chapter 5 help to understand the NMR results seen in the Nafion/ZrP composites in Chapter 6. Special emphasis is placed on the interaction of ZrP and the sulfonic acid proton of Nafion.

The studies of S-PEEK with variable degree of sulfonation, and prepared from different casting solvents, are shown in Chapter 7. Their conductivity differences are discussed according to the proton environments and polymer chain mobility in these samples. The investigation of crosslinked S-PEEK is presented in Chapter 8. In this chapter the superb conductivity of this polymer is better understood through interpretation of 2D EXSY NMR results. In the last chapter a summary is presented followed by an outlook for this exciting field of research.

1.8 References

[1] K. M. Nouel, P. S. Fedkiw, *Electrochim. Acta*, **1998**, 43, 2381-2387.

[2] F. Barbir, *PEM Fuel cells: Theory and Practice*, Elsevier Academic Press, **2005**, p 13.

[3] Peter Hoffmann, *Tomorrow's Energy: hydrogen, fuel cells, and the prospects for a cleaner planet*, The MIT press, **2001**, p. 146.

[4] Anno., *Business Week* 33, **1959**, Sept. 19.

[5] M. Nadal, F. Barbir, *Development of a Hybride Fuel Cell/Battery Powered Electric Vehicle*, in D.L Block and T. N. Veziroglu, Hydrogen Energy Progress X, Vol. 3, pp. 1427-1440.

[6] P. W.Atkins, *Physical Chemistry*, Sixth Edition, W.H.Freeman and Company, New York, **2000**, p. 258.

[7] L. Carrette, K. A. Friedrich, U. Stimming, *Fuel cells*, **2001**, 1, 5-39.

[8] K. D. Kreuer, in *Handbook of Fuel Cell Fundamentals, Technology, and Applications*; Vielstich *et al.*, Eds.; John Wiley: Chichester, UK, **2003**, Vol. 3, Part 3, Chapter 33, pp. 420.

[9] W. T. Grubb, General Electric, US Patent, 2, 913, 511, **1959**.

[10] K. Kolbrecka, J. Przyluski, *Electrochim. Acta*, **1994**, 39, 1591-1595.

[11] H. F. Oetjen, V. M. Schmidt, U. Stimming, F. Trila, *J. Electrochem. Soc.*, **1996**, 143, 3838-3842.

[12] K. H. Choia, D. J. Park, Y. W. Rho, Y. T. Kho, T. H. Lee, *J. Power Sources*, **1998**, 74, 146-150.

[13] M. Watanabe, H. Uchida, Y. Seki, M. Emori, *J. Electrochem. Soc.*, **1996**, 143, 3847-3852.

[14] L. Carrette, K. A. Friedrich, S. Ulrich, *Chemphyschem*, **2000**, 1, 162-193.

[15] S. Gottesfeld, T. A. Zawodzinski, Polymer Electrolyte Fuel Cells, in R. C. Alkire, H. Gerischer, D. M. Kolb, C. W. Tobias (Editors), *Advances in Electrochemical Science and Engineering*, Vol. 5 (Wiley-VCH, New York, **1997**).

[16] M. Rikukawa, K. Sanui, *Prog. Polym. Sci.*, **2000**, 25, 1463-1502.

[17] P. D. Beattie, F. P. Orfino, V. I. Basura, K. Zychowska, J. Ding, C. Chuy, J. Schmeisser, S. Holdcroft, *J. Electroanal. Chem.*, **2001**, 503, 45-56.

[18] A. V. Anantaraman, C. L. Gardner, *J. Electroanal. Chem.*, **1996**, 414, 115-120.

[19] T. D. Gierke, G. E. Munn, F. C. Wilson, *J. Polym. Sci., Polm. Phys.*, **1981**, 19, 1687-1704.

[20] W. Y. Hsu, T. D. Gierke, *Macromolecules*, **1982**, 15, 101-105.

[21] W. Y. Hsu, T. D. Gierke, *J. Membr. Sci.*, **1983**, 13, 307-326.

[22] M. Fujimura, T. Hashimoto, H. Kawai, *Macromolecules*, **1981**, 14, 1309-1315.

[23] M. Fujimura, T. Hashimoto, H. Kawai, *Macromolecules*, **1982**, 15, 136-144.

[24] W. J. MacKnight, W. P. Taggert, R. S. Stein, *J. Polym. Sci., Polym. Symp.*, **1974**, 45, 113.

[25] E. J. Roche, R. S. Stein, T. P. Russell, W. J. MacKnight, *J. Polym. Sci., Polym. Phys. Ed.*, **1980**, 18, 1497-1512.

[26] E. J. Roche, M. Pineri, R. Duplessix, *J. Polym. Sci., Polym. Phys. Ed.*, **1982**, 20, 107-116.

[27] G. Gebel, J. Lambard, *Macromolecules*, **1997**, 30, 7914-7920

[28] G. Gebel, R. B. Moore, *Macromolecules*, **2000**, 33,4850-4855

[29] A. L. Rollet, G. Gebel, J. P. Simonin, P. Turq, *J. Polym. Sci., Part B: Polym. Phys.*, **2001**, 39, 548-558.

[30] G. Gebel, *Polymer*, **2000**, 41, 5829-5838.

[31] L. Rubatat, A. L. Rollet, G. Gebel, O. Diat, *Macromolecules*, **2002**, 35, 4050-4055.

[32] H. G. Haubold, T. Vad, H. Jungbluth, P. Hiller, *Electrochim. Acta,* **2001**, 46, 1559-1563.

[33] K. D. Kreuer, *J. Membr. Sci.*, **2001**, 185, 29-39.

[34] G. Alberti, M. Casciola, L. Massinelli, B. Bauer, *J. Membr. Sci.*, **2001**, 185, 73-81.

[35] M. Gil, X. Ji, X. Li, H. Na, J. E. Hampsey, Y. Lu, *J. Membr. Sci.*, **2004**, 75-81.

[36] R. Jiang, H. R. Kunz, J. M. Fenton, *J. Power Sources*, **2005**, 150, 120-128.

[37] R. W. Koptzke, C. A. Linkous, H. R. Anderson, G. L. Nelson, *J. Electrochem. Soc.*, **2000**, 147 (5), 1677-1681.

[38] B. Yang, A. Manthiram, *J. Power Sources*, **2006**, 153, 29-35.

[39] C. Zhao, X. Li, Z. Wang, Z. Dou, S. Zhong, H. Na, *J. Membr. Sci.*, **2006**, 280, 643-650.

[40] C. Zhao, H. Lin, K. Shao, X. Li, H. Ni, Z. Wang, H. Na, *J. Power Sources*, **2006**, 162, 1003-1009.

[41] S. Kaliaguine, S.D. Mikhailenko, K. P. Wang, P. Xing, G. Roberson, M. Guiver, *Catalysis Today*, **2003**, 82, 213-222.

[42] G. P. Roberson, S. D. Mikhailenko, K. P. Wang, P.Xing, M. D. Guiver, S. Kaliaguine, *J. Membr. Sci.*, **2003**, 219, 113-121.

[43] A. R. Valencia, S. Kaliaguine, M. Bousmina, *J. Applied Polymer Sci.*, **2006**, 99,

756-774.

[44] S. D. Mikhailenko, K. Wang, S. Kaliaguine, P. Xing, G. P. Robertson, M. D. Guiver, *J. Membr. Sci.*, **2004**, 233, 93-99.

[45] S. D. Mikhailenko, G. P. Robertson, M. D. Guiver, S. Kaliaguine, *J. Membr. Sci.*, **2006**, 285, 306-316.

[46] X. Glipa, M. E. Haddad, D. J. Jones, J. Roziere, *Solid State Ionics*, **1997**, 97, 323-331.

[47] K. Tsuruhara, K. Hara, M. Kawahara, M. Rikukawa, K. Sanui, N. Ogata, *Electrochim. Acta*, **2000**, 45, 1223-1226.

[48] M. Kawahara, M. Rikukawa, K. Sanui, *Polym. Adv. Technol.*, **2000**, 11, 544-547.

[49] J. M. Bae, I. Honma, M. Murata, T. Yamamoto, M. Rikukawa, N. Ogata, *Solid State Ionics*, **2002**, 147, 189-194.

[50] N. Cornet, O. Diat, G. Gebel, F. Jousse, D. Marsacq, R. Mercier, M. Pineri, *J. New Mater. Electrochem. Syst.*, **2000**, 3, 33-42.

[51] X. Ye, H. Bai, W. S. W. Ho, *J. Membr. Sci.*, **2006**, 279, 570-577.

[52] V. Deimede, G. A. Voyiatzis, J. K. Kallitsis, O. Li, N. J. Bjerrum, *Macromolecules*, **2000**, 33, 7609-7617.

[53] T. Kobayashi, M. Rikukawa, K. Sanui, N. Ogata, *Solid State Ionics*, **1998**, 106, 219-225.

[54] K. Miyatake, H. Iyotani, K. Yamanoto, E. Tscuchida, *Macromolecules*, **1996**, 29, 6969-6971.

[55] Q. Li, R. He, J. O. Jensen, N. J. Bjerrum, *Chem. Mater.*, **2003**, 15, 4896-4915.

[56] M. Watanabe, H. Uchida, Y. Seki, M. Emori, P. Stonehart, *J. Electrochem. Soc.*, **1996**, 143, 3847-3852.

[57] H. Wang, B. A. Holmberg, L Huang, Z. Wang, A. Mitra, J. M. Norbeck, Y. Yan, *J. Mater. Chem.*, **2002**, 12, 834-837.

[58] A. S. Arico, V. Baglio, V. Antonucci, I. Nicotera, C. Oliviero, L. Coppola, P. L. Antonucci, *J. Membr. Sci.*, **2006**, 270, 221-227.

[59] B. Boonet, D. J. Jones, J. Roziere, L. Tchicaya, G. Alberti, *J. New Mater. Electrochem. Syst.*, **2000**, 3,87-92.

[60] B. Mecheri, A. D'Epifanio, M. L. D. Vona, E. Traversa, S. Licoccia, M. Miyayama, *J. Electrochem. Soc.*, **2006**, 153(3), A463-A467.

[61] L. A. S. De A. Prado, H. Wittich, K. Schulte, G. Goerigk, V. M. Garamus, R. Willumeit, S. Vetter, B. Ruffmann, S. P. Nunes, *J. Polymer Sci., Part B: Polymer Phys.*, **2003**, 42, 567-575.

[62] S. P. Nunes, B. Ruffmann, E. Rikowski, S. Vetter, K. Richau, *J. Membr. Sci.*, **2002**, 203, 215-225.

[63] Q. Deng, R. B. Moore, K. A. Mauritz, *Chem. Mater.*, **1995**, 7, 2259-2268.

[64] Q. Deng, Y. Hu, R. B. Moore, C. L. McCormick, K. A. Mauritz, *Chem.Mater.*, **1997**, 9, 36-44.

[65] K. A. Mauritz, *Material Science and Engineering C*, **1998**, 6, 121-133.

[66] K. A. Mauritz, R. M. Warren, *Macromolecules*, **1989**, 22, 1730-34.

[67] K. A. Mauritz, I. D. Stefanithis, *Macromolecules*, **1990**, 1380-1388.

[68] B. Baradie, J. P. Dodelet, D. Guay, *J. Electroanal. Chem.*, **2000**, 489, 101-105.

[69] K. T. Adjemian, S. Srinivasan, J. Benziger, A. B. Bocarsly, *J. Power Sources*, **2002**, 109, 356-364.

[70] K. T. Adjemain, S. J. Lee, S. Srinivasan, J. Benziger, A. B. Bocarsly, *J. Electrochem. Soc.*, **2002**, 149, A256-A261.

[71] Y. Abe, G. Li, M. Nogami, T. Kasuga, *J. Electrochem. Soc.*, **1996**, 143, 144-147.

[72] N. J. Clayden, *J. Chem. Soc. Dalton Trans*, **1987**, 1877-1881.

[73] A. Clearfield, *Ann. Rev. Mater. Sci.*, **1984**, 14, 205-229.

[74] P. Costamagna, C. Yang, A. B. Bocarsly, S. Srinivasan, *Electrochim. Acta*, **2002**, 47, 1023-1033.

[75] C. Yang, S. Srinivasan, A. B. Bocarsly, S. Tulyani, J. B. Benziger, *J. Membr. Sci.*, **2004**, 237, 145-161.

[76] E. Chalkova, M. V. Fedkin, S. Komarneni, S. N. Lvov, *J. Electrochem. Soc.*, **2007**, 154(2), B288-B295.

[77] F. Bauer, M. W. Porada, *J. Membr. Sci.*, **2004**, 233, 141-149.

[78] F. Bauer, M. W. Parada, *Fuel Cells*, **2006**, 3-4, 261-269.

[79] G. Alberti, M. Casciola, *Annu. Rev. Mater. Res.*, **2003**, 33, 129-154.

[80] M. Casciola, G. Alberti, S. Ciarletta, A. Cruccolini, P. Piaggio, M. Pica, *Solid State Ionics*, **2005**, 176, 2985-2989.

[81] G. Alberti, U. Costantino, M. Casciola, S. Ferroni, L. Massinelli, P. Staiti, *Solid State Ionics*, **2001**, 145, 249-255.

[82] G. Alberti, M. Casciola, E. D'Alessandro, M. Pica, *J. Mater. Chem.*, **2004**, 14, 1910-1914.

[83] G. Alberti, M. Casciola, M. Pica, T. Tarpanelli, M. Sganappa, *Fuel cells*, **2005**, 5(3), 366-374.

[84] P. Krishnan, J. Park, T. Yang, W. Lee, C. Kim, *J. Power Sources*, **2006**, 163, 2-8.

[85] O. Nakamura, I. Ogino, T. Kodama, *Solid State Ionics*, **1981**, 3-4, 347-351.

[86] V. Ramani, H. R. Kunz, J. M. Fenton, *J. Membr. Sci.*, **2005**, 266, 110-114.

[87] B. Tazi, O. Savadogo, *Electrochim. Acta*, **2000**, 45, 4329-4339.

[88] B. Tazi, O. Savadogo, *J. New Mater. Electrochem. Syst.*, **2001**, 4, 187-196.

[89] M. J. Zaidi, S. D. Mikhailenko, G. P. Robertson, M. D. Guiver, S. Kaliaguine, *J. Membr. Sci.*, **2000**, 173, 17-34.

[90] R. Savinell, E. Yeager, D. Tryk, U. Landau, J. Wainright, D. Weng, K. Lux, M. Litt, C. Rogers, *J. Electrochem. Soc.*, **1994**, 141, L46-L48.

[91] O. Savadogo, *J. Power Sources*, **2004**, 127, 135-161.

[92] O. Savadogo, B. Xing, *J. New Mater. Electrochem. Syst.*, **2000**, 3, 345-349.

[93] D. A. Boysen, C. R. I. Chisholm, S. M. Haile, S. R.. Narayananb, *J. Elelctrochem. Soc.*, **2000**, 147(10), 3610-3613.

[94] S. D. Mikhailenko, S. M. J. Zaidi, S. Kailiaguine, *Catalysis Today*, **2001**, 67, 225-236.

Chapter 2 Experimental Techniques

In this chapter, experimental techniques used in this thesis are introduced. First, an introduction for solid state NMR is presented. The focus of this section is the recoupling of dipolar coupling using the Back to Back (BaBa) pulse sequence, which was used in this thesis to investigate proton mobility in proton exchange membranes. In the following section pulse-field gradient (PFG) NMR is introduced. This technique was used to investigate proton motion on a macroscopic level, providing information for long-range proton motion. Since PFG NMR cannot distinguish proton motion contributed by dissociated protons from that of associated protons, impedance spectroscopy was also used to study the macroscopic proton conductivity contributed by dissociated protons. The principles of impedance measurements are presented in this chapter.

2.1 Solid state NMR

Solid state NMR is a powerful and widely used technique for the study of both ordered and disordered solids, providing not only structural but also dynamic information. Compared with spectra in solution state NMR, spectra in solid state NMR for static samples usually do not present any peak resolution. This is due to slow molecular tumbling in solids which is unable to average anisotropic interactions, such as heteronuclear and homonuclear dipolar coupling, quadrupolar coupling (for spins of I>1/2, where I is the spin quantum number) and chemical shielding anisotropy. In many cases, well resolved spectra can be obtained for spins with I=1/2 (which are the focus of the thesis) by applying NMR techniques such as magic angle spinning (MAS) and dipolar decoupling. However, the interactions which broaden the NMR spectra contain valuable pieces of information which are usually lost when using these techniques. Since this information is valuable when trying to understand the properties of materials, NMR techniques that reintroduce this information - such as dipolar recoupling experiments - are used to access this information. [1] This makes solid state NMR a challenging yet very powerful tool and very important in this research.

2.1.1 NMR basics

It is known from basic quantum mechanics that angular momentum for a spin is always quantized in half-integral or integral multiples of $\hbar$, where $\hbar$ is Planck's constant h divided by 2π. Therefore, the maximum component of angular momentum for a spin with spin quantum number I ($I \neq 0$) is:

$$p = I \cdot \hbar = I \cdot \mathrm{h} / 2\pi \qquad (2\text{-}1)$$

The corresponding magnetic moment μ is proportional to the gyromagnetic ratio γ.

$$\boldsymbol{\mu} = \gamma \cdot \boldsymbol{p} \qquad (2\text{-}2)$$

Where the boldface type denotes vector quantities of the magnetic moment and the angular momentum. When the spin is placed in an applied magnetic field $\mathbf{B}_0$, the magnetic moment interacts with this field, which is referred to as the Zeeman interaction. According to quantum theory, the Zeeman interaction appears in the Hamiltonian operator $\hat{\boldsymbol{H}}$:

$$\hat{\boldsymbol{H}} = - \mu \cdot \mathbf{B}_0 = - \gamma \cdot \hbar \cdot \boldsymbol{I} \cdot \mathbf{B}_0 \tag{2-3}$$

Where $\boldsymbol{I}$ represents a quantum mechanical operator. The solution of the Hamiltonian gives energy levels as follows:

$$E_m = - \gamma \cdot \hbar \cdot m \cdot \mathbf{B}_0 \tag{2-4}$$

Where m is the quantum number. The values for m can be: $-I$, $-I + 1$, …, $I - 1$, I. Therefore, the energy separation between states linearly depends on the magnetic field strength. However, the selection rule $\Delta m = \pm 1$ permits transitions only between adjacent energy levels. As a result, the energy difference for a transition between states is:

$$\Delta E = \gamma \cdot \hbar \cdot \mathbf{B}_0 \tag{2-5}$$

This transition results in an observed frequency ν in a NMR spectrum.

$$\nu = \Delta E / h = \gamma \cdot \mathbf{B}_0 / 2\pi \tag{2-6}$$

This frequency is the Larmor frequency. The Larmor frequency of a nucleus is influenced by its local environment which creates chemical shielding of the external magnetic field $\mathbf{B}_0$. Therefore, different frequencies will be observed in a NMR spectrum for nuclei in distinct chemical environments.

Nevertheless, a difference of population of spins in the two adjacent energy levels is necessary in order to observe this transition. This is shown by the Boltzman distribution. For two adjacent energy levels α and β, the corresponding number of spins N_α and N_β on each level has the following form:

$$\frac{N_\beta}{N_\alpha} = e^{-\gamma\hbar B_0 / kT} \tag{2-7}$$

Where k is the Boltzman constant and T is the temperature. At room temperature, the difference in the number of spins of the two energy levels is very small, which is an important factor in determining the intensity of the NMR signal. The NMR signal is usually enhanced with more scans. However, a delay time between two continuous scans is determined by the spin-lattice relaxation time T_1 which is a time constant describing how fast the longitudinal magnetization (from equilibrium magnetization flipped by a radiation pulse into a plane perpendicular to the direction of $\mathbf{B}_0$) returns to its equilibrium magnetization. In NMR, there are many interactions, such as dipole-dipole coupling, chemical shielding, scalar coupling (J coupling), spin rotation coupling and quadrapolar coupling, which contribute to the relaxation. [2] These interactions are very important not only for the relaxation process but also for exploring the structural information of compounds. This thesis will focus on the interactions of chemical shielding and dipole-dipole coupling. More details for these two interactions will be presented in the following sub-sections.

2.1.2 Chemical shift anisotropy (CSA)

The origin of the chemical shift is due to the chemical shielding effect resulting from a small magnetic field produced by the circulating current of electrons which is induced by the external magnetic field. Generally, the electron distribution around a nucleus in a molecule is not spherically symmetric. This results in a variable size of the electron current around the nucleus when the molecule changes its orientation in the external magnetic field, generating different sizes of chemical shielding. Therefore, the chemical shift is orientation dependent in the magnetic field. The chemical shift Hamiltonian H_{CS} can be expressed by an isotropic term and an anisotropic term as follows:

$$H_{cs} = \gamma B_0 I_z \left[1 - \left(\sigma_{iso} + \Delta\sigma(3\cos^2\theta - 1 + \eta_{CS}\sin^2\theta\cos 2\phi)\right)\right] \quad (2\text{-}8)$$

Where θ and ϕ are the polar angles of the chemical shielding tensor relative to the magnetic field, σ_{iso} is the isotropic chemical shielding, $\Delta\sigma$ is the chemical shielding anisotropy and η_{CS} is the asymmetry in chemical shielding. They are further described as follows:

$$\sigma_{iso} = (\sigma_{11} + \sigma_{22} + \sigma_{33}) / 3 \quad (2\text{-}9)$$

$$\Delta\sigma = \sigma_{33} - (\sigma_{11} + \sigma_{22})/2 \quad (2\text{-}10)$$

$$\eta_{cs} = (\sigma_{22} - \sigma_{11}) / (\sigma_{33} - \sigma_{iso}) \quad (2\text{-}11)$$

Where σ_{11}, σ_{22} and σ_{33} ($\sigma_{11} < \sigma_{22} < \sigma_{33}$) are the principal components of the chemical shielding tensor.

In solution state, only the isotropic chemical shift is observed since the CSA is averaged to zero by the rapid molecular tumbling. However, in solids, the CSA is not averaged to zero, resulting in a broadened spectrum with contributions from all possible orientations of the nuclei in the magnetic field. This makes observation of the isotropic chemical shift difficult in a static solid state NMR spectrum. Thus, techniques which can remove CSA are needed in order to be able to resolve different sites in the solid state NMR spectra.

2.1.3 Homonuclear and heteronuclear dipolar coupling

The dipolar coupling results from an interaction of magnetic moments from different nuclear spins. It is also called dipole-dipole coupling. Different from scalar (J) coupling which is an indirect coupling of the nuclear spins through electrons, the dipolar coupling is a direct coupling of the nuclear spins through space. [3] In the solution state dipolar coupling is averaged to zero by fast molecular tumbling allowing for scalar coupling to be well observed in solution state. However, in solid state the dipolar coupling is not averaged to zero, which results in broadened lineshapes. Due to the broadened lineshapes and the large dipolar coupling, scalar coupling is usually not observed in solid state NMR.

Homonuclear dipolar coupling is a through space coupling between the same nuclear spin. The Hamiltonian can be expressed by: [4]

$$H_D^{(i,j)} = I^{(i)} \cdot D^{(i,j)} \cdot I^{(j)} \tag{2-12}$$

Where the dipolar coupling tensor $D^{(i,j)}$ in the principal axes system (PAS) has the following form:

$$D^{(i,j)} = -2D_{ij} \cdot \begin{pmatrix} -1/2 & 0 & 0 \\ 0 & -1/2 & 0 \\ 0 & 0 & 1 \end{pmatrix} \tag{2-13}$$

Where the dipolar coupling constant D_{ij} is:

$$D_{ij} = -\frac{\mu_0 \hbar \gamma_i \gamma_j}{4\pi r_{ij}^3} \tag{2-14}$$

Where μ_0 is permeability of free space, γ_i and γ_j are the gyromagnetic ratios, r_{ij} is the distance between spins.

Transforming the Hamiltonian from the PAS into the laboratory frame (LAB) in which the z-direction is defined by the external magnetic field, B_0, results in:

$$H_D^{(i,j)} = -\frac{\mu_0 \hbar \gamma_i \gamma_j}{4\pi} \cdot \left[\frac{3\left(I^{(i)} \cdot \boldsymbol{r}_{ij}\right)\left(I^{(j)} \cdot \boldsymbol{r}_{ij}\right)}{r_{ij}^5} - \frac{I^{(i)} \cdot I^{(j)}}{r_{ij}^3} \right] \tag{2-15}$$

Where $\boldsymbol{r}_{ij}$ is the vector describing the orientation of r_{ij} with respect to the laboratory frame. Thus, the secular part of the Hamiltonian is expressed as:

$$H_{D,\mathrm{sec}}^{(i,j)} = D^{(ij)} \cdot \frac{1 - 3\cos^2\theta}{2} \cdot \left[2I_z^{(i)} I_z^{(j)} - \left(I_+^{(i)} I_-^{(j)} + I_+^{(j)} I_-^{(i)} \right) \right] \tag{2-16}$$

Where θ is the angle of the dipolar tensor with respect to the laboratory frame. The effect of homonuclear dipolar coupling in a multispin system is to broaden the spectral lineshape. Generally, the ^{1}H linewidth in organic solids is several tens of kHz.

The heteronuclear dipolar coupling is the dipolar coupling between different nuclear spins. According to equation (2-16), when the two spins have different resonance frequencies, the $I_+^{(i)}I_-^{(j)} + I_+^{(j)}I_-^{(i)}$ terms are insignificant. So the Hamiltonian for heteronuclear dipolar coupling becomes:

$$H_{D,\sec}^{(i,j)} = D^{(ij)} \cdot (1 - 3\cos^2\theta) \cdot I_z^{(i)} I_z^{(j)} \tag{2-17}$$

Where i and j now represent spins from different nuclei. As can be seen from the equation, the effect of heteronuclear dipolar coupling on the spectrum is much simpler than that of homonuclear dipolar coupling. This makes it easier to remove the heteronuclear dipolar coupling. For example, by constantly applying radio-frequency (RF) pulses on the i spin, the sign of the energy determined by $I_z^{(i)} I_z^{(j)}$ oscillates between positive and negative, which averages the heteronuclear dipolar coupling to zero in the spectrum of the j spin. In addition, the heteronuclear dipolar coupling is often much smaller than homonuclear proton dipolar coupling in organic solids, which also benefits from the averaging of heteronuclear dipolar coupling by magic angle spinning of the sample (see below).

Clearly, both homonuclear dipolar coupling and heteronuclear dipolar coupling depend on the distance between nuclei, providing structural information for the sample under investigation. Also, both dipolar couplings are orientation dependent. This makes it possible to extract information about the motions of nuclei, which is crucial for the study of proton mobility in this research.

2.1.4 Magic angle spinning (MAS)

Magic angle spinning is now used routinely in solid state NMR experiments. In the MAS NMR experiments, the rotor in which the sample is held is spun at an angle of 54.74° with respect to the external magnetic field, as shown by Figure 2-1. Under MAS conditions, the Hamiltonian for dipolar coupling interaction is time dependent. Since the axis of rotor is fixed at the magic angle, this reference frame is called rotor frame (ROT). Therefore, by a successive coordinate transformation from PAS frame to ROT frame and then from ROT frame to LAB frame, the spatial part of Hamiltonian for the dipolar interaction, which is represented by a second-rank tensor component, has the following form: [4]

$$A_{2,0}^{(LAB)}(t) = \sum_{m=-2}^{2} A_{2,0}^{(PAS)} \underbrace{D_{0,m}^{(2)}(\alpha,\beta,\gamma)}_{(PAS)\rightarrow((ROT)} \underbrace{D_{m,0}^{(2)}(\omega_R t,\theta_m,0)}_{(ROT)\rightarrow((LAB)} \qquad (2\text{-}18)$$

Where $D_{0,m}^{(2)}$ and $D_{m,0}^{(2)}$ denote the components of Wigner rotation matrices. The angles α,β and γ denote the orientation of the PAS frame with respect to the ROT frame. The angle $\omega_R t$ is the rotor phase. The θ_m is the magic angle. Using the reduced rotation matrices, the spatial part of the Hamiltonian becomes:

$$A_{2,0}^{(LAB)}(t) = A_{2,0}^{(PAS)} \cdot \left[\frac{1}{2}\sin^2\beta\cos(2\omega_R t + 2\gamma) - \frac{1}{\sqrt{2}}\sin 2\beta\cos(\omega_R t + \gamma)\right]$$

(2-19)

Therefore, the introduction of magic angle spinning results in the change of orientational dependence from $\frac{1}{2}(1-3\cos^2\beta)$ in the static case to $\left[\frac{1}{2}\sin^2\beta\cos(2\omega_R t+2\gamma)-\frac{1}{\sqrt{2}}\sin 2\beta\cos(\omega_R t+\gamma)\right]$. This means that the Hamiltonian for the dipolar interaction will collapse after each rotor period, leading to a narrowed spectrum, if the rotor spinning is fast enough. In the simplest case, when the time dependent Hamiltonian commutes with itself, it can be described by the integration of the time dependent spatial part over a period of $[t_0, t_1]$:

$$\Omega(t_0,t_1)=\int_0^{t_1}A_{2,0}^{(LAB)}(t)dt=\frac{A_{2,0}^{(PAS)}}{2\omega_R}\left[\frac{1}{2}\sin^2\beta(\sin(2\omega_R t_1-2\gamma)-\sin(2\omega_R t_0-2\gamma))\right.$$
$$\left.-\sqrt{2}\sin 2\beta(\sin(\omega_R t_1-\gamma)-\sin(\omega_R t_0-\gamma))\right] \qquad (2\text{-}20)$$

Thus, the state of the spin system is fully refocused after each rotor period when it is subject to inhomogeneous interactions. This results in a spectrum with much narrowed peaks.

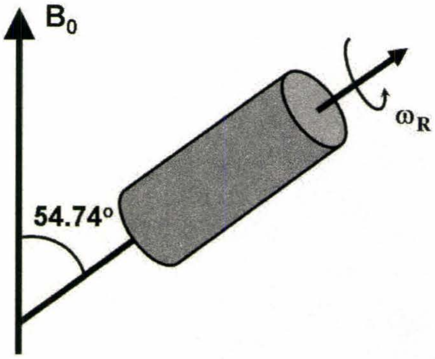

Figure 2-1. The magic angle spinning (MAS) relative to the external magnetic field B_0. ω_R is the spinning speed.

Magic angle spinning can also work to average the chemical shift anisotropy. Under MAS conditions, similar to the case of dipolar interactions, the Hamiltonian for chemical shielding interaction is time dependent as well. Over one rotor period the integration for the anisotropic part of this interaction is zero if the spinning speed of the rotor is fast enough, leading to observation of only isotropic chemical shifts. In MAS NMR experiments, the CSA values of all crystallites in a powder sample are time dependent. Since the axis of rotation, which has an angle of 54.74° relative to the external magnetic field, is the direction of the space diagonal of a cube, each crystallite thereby experiences the average chemical shielding σ_{iso} over one rotation period. [5] Thus, MAS can be viewed as a dynamic implementation of cubic symmetry, which removes the CSA from the obtained spectrum.

However, if the spinning speed is moderate, the MAS will have different effect on the CSA and the dipolar coupling. In the case of inhomogeneous Hamiltonian, [6] such as chemical shielding anisotropy, in which the Hamiltonian at different times commutes with itself, the sample rotation results in a sideband pattern which consists of peaks with integer multiples of the spinning speed centered at the isotropic chemical shift resonance. The spinning sidebands can be minimized by spinning the sample at a frequency greater than the width of the CSA. Nevertheless, in the case of homogeneous Hamiltonian in which the Hamiltonian at different times does not commute, such as the multi-spin homonuclear dipolar coupling, the anisotropic interaction is not completely refocused if the spinning speed is not fast (less than dipolar coupling constant which is generally large in rigid solids). Consequently, a broadened spectrum instead of a sideband pattern is often observed. In most cases, MAS at 25 kHz, which is commonly used in this research, allows proton dipolar coupling to be well suppressed for narrower linewidths.

2.1.5 Recoupling of homonuclear dipolar coupling

As introduced above, dipolar coupling is useful for extracting structural and dynamic information of investigated materials. Particularly, the proton-proton homonuclear dipolar coupling can be used as a probe to explore the proton mobility of polymer electrolyte membranes. This helps to develop an understanding of the proton conductivity of the membranes. However, this information cannot be extracted from regular high resolution MAS NMR spectra since the dipolar coupling is often averaged by the fast magic angle spinning. In order to retrieve the dipolar coupling information, NMR techniques which can recouple the homonuclear dipolar coupling averaged by MAS have been developed, such as DRAMA, [7] RFDR, [8, 9] DREAM, [10] and $C7_2^1$. [11] These pulse sequences have limitations. For example, DRAMA is not efficient for powder samples since the recoupling effect displays an orientation dependence. The $C7_2^1$ is applicable only under moderate spinning speeds (MAS up to ~15 kHz) as this pulse sequence requires a RF pulse of $\omega_{RF} = 7\omega_R$. This is experimentally not applicable under fast MAS conditions (MAS>25 kHz) for conventional NMR spectrometers and MAS probes. For instance, when the MAS is equal to 30 kHz, this pulse sequence requires the ω_{RF} equal to 210 kHz which corresponds to a $\pi/2$ pulse with pulse length of 1.2 μs. Such a short pulse in turn requires very strong power. Furthermore, since $C7_2^1$ consists of a large number of continuous 2π pulses which have different phases, the strong power with a very long total pulse time is difficult for conventional probes. This limits the application of this pulse sequence. At present, the Back to Back (BaBa) pulse sequence shown in Figure 2-2 (a) is very popular for dipolar recoupling due to its simplicity and robustness. [12]

The BaBa pulse sequence consists of pairs of $\pi/2$ pulses which are spaced by intervals of half rotor periods. During the excitation in the BaBa pulse sequence shown in Figure 2-2 (a), pairs of spins change their spin states between ↓↓ and ↑↑, corresponding to the transition between M= -1 and M= +1, which creates double-quantum coherence (DQC) ($\Delta M=2$). The DQC then evolves during a time period t_1. After that, it is reconverted into zero quantum coherence and then into observable single quantum coherence (SQC) for detection during which the spin states change between M= -1/2 and M= +1/2 ($\Delta M=1$). Thus, the selected coherence transfer pathway, as shown in Figure 2-2 (b), is:

$$0 \xrightarrow{excitation} \pm 2 \xrightarrow{reconversion} 0 \xrightarrow{read} -1 \qquad (2\text{-}21)$$

The signal contributed by unwanted coherence pathways can be suppressed by phase cycles employed in the BaBa pulse sequence. [13] Therefore, it is possible to use DQC as a tool for observing two spin correlations in BaBa NMR spectra.

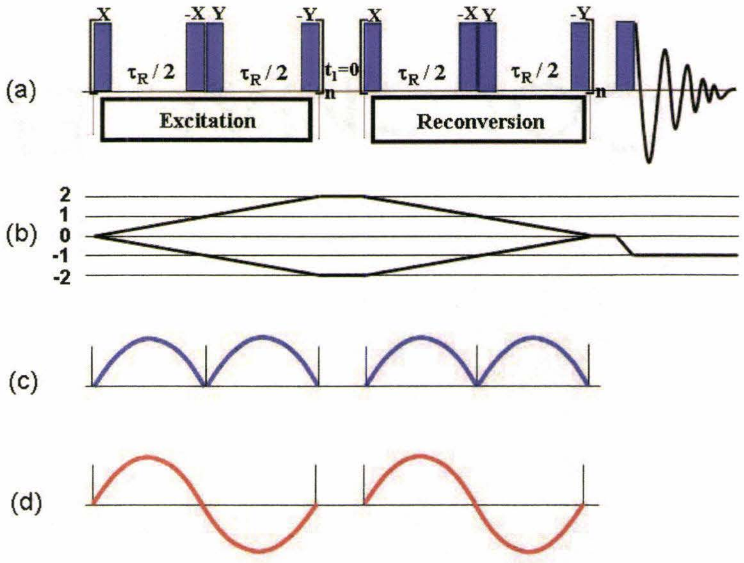

Figure 2-2. (a) Back to Back (BaBa) pulse sequence; (b) coherence transfer pathway diagram; (c) dipolar coupling evolution in BaBa pulse sequence; (d) dipolar coupling evolution in a regular single pulse experiment

As shown in Figure 2-2 (d), the dipolar coupling in a regular single pulse MAS experiment has the opposite sign in the first and the second half of the rotor period, which results in the integration of dipolar coupling over one rotation period to be zero. Therefore no dipolar coupling information can be extracted from the obtained single pulse MAS NMR spectra. However, Figure 2-2 (c) shows that the dipolar coupling in the BaBa experiment has the same sign in both half rotor periods. This leads to a non-zero integration of the dipolar coupling over one rotor period. Therefore, dipolar coupling information can be retrieved from the obtained BaBa spectrum. In the BaBa spectrum, the detected signal intensity for a spin pair is given by the sum over all intensities I_{DQ}^{ij} for each single pair of spins: [14]

$$I_{DQ} = \sum_{i<j} I_{DQ}^{(ij)} \propto \sum_{i<j} \left(D^{(ij)} \tau_{exc}\right)^2 \propto \tau_{exc}^2 \sum_{i<j} \frac{1}{r_{ij}^6} \propto \frac{\tau_{exc}^2}{r_{eff}^6} \qquad (2\text{-}22)$$

Where τ_{exc} is the excitation time, the $D^{(\mathrm{ij})}$ and r_{ij} are the dipolar coupling constant and the distance between spins for an individual pair of spins, respectively, and the r_{eff} is the effective distance between the spin pairs. Thus, the BaBa pulse sequence works as a filter which effectively scales the observed signal intensities by the strength of homonuclear dipolar couplings experienced by respective spins. Namely, only dipolar couplings with certain strength can be efficiently excited and reconverted for detection. Those weak dipolar couplings will be filtered out of the BaBa spectrum. This allows us to distinguish the mobile protons from rigid ones by comparing a BaBa spectrum with a regular single pulse MAS NMR spectrum. [15, 16]

Generally, the 1D double quantum filtered (DQF) BaBa spectrum only provides information about whether and to what degree spins are subject to dipolar couplings. The correlations between spins which have dipolar coupling interactions remain unknown. Therefore, it is necessary to acquire a rotor-synchronized 2D DQ spectrum in which the spins with dipolar couplings can be correlated through dipolar DQCs. In this 2D experiment, the t_1 increment in the BaBa pulse sequence shown in Figure 2-2

(a) is often set to be one rotation period, which makes the excitation and reconversion of DQC have identical phases. Thus, it is called a rotor-synchronized experiment. [13] A schematic rotor-synchronized 2D DQ spectrum is shown in Figure 2-3. In this spectrum the two single-spin resonances A and B are shown in the single quantum (SQ) dimension. In the DQ dimension, the A-A, A-B and B-B correspond to DQC for spin pairs of A and A, A and B, and B and B, respectively. The chemical shift of each resonance is the sum of the nuclei involved in the DQC. Clearly, the 2D DQ spectrum allows us to identify the correlation of dipolar coupling between spins.

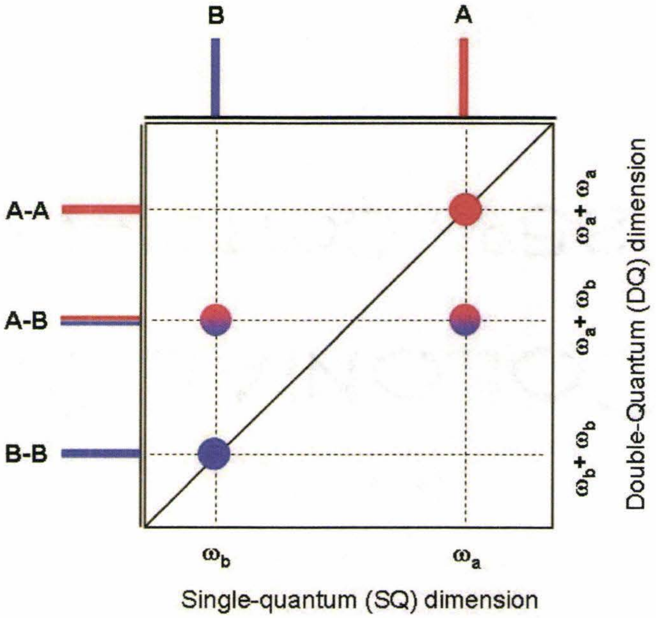

Figure 2-3. A schematic representation of 2D BaBa spectrum

2.1.6 DQ buildup curve for measurement of the dipolar coupling constant

Although a rotor-synchronized 2D BaBa spectrum provides more information about dipolar couplings, no quantitative or semi-quantitative information can be achieved from a single 2D BaBa spectrum. As shown by equation (2-16), the signal intensity for a pair of spins is proportional to the excitation time in the BaBa pulse sequence. If the excitation time is varied in rotor-synchronized 2D BaBa experiments, the integration of the resonance for the spin pair will change accordingly. Therefore, a plot of DQ signal intensity as a function of excitation time, called a DQ buildup curve, would allow one to obtain the dipolar coupling constant by fitting the following equation: [13]

$$I_{DQ}^{(ij)}(\tau_{exc}) = A \cdot \left(D^{(ij)}\tau_{exc}\right)^2 \cdot \exp\left(\frac{\tau_{exc}}{\tau}\right) \tag{2-23}$$

Where A is a constant for experiments with variable excitation time τ_{exc}, $D^{(ij)}$ is the dipolar coupling constant for the spin pair, and τ is the decay time which represents the effective relaxation time of the spin pair during the DQ excitation.

However, in rigid proton systems, strong dipolar couplings produce distinct DQ signal decay effects, which need very short excitation times for the initial DQ buildup curve. This requires very fast MAS experiments. In fact, the DQ buildup approach is usually more suitable for systems with dipolar coupling significantly weaker than that in rigid proton systems, such as mobile polymer melts. [17, 18]

2.1.7 Sidebands for measurement of dipolar coupling constants

An alternative way to achieve the dipolar coupling constant information is by a non-rotor-synchronized 2D DQ experiment in which the t_1 increment is not equal to τ_r. According to the BaBa pulse sequence shown in Figure 2-2 (a), when t_1 is not a multiple of τ_r, the rotor orientations at the beginning of the excitation will be different from those at the beginning of the reconversion period. This causes the rotor phase for the reconversion of DQC to be shifted relative to that for the excitation of DQC. Namely, the reconversion is now rotor encoded. This is called reconversion rotor encoding (RRE) mechanism. The time signals for spin-pair DQCs can be written as follows: [14]

$$S_{DQ}^{(ij)}(t_1) \propto \sin\left(C_{ij}\sin(\omega_R t_1)\right) = 2\sum_{n=1}^{\infty} J_{2n+1}(C_{ij})\sin\left((2n-1)\omega_R t_1\right) \qquad (2\text{-}24)$$

Where J_{2n+1} (C_{ij}) is the (2n+1) order of the Bessel functions, C_{ij} represents terms which do not depend on t_1, but only on the orientation of the dipolar coupling vector and the ratio of dipolar frequency $\omega_D^{(ij)}(=3D^{(ij)})$ to the rotor spinning frequency ω_R. Obviously, the DQ signal is modulated by the odd multiples of the spinning frequency. A Fourier transformation of the signal in t_1 will result in the spin pair DQ spectrum containing only odd-order MAS sidebands.

Generally, if a spin pair is not subjected to the other spins, the MAS sideband patterns should consist of only odd-order sidebands. [14] The presence of the perturbing interaction by other spins usually results in a weak intensity at the centerband and even-order sidebands in the DQ spectrum which is an extracted slice for a proton site in the F2 dimension. Therefore, dipolar coupling information can be achieved by fitting the MAS sideband pattern provided that it consists of only odd-order sidebands. More importantly, the dipolar coupling constants can be used to analyze the mobility of the spins by comparing it with the calculated dipolar coupling constant based on crystallographic data when they are available.

Clearly, a sideband pattern with higher order sidebands, such as the 5th order sidebands, will allow a better fit and therefore a better determination of dipolar coupling constants. Since the observation of the higher order sidebands requires a larger spectra width, the t_1 increment has to be as small as possible. Moreover, the recoupling time should be long enough to allow the excitation of the higher order sidebands as well. Thus, in this thesis the recoupling time in a non-rotor-synchronized 2D DQ experiment is usually set to be 4 rotor periods and the t_1 increment is chosen to be 2 μs for a sample spun at 25 kHz. Under this condition, the 5th order of sidebands can be observed very clearly for most proton sites in the samples investigated in this thesis.

2.2 Pulse field gradient (PFG) NMR

It has been shown in the previous sections that solid state NMR can provide local mobility information of protons by a dipolar recoupling pulse sequence such as Back-to-Back. While this information gives a good description of short range proton motion, information for long range proton motion is still needed to understand macroscopic proton mobility. Usually, there are two ways in NMR to measure the long range proton motion which is measured as a self-diffusion coefficient for translational proton motion. One way is by the analysis of relaxation data, [19] which gives the rotational correlation time, τ_c. Then the translational diffusion coefficient can be determined using the Debye equation and the Stokes-Einstein equation. [20] However, this method requires several assumptions to be satisfied. For example, the molecules are assumed to be spherical in order to be characterized by a single correlation time. The relaxation by intermolecular contribution can be separated from that by intramolecular contribution. [21] Beside these assumptions, the determination of the Stokes radius which is used in the Stokes-Einstein equation to calculate the diffusion coefficient is not straightforward. All these features limit the application of this method, which makes another approach, pulse field gradient (PFG) NMR, very popular.

In PFG NMR, a gradient pulse is often used to create a gradient field in the direction of the B_0 field (denoted as the Z direction). As a result, magnetically equivalent nuclei will have different Larmor frequencies at different positions of the Z direction. This means that any nuclear motion in the Z direction will cause the change of their precession frequencies. Therefore, if an echo pulse sequence, in which the gradient pulses are included, is applied, nuclei which experience motion in the Z direction, will not be refocused at the end of the pulse sequence. Consequently, an attenuated signal is observed. With increasing strength of the gradient field, the signal will exhibit more attenuation. By comparing these attenuated signals with a reference signal which is obtained without applying gradient pulses, the diffusion coefficient for translational motion can be determined.

A pulse sequence applied for PFG NMR measurements in this research is shown in Figure 2-4. [22] A pair of symmetrically spaced field gradient pulses is superimposed onto a standard spin-echo sequence. This is known as the stimulated echo (STE) pulse sequence. A very important feature of the STE pulse sequence is that magnetization is aligned along the –Z direction and only subject to longitudinal relaxation during τ_2. However, the magnetization is subject to transverse relaxation during the two τ_1 periods. Moreover, in the STE sequence it is typical to keep $\tau_1 << \tau_2$, which allows longer time for diffusion provided that the transverse relaxation is fast. This benefits the samples with very slow diffusion coefficients which otherwise require stronger gradient pulses for observable signal attenuation. Due to the longer spin-lattice relaxation time (T_1) for macromolecules ($T_1 > T_2$, where T_2 is the spin-spin relaxation time), the STE pulse sequence is usually preferred to Stejskal and Tanner pulsed-field gradient NMR sequence in which the second and the third $\pi/2$ pulses are replaced by a single π pulse.

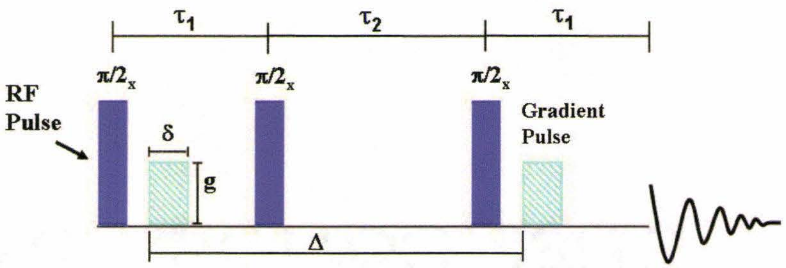

Figure 2-4. Stimulated echo (STE) pulse sequence for diffusion coefficient measurement

The predicted dependence of the observed signal attenuation on gradient strength is: [20]

$$E(2\tau) = \frac{S(2\tau)}{S(2\tau)_{g=0}} = \exp(-\gamma^2 g^2 D\delta^2 (\Delta - \delta/3)) \qquad (2\text{-}25)$$

where S (2τ) is the observed signal intensity with an applied gradient pulse g, $S(2\tau)_{g=0}$ is the signal intensity observed in the absence of an applied gradient, γ is the nuclear gyromagnetic ratio, D is the self-diffusion coefficient, δ is a pulse width of the applied gradient, and Δ is the separation in time between the leading edges of the two gradient pulses (also referred to as the "diffusion time"). Generally, a series of spectra are obtained at increasing gradient strengths with all other parameters kept constant.

The diffusion coefficient is obtained by fitting the plot of the ratio of attenuated signal intensity to reference signal intensity as a function of gradient strength.

In contrast to the relaxation approach, no assumptions are needed regarding the relaxation mechanism and the geometry of the molecule. A fundamental requirement of a PFG NMR experiment is that the diffusional attenuation must be significant relative to the attenuation caused by relaxation of the observed nuclei. Determination of diffusion coefficients by PFG NMR measurements will be difficult or infeasible if relaxation is too rapid. Another basic requirement is that the spectrum should have high resolution for a static sample (MAS is not applied in PFG NMR experiments), since only a well resolved spectrum will allow one to precisely determine the intensity of the attenuated signal. With this limitation, the PFG NMR experiment was only performed for the samples of Nafion and Nafion composites in this thesis.

2.3 Impedance spectroscopy

While PFG NMR experiments can provide information about proton translational motion in the electrolyte, this technique is not able to distinguish proton motion contributed by associated protons from that by dissociated ones. According to the Nernst-Einstein equation shown below, [23] all species involved in diffusion must be responsible for conductivity.

$$\sigma = \frac{C_+ \cdot q_+^2 \cdot D_+ + C_- \cdot q_-^2 \cdot D_-}{k_B T} \tag{2-26}$$

Where σ is conductivity, C_+ and C_- are the concentration of charge carriers, q_+ and q_- are their charges, D_+ and D_- are their diffusion coefficients, k_B is the Boltzman constant, T is the temperature. Therefore, in strong electrolytes in which the concentration of ions is equal to the number of charge carriers, the calculated conductivity based on the diffusion coefficients from PFG NMR measurements will be equal to that obtained from impedance spectroscopy. However, in weak electrolytes, particularly in polymer electrolytes, the concentration of ions is not equal to that of charge carriers as the ions are not fully dissociated. Apparently, these associated ions, presented as neutral ion pairs, will not have much contribution to the measured conductivity. This means that the calculated conductivity based on Nernst-Einstein equation using diffusion coefficients from PFG NMR will be higher than the measured conductivity by impedance spectroscopy. Therefore, it is necessary to measure the conductivity directly by impedance spectroscopy.

2.3.1 Basic principles of impedance spectroscopy

Impedance spectroscopy is a very powerful and popular technique for characterization of electrolytes. It has been widely used in characterizing batteries, [24, 25] fuel cells [26, 27] and corrosion phenomena. [28, 29] The basic principle of impedance spectroscopy is to apply a small amplitude sinusoidal excitation signal (voltage or current) to a system under investigation and measure the response (current or voltage, correspondingly). [30] The impedance Z (ω) is defined as the ratio of the voltage ($V=V_m \sin(\omega t)$) to the current ($I=I_m \sin(\omega t+\theta)$) at a given frequency (ω), shown below:

$$Z(\omega) = \frac{V_m \sin(\omega t)}{I_m \sin(\omega t + \theta)} \tag{2-27}$$

$$Z^{'} = |Z(\omega)| \cos \theta \tag{2-28}$$

$$Z^{''} = |Z(\omega)| \sin \theta \tag{2-29}$$

Where the $Z^{'}$ and the $Z^{''}$ are the real part (resistance) and the imaginary part (reactance), respectively. θ is the phase difference between the voltage and the current. Generally, the magnitude of the impedance and the phase difference θ are frequency dependent. Therefore, the impedance of an electrolyte as a function of frequency can be obtained by varying the frequency.

The resulting impedance data are usually presented by a Nyquist plot and/or a Bode plot, shown in Figure 2-5 and Figure 2-6, respectively. In a Nyquist plot, the imaginary part of the impedance is graphed against the real part of the impedance. The Nyquist plot requires that the real axis and the imaginary axis have the same scale in order not to distort the shape of the impedance curve. This is the advantage of the Nyquist plot as the shape of the curve allows one to have a quick overview of the data and to make some qualitative explanations. However, the disadvantage of the Nyquist plot is the lack of a frequency dimension. This makes the Bode plot very useful. In a Bode plot, the logarithm of the absolute value of impedance ($\log|Z|$) and the phase difference (θ) are plotted against the logarithm of the frequency ($\log \omega$). The axes for the $\log|Z|$ and for θ are often set at the left and the right of the Bode plot, respectively. This is a more complete way to present the impedance data. The change of impedance and phase difference with frequency can be easily identified from the Bode plot.

The interpretation of impedance data is usually performed by fitting the impedance curve of the Nyquist plot with a proper equivalent circuit. The shape of the curve can usually be correlated to a certain type of equivalent circuit in which some of the elements such as resistors, capacitors, inductors and Warburg impedance elements are involved. These elements can be combined in series and parallel to give a complex circuit. The fitting of the impedance curve allows one to determine these elements in the electrochemical system.

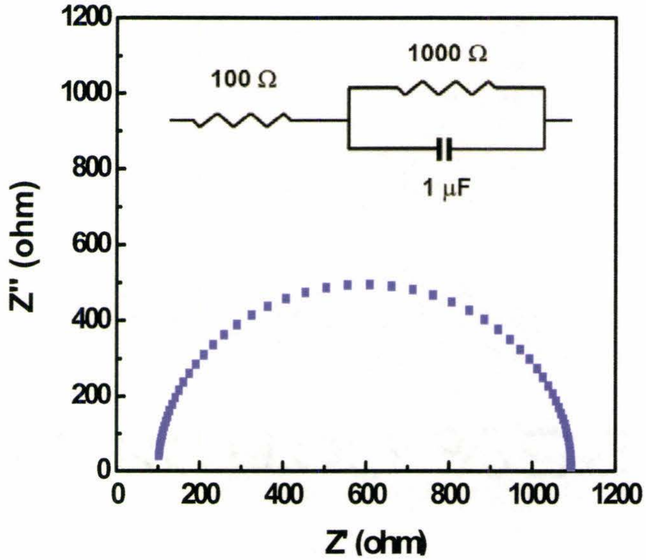

Figure 2-5. An example of a Nyquist plot. The equivalent circuit shown in the figure consists of a 100Ω resistor which is in series with a 1000 Ω resistor and a 1 μF capacitor in parallel. The intercepts on real axis clearly shows the resistances of the two resistors.

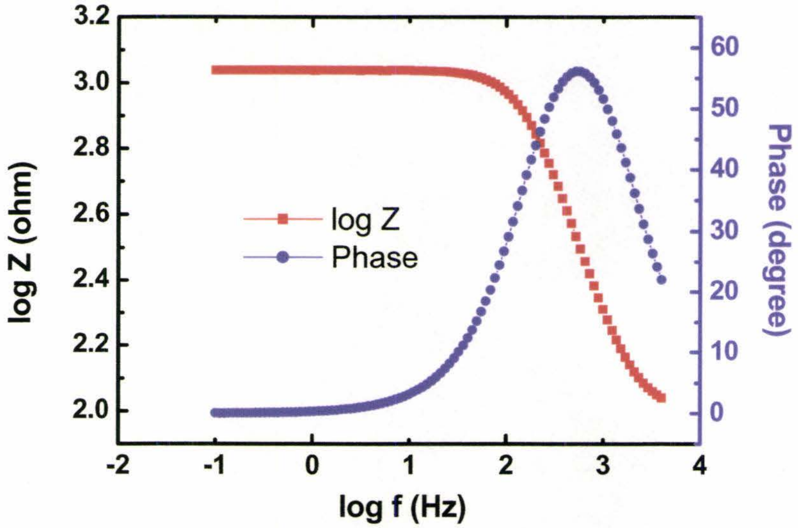

Figure 2-6. An example of a Bode plot. The equivalent circuit is same as the one for Figure 2-5. At low frequency, the impedance is independent of frequency and the phase is zero. The circuit behaves as a pure resistor at low frequency which has a total value of 1100 Ω

2.3.2 Connection modes for impedance measurements

Most electrochemical measurement systems provide at least four connections to the cell. The connections consist of a counter electrode, a working electrode, and two reference electrodes. Generally, impedance can be measured by two-probe method or four-probe method. The difference in the two methods is the configuration of electrodes for voltage supply and electrodes for current measurement. [31] In the two-probe method, the current is supplied via the same two electrodes for measuring potential. In the four-probe method, the electrodes which provide current are separated from the electrodes for potential recording. Usually, the two inner electrodes (the two reference electrodes) and the two outer electrodes (the counter and the working electrodes) are used to record voltage and to provide current, respectively.

The two-probe method has advantages of simplicity and convenience. It is often used for measuring materials with high impedance, such as impedance greater than 10 kΩ, in which case the impedance of the cables is not significant. When the sample under investigation has low impedance, the extra impedance derived from leads connecting with electrodes will be added to the measured impedance, which makes data analysis very difficult. However, a four-probe method can eliminate the contribution of the leads to the measured impedance. This is due to the separation of electrodes for current from those for voltage, which results in no current through the leads connecting with electrodes for voltage. Therefore, the four-probe method is often used to measure low impedance devices such as fuel cells.

In the two-probe method, the impedance measurement of polymer electrolytes is generally performed by sandwiching a polymer membrane with two disc-like electrodes, generally have diameter of 1 cm. [32] This measures the resistance of the membrane in the transverse direction (corresponding to resistance across the membrane in PEMFC). One shortcoming of this geometry is the difficulty of controlling the humidification of the membrane. This issue is better dealt with using the four-probe method in which the two outer platinum foil electrodes and two inner platinum wire electrodes are placed on the same side of the membrane separately. The geometry of the four-probe method is shown in Figure 2-7. Clearly, this geometry allows the membrane to establish equilibrium of hydration quickly by exposing it to the controlled humidity. It should be pointed out that the geometry measures the conductivity of the membrane in the longitudinal direction instead of the transverse direction. For most polymer membranes which have an amorphous structure, their conductivities are expected to be direction independent, which is consistent with literature. [33, 34, 35]

In this research, the four-probe method is taken for impedance measurement of membranes. The ohmic resistance of membrane can be derived directly from the Bode plot. When the phase angle is close to zero over a reasonable frequency range, the impedance is constant and dominated by the ionic conductance. Thus, the impedance is the ohmic resistance of the membrane. Then, the conductivity of the membrane can be calculated using equation (2-30):

$$\sigma = d \,/\, R \cdot l \cdot h \tag{2-30}$$

Where σ, d, R, l and h denote the ionic conductivity, distance between the two inner electrodes, the measured resistance of the membrane, the width of the membrane, and the thickness of the membrane, respectively.

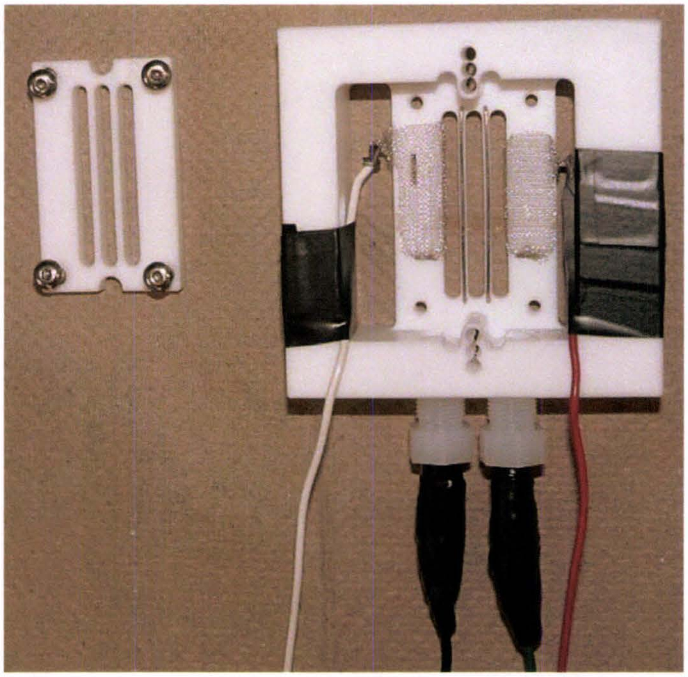

Figure 2-7. The four-probe cell for proton conductivity measurement used in this research. The two platinum foils are used as outer electrodes for current. The two platinum wires are used as inner electrodes for voltage.

2.4 Mechanism of proton conduction

In general, it is widely accepted that the proton conduction can take place via two mechanisms. One is the so-called Grotthuss mechanism, [36, 37] in which the proton transport is completed by the formation/cleavage of hydrogen bonds between hydroniums and water molecules. The other is the vehicle mechanism in which the proton migrates through the motion of the hydronium. [38] The rate of proton transport by the Grotthuss mechanism is faster than that by the vehicle mechanism, leading to the very high proton mobility of hydronium ion compared with that of other ions with similar size. [39] For proton conduction taking place in proton exchange membranes such as Nafion, Datta proposed a third mechanism. [39] This mechanism - called the surface diffusion mechanism - describes the proton transport from the sulfonic acid group of Nafion to the water molecule. The rate of proton transport by this mechanism is even slower than that by the vehicle mechanism. Clearly, the determination of proton conduction contributions from each mechanism will be particularly useful for a full understanding of measured proton conductivity.

By referring to the equation (2-26), the mobility of the protonic charge carrier (D_σ) can be calculated using the measured proton conductivity, assuming that the sulfonic acid groups are fully dissociated and the conductivity contributed by the anion of the sulfonic group (since it is connected with polymer chain) is negligible. The comparison of D_σ with the diffusion coefficient of water will allow one to determine the contribution of proton conductivity resulting from the Grotthuss mechanism and the vehicle mechanism. [40] Since the proton diffusion measured using PFG NMR in this thesis results from several processes including proton transfer between the sulfonic acid group and the water molecule (the surface diffusion mechanism), proton transfer between water molecules (Grotthuss mechanism), and translational motion of hydronium (vehicle mechanism), the diffusion coefficient of water cannot be determined unambiguously in the experiment (due to fast proton exchange between the sulfonic acid group, the hydronium, and the water molecule, these protons are not distinguishable on the NMR time scale). Therefore, no attempt will be made in this thesis to determine the contribution of different mechanisms to the proton conduction by comparing the proton conductivity data with the proton diffusion coefficient data. Instead, these data will be used in combination with solid state NMR data to interpret on the molecular level how the preparation of polymer and polymer composites can change the long range proton motion in these materials.

2.5 References

[1] S. P. Brown, H. W. Spiess, *Chem. Rev.*, **2001**, 101, 4125-4155.

[2] M. H. Levitt, Spin Dynamics, *Basics of Nublear Magnetic Resonance*, John Wiley & Sons, LTD, **2002**, Chapter 16.

[3] E. D. Becker, *High Resolution NMR: Theory and Chemical Applications*, Third

Edition, Acdemic Press, **2000**, p184.

[4] I. Schnell, H. W. Spiess, *J. Magn. Reson.*, **2001**, 151, 153-227

[5] D. D. Laws, H. L. Bitter, A. Jerschow, *Angew. Chem. Int. Ed.*, **2002**, 41, 3096-3129.

[6] C. Filip, S. Hafner, I. Schnell, D. E. Demco, H. W. Spiess, *J. Chem. Phys.*, **1999**, 110, 423-440.

[7] R. Tycko, G. Dabbagh, *J. Am. Chem. Soc.*, **1991**, 113, 9444-9448.

[8] A. E. Bennett, J. H. Ok, R. G. Grinffin, S. Vega, *J. Chem. Phys.*, **1992**, 96, 8624-8627.

[9] A. E. Bennett, C. M. Rienstra, J. J. Griffiths, W. G. Zhen, P. T. Lansbury, R. G. Griffin, *J. Chem. Phys.*, **1998**, 108, 9463-9479.

[10] R. Verel, M. Ernst, B. H. Meier, *J. Magn. Reson.*, **2001**, 150, 81-99.

[11] Y. K. Lee, N. D. Kurur, M. Helmle, O. G. Johannessen, N. C. Nielsen, M. H. Levitt, *Chem. Phys. Lett.*, **1995**, 242, 304-309.

[12] M. Feike, D. E. Demco, R. Graf, J. Gottwald, S. Hafner, H. W. Spiess, *J. Magn. Reson.* A, **1996**, 122, 214-221.

[13] I. Schnell, *Prog. Nucl. Magn. Reson. Spectrosc.*, **2001**, 39, 191-267.

[14] I. Schnell, H. W. Spiess, *J. Magn. Reson.*, **2001**, 151, 153-227.

[15] I. Schnell, S. P. Brown, H. Y. Low, H. Ishida, H. W. Spiess, *J. Am. Chem. Soc.*, **1998**, 120, 11748-11795.

[16] G. R. Goward, M. F. H. Schuster, D. Sebastiani, I. Schnell, H. W. Spiess, *J. Phys. Chem.* B, **2002**, 106, 9322-9334.

[17] R. Graf, D. E. Demco, S. Hafner, H. W. Spiess, *Solid State Nucl. Magn. Reson.*, **1998**, 12, 139-152.

[18] R. Graf, A. Heuer, H. W. Spiess, *Phys. Rev. Lett.*, **1998**, 80, 5738-5741.

[19] W. S. Price, P. W. Kuchel, B. A. Cornell, *Biophys. Chem.*, **1989**, 33, 205-215.

[20] W. S. Price, *Concepts in Magnetic Resonance*, **1998**, 9, 299-336.

[21] W. S. Price, B. C. Perng, C. L. Tsai, L. P. Hwang, *Biophys. J.*, **1992**, 61, 621-630.

[22] W. S. Price, *Concepts in Magnetic Resonance*, **1998**, 10(4), 197-237.

[23] P. G. Bruce, Solid State Electrochemistry, Cambridge University Press, **2003.**

[24] J. P. Diard, B. L. Gorrec, C. Montella, P. Landaud, *Electrochimica Acta*, **1997**, 42(23-24), 3417-3420.

[25] V. G. Kumar, N. Munichandraiah, A. K. Shukla, *J. Power Sources*, **1996**, 63(2), 203-208.

[26] N. Wagner, *J. Appl. Electrochem.*, **2002**, 32, 859-863.

[27] J. J. Fontannella, M. G. Mclin, M. C. Wintersgill, J. P. Calame, S. G. Greenbaum, *Solid State Ionics*, **1993**, 66, 1-4.

[28] N. Etteyeb, L. Dhouibi, H. Takenouti, M. C. Alonso, E. Triki, *Electrochimica Acta*, **2007**, 52(27), 7506-7512.

[29] S. Y. Sayed, M. S. Ei-Deab, B. E. EI-Anadouli, B. G. Ateya, *J. Phys. Chem.* B, **2003**, 107(23), 5575-5585.

[30] J. R. Macdonald, *Impedance Spectroscopy: Theory, Experiment, and Applications*, Second Edition, John Wiley & Sons, Inc., New Jersey, **2005.**

[31] C. H. Lee, H. B. Park, Y. M. Lee, R. D. Lee, *Ind. Eng. Chem. Res.*, **2005**, 44, 7617-7626.

[32] B. D. Cahan, J. S. Wainright, *J. Electrochem. Soc.*, **1993**, 140(12), L185-L186.

[33] J. J. Sumner, S. E. Creager, J. J. Ma, D. D. DesMarteau, *J. Electrochem. Soc.*,

1998, 145(1), 107-110.

[34] Y. Sone, P. Ekdunge, D. Simonsson, *J. Electrochem. Soc.*, **1996**, 143(4), 1254-1259.

[35] J. Halim, F. N. Buchi, O. Haas, M. Stamm, G. G. Scherer, *Electrochimica Acta*, **1994**, 39, 1303-1307.

[36] B. E. Conway, J. O'M. Bockris, H. Linton, *J. Chem. Phys.*, **1956**, 24, 834.

[37] N. Agmon, *Chem. Phys. Lett.*, **1995**, 244, 456-462.

[38] K. D. Kreuer, A. Rabenau, W. Weppner, *Angew. Chem. Int. Ed. Engl.*, **1982**, 21, 208-209.

[39] P. Choi, N. H. Jalani, R. Datta, *J. Electrochem. Soc.*, **2005**, 152(3), E123-E130.

[40] K. D. Kreuer, *J. Membr. Sci.*, **2001**, 185, 29-39.

Chapter 3

A Comparative Study of Nafion and S-PEEK Using Solid State NMR

This chapter has been published on *Macromolecules* (**2006**, 39, 3283-3290). The co-authors are N. Janzen and G. R. Goward. The manuscript was initially prepared by me. Then it was revised by me and G. R. Goward for submission. My contribution to this paper includes: the sample preparations and the NMR experiments for both Nafion® and S-PEEKs, and a proposed model to understand the difference of proton dynamics of Nafion and S-PEEK in different hydrating states. In this chapter, the solid state NMR studies on Nafion and S-PEEKs demonstrated proton exchange between sulfonic acid groups and water within these samples. Variable temperature experiments were used to determine the activation energy for proton transport in pure Nafion, found to be 11.0 kJ/mol, which is lower than those determined for S-PEEKs with different degrees of sulfonation. Increasing proton exchange rates with increasing temperature indicate the expected dependence of proton mobility on temperature. A rotor-synchronized homonuclear double quantum filter sequence (BaBa) was used to disclose the nature of the H-bonding interactions in the two polymers, from which a model of the proton interactions in the polymers is developed.

3.1 Introduction

Proton exchange membrane fuel cells (PEMFCs) are promising new power sources for both portable and stationary applications, ranging from portable electronics and vehicles to industries and residences. [1] Membranes currently used in PEMFCs are sulfonated perfluorinated polymers such as Nafion (shown in Figure 1-2) designed by Dupont or Nafion-like polymers supplied by Dow. [2] These membranes have good proton conductivity and long-term stability. However, the high cost of perfluorinated polymers limits the large-scale commercialization of PEMFCs. Another drawback for these membranes is methanol cross-over which occurs when they are used in direct methanol fuel cells (DMFC). [3] This leads to a decreased fuel cell performance due to depolarization of the oxygen reducing cathode. [4] The problem caused by methanol crossover can be relieved to some extent by doping with various inorganic fillers. [5, 6] Dopants such as silica and zirconium phosphate (ZrP) that have surface hydroxyl groups, are preferred since these groups are assumed to retain water even at temperatures higher than 100 °C. Data on the interactions between Nafion acid protons and protons of hydroxyl group of dopants is elusive, and yet important to understand the performance of these composites. Such data can be provided by solid-state NMR studies.

Sulfonated aromatic polyether ether ketones (shown in Figure 1-6) have been studied as an alternative to Nafion due to the good mechanical properties, thermal stability and conductivity exhibited by this polymer. [4, 7, 8] These properties have been shown to depend on the degree of sulfonation of the polymer. Although a high degree of sulfonation (DS) degrades the mechanical properties of humidified S-PEEK, it does give improved proton conductivity under high relative humidity (RH) conditions. This is a typical juxtaposition of polymer electrolyte membranes: good conductivity is achieved at the expense of structural integrity. Such problems motivate the efforts to understand the molecular-level processes at work in the proton transport mechanism and thereby contribute to the development of new materials.

Many studies on these proton-conducting materials have been carried out by impedance spectroscopy measurements, [9, 10, 11] which provide standard proton conductivity data. Such studies probe proton mobility indirectly, through a measurement of a bulk property of the material. Small angle X-ray scattering (SAXS) [12, 13] and small angle neutron scattering (SANS) [14] have been used to obtain details on the structures of membranes, however dynamic information about proton mobility is not available from these methods.

Solid-state NMR can provide useful information concerning proton mobility of conducting polymers on the molecular level [15, 16] because it is able to probe local chemical environments. Such information is helpful to give a fundamental understanding of the observed differences in proton conductivity. For a powder sample, the ^{1}H NMR spectrum exhibits noticeably broadened peaks due to the random orientation of molecules and very strong ^{1}H-^{1}H homonuclear dipolar coupling in a rigid polymer. Fast magic angle spinning (MAS) is used to average the dipolar couplings on the timescale of the rotor period and thereby achieve significant line narrowing. Since the strength of dipolar interactions can be used to determine the relative mobility of protons, methods which can selectively retrieve information about the dipolar interaction removed by MAS are desirable. Double quantum filtering (DQF) pulse sequences, such as Back-to-Back (BaBa) [17, 18] allows us to recouple the dipolar couplings between protons which are rigid on the timescale of the pulse sequence, and which are close to each other in space. As shown by equation (2-8) in chapter 2, the dipolar coupling is very sensitive to both the distance between nuclei and the motion of nuclei. Thus, the observation of a weak dipolar coupling will be due to either fast tumbling of molecules (termed the residual dipolar coupling) or a long distance between nuclei. The BaBa sequence is used here to detect proton interactions, and gauge their relative mobilities. The intensity of the double quantum coherence (DQC) depends on the product of coupling strength and the excitation time, meaning DQCs based on strong dipolar coupling will be efficiently excited in a short recoupling time. Mobile protons which generate weak or no dipolar coupling will be absent from the DQF MAS NMR spectrum due to inefficient excitation of the DQC. Hence we can ascertain the relative mobilities of protons by comparing ^{1}H MAS NMR with ^{1}H DQF MAS NMR. By extending the length of the recoupling (excitation) time, the DQF sequence can be used to detect weak dipolar couplings which are partially dynamically averaged by local mobility, or where the dipolar coupling occurs over a long distance. [17]

In this chapter, proton mobility in Nafion, Nafion composites and S-PEEK with different degrees of sulfonation was investigated. Several samples exposed to different relative humidity were used to understand proton interactions between water and sulfonic acid groups. Homonuclear DQF experiments are performed to distinguish strong dipolar couplings from weak ones. The differences in proton mobility are compared and discussed.

3.2 Experimental

3.2.1 Preparation of S-PEEK

S-PEEKs with different degrees of sulfonation were prepared as follows: 20 g of commercial PEEK (Victrec Company) was dissolved in 300 ml of 98% H_2SO_4 at room temperature. In intervals of tens of hours, samples were taken periodically from the previous mixture and added to ice water under strong agitation. To remove any residual acid, the polymer precipitate was washed until a constant pH was obtained. After that, it was dried first at room temperature for two days and then at 343K for a few days. Finally, polymer beads of 1-2 mm diameter were obtained; the color of the beads varied with the DS. The DS of S-PEEK was determined using solution NMR. For these studies, samples of S-PEEK were dissolved in DMSO-d_6. For solid-state NMR measurements, powder samples are preferred to facilitate rotor spinning. Powders were prepared by grinding previously dried S-PEEK in liquid nitrogen. Afterwards the powder samples were treated at 353K in an oven for dried samples. The humidified samples were prepared by storing S-PEEK in a humidity chamber (model 9000, VWR) at 323K for 24 hrs. The RH of the chamber was set at 50% or 100% to control the amount of water in hydrated S-PEEK.

3.2.2 Preparation of Nafion composites

Treatment of Nafion112 was performed in two ways. Method I: Nafion112 was first washed in 1M NaOH for 1 hour and then in distilled deionized water for another hour, during which time the water was refreshed four times. Subsequently, the membrane was again washed in 1M HCl for 1 hour. Finally, it was washed in distilled deionized water until a constant pH was obtained. Method II: Nafion112 was first washed in 3% H_2O_2 for 1 hour and then in distilled deionized water for another hour, again changing the water four times. Subsequently, it was washed in 1M H_2SO_4 for 1 hour. Finally, it was washed in distilled deionized water until a constant pH was obtained. The dried Nafion samples were prepared by drying the treated Nafion membranes at 353 K from 2 days to 1 week.

Nafion/SiO_2 composite membranes were prepared according to the procedure reported by Deng. [19] Nafion treated by Method I was first swollen in MetOH: H2O (V/V) = 5:1 for 24 hours. It was then immersed in TEOS: H_2O (mol/mol) = 1:1 for 9 min to allow permeation of TEOS into Nafion. After that, it was dried at 353K overnight to remove the excess methanol. The polymerization of TEOS to silica is an acid catalyzed process. Since the sulfonic acid groups within Nafion are the only source of acid, it is assumed that the silica is formed within the Nafion membrane. Nafion/ZrP composite membranes were prepared following the procedure reported by Costamagna. [20] Nafion treated by Method II was first swollen in boiling MetOH: H_2O (V/V) = 1:1 for 2~3 hours. Subsequently the material was washed in 1M zirconyl chloride solution at 353K for 1 hour. In order to remove excess zirconyl chloride, it was quickly rinsed in distilled deionized water and then put in 1M H_3PO_4 at 353K overnight. Finally, it was washed in distilled deionized water and dried at 353K overnight.

3.2.3 ^{1}H NMR

^{1}H solution NMR experiments were carried out on a Bruker AV 200 spectrometer at a ^{1}H Larmor frequency of 200.13 MHz. The 3% S-PEEK solution was prepared by dissolving beads of S-PEEKs in DMSO-d_6. Tetramethylsilane (TMS) was added as the internal standard. NMR data were acquired with a 90° pulse length of 6.35 μs at room temperature.

^{1}H solid-state NMR experiments were performed on a Bruker AV 500 spectrometer at a ^{1}H Larmor frequency of 500.13 MHz. Rotor diameters of 4 mm and 2.5 mm rotors were used for Nafion samples and S-PEEK samples, respectively. The former rotor was spun at 5 or 10 kHz and the latter at 25 kHz. In both cases a recycle delay of 3 s was used. The spectra are referenced to adamantane (1.63 ppm for ^{1}H). Solid-state ^{1}H NMR spectra were acquired with a 90° pulse length of 2.5 μs. Variable temperature experiments were performed in the range of 300-360K, with the sample temperature corrected to include heating effect arising from the high-speed MAS. [21] The ^{1}H linewidth as a function of temperature reflects changes of spin-spin relaxation time (T_2) with temperature, which is used to fit the activation energy for proton transport in this work. Due to inhomogeneity of an applied magnetic field B_0, the effective T_2 is denoted as T_2^* in terms of the observed line width. [22] Since the chemical shift of sulfonic acid proton, which is humidity sensitive, does not show any noticeable shift within 2 days once samples were put in the rotor, this suggests that the humidity of samples in the rotor does not change during that time. Thus the humidification of the samples is maintained during measurement. The rotor-synchronized DQF MAS spectra were recorded by using the Back-to-Back (BaBa) pulse sequence, with variable excitation times, τ_{exc}, from τ_r to $8\tau_r$ and 512 scans. [23]

The decomposition of S-PEEK ^1H MAS NMR spectra is performed by both Bruker Topspin 1.2 and MestRe-C software to determine linewidth of sulfonic acid proton and aromatic proton resonances. Error bars of E_a within 1% were determined by comparing the goodness of fit from the two routines. Since the difference in activation energies determined for different samples, prepared at different times, is less than 4%, this is taken as the error bar for each measurement.

3.3 Results and discussion

3.3.1 Determining the degree of sulfonation

Two examples of ^1H NMR spectra of S-PEEK samples dissolved in DMSO-d_6 are shown in Figure 3-1. The DS can be determined quantitatively by ^1H NMR. [24] The presence of the sulfonic acid group increases the deshielding effect for proton H_A in Figure 3-2, causing the H_A resonance to move to a higher chemical shift compared with proton H_B and H_C. Therefore, a distinct signal for H_A can be observed from NMR spectra. The ^1H NMR signal for the sulfonic acid group cannot be recorded directly since the sulfonic acid proton is highly mobile. Nevertheless, the number of the H_A is exactly equal to that of the sulfonic acid protons. Thus, if the degree of sulfonation (DS) is defined as a ratio of sulfonated units to total units, the DS can be calculated as follows: [24]

$$\mathrm{DS} = \frac{\mathrm{Area}_{\mathrm{H_A}}}{[\mathrm{Area}_{\mathrm{H_{B,B',C,C',D,D',E,E'}}} + 2 * \mathrm{Area}_{\mathrm{H_A}}]/12} \tag{3-1}$$

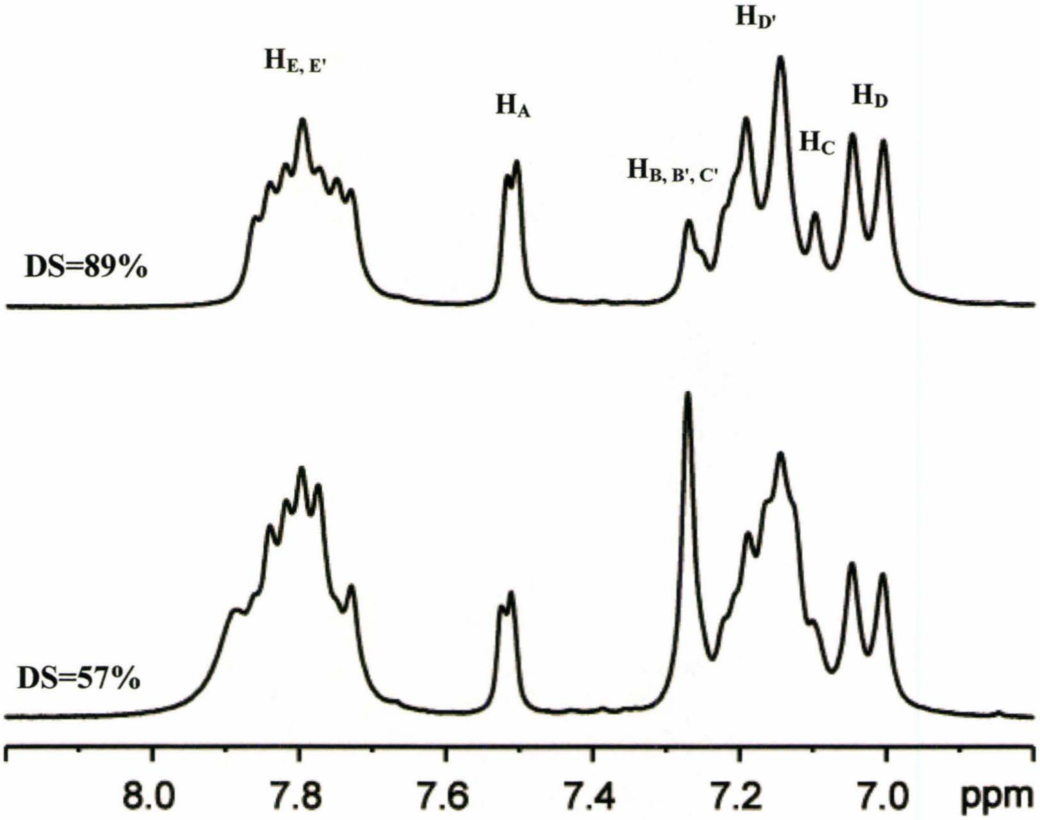

Figure 3-1. Solution-state ^{1}H NMR spectra of sulfonated PEEK (S-PEEK)

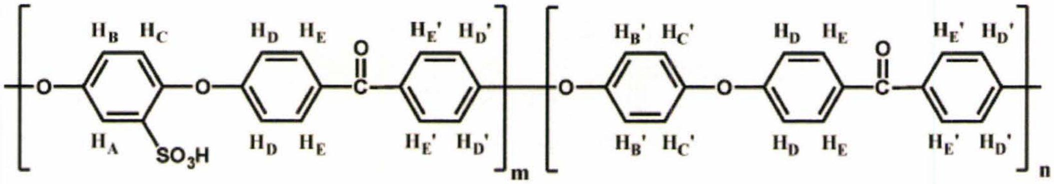

Figure 3-2. Structure of S-PEEK

The DS calculated from the ^{1}H NMR spectra of seven S-PEEK samples is plotted in Figure 3-3. In our experiments, when the sulfonation time increases from 70 hours to 336 hours, the DS changes from 51% to 89%. Due to differences in experimental conditions, such as the concentration of PEEK in H_2SO_4 and the reaction temperature, Huang reported S-PEEK with higher DS but shorter sulfonation time. [25]

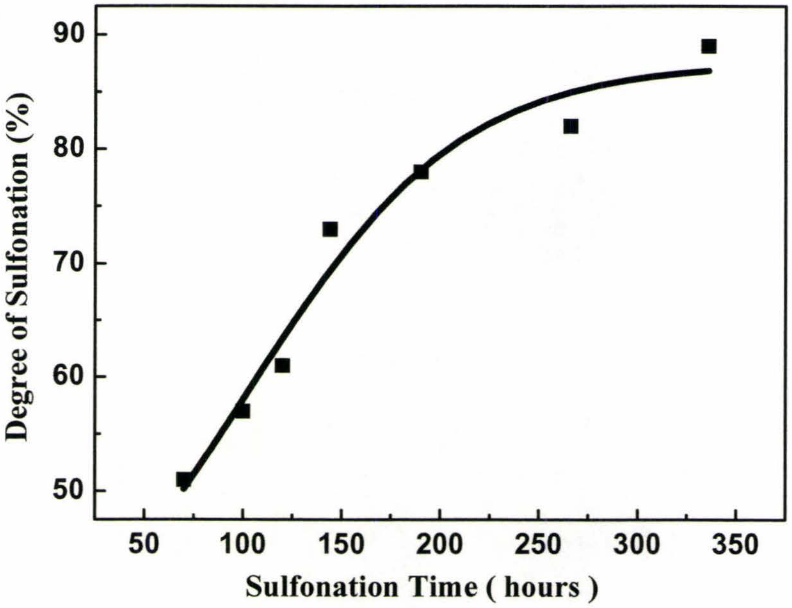

Figure 3-3. DS of S-PEEK as a function of sulfonation time. The curve is included as guide for the eye

3.3.2 Proton exchange between water and sulfonic acid group

Figure 3-4 shows a series of ^{1}H MAS NMR spectra of Nafion treated under different conditions. After Nafion was fully acidified and heated, the broad peak at 9.7 ppm in Figure 3-4(c) indicates that the only protons remaining are from the sulfonic acid group and they are immobile. When the sulfonic acid protons were replaced with

Na^+ in Nafion treated with NaOH (aq), a narrow peak at 4.2 ppm, similar to the chemical shift of pure water, is observed in Figure 3-4(a). [26] Based on these two assignments, it follows that the narrow resonance at 6.7 ppm observed for the fully acidified and hydrated Nafion membrane in Figure 3-4(b) likely represents fast proton exchange between water and the sulfonic acid group. Similar fast proton exchange has been also reported by C.A.Fyfe [27] and J.Fraissard. [28]

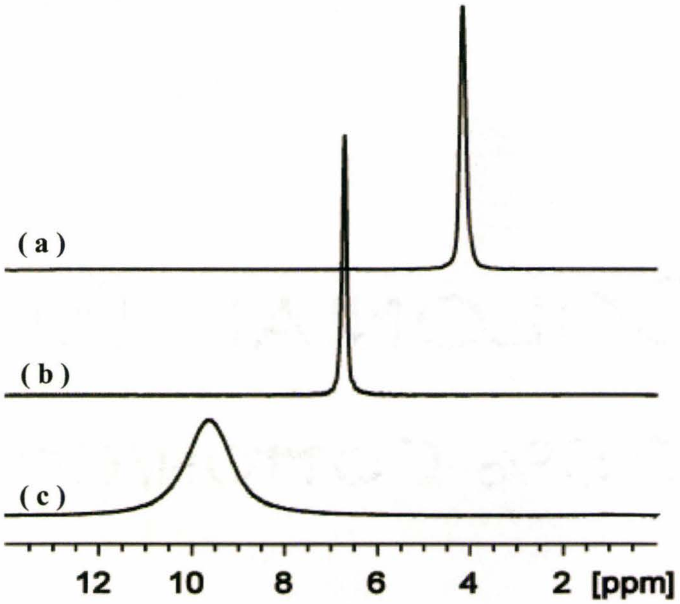

Figure 3-4. ^1H MAS NMR spectrum at 5kHz for Nafion 112 treated by (a) $NaOH_{(aq)}$; (b) fully acidified and hydrated; (c) fully acidified and dried at 80 °C for 12hr

Figure 3-5 shows a series of ^1H MAS NMR spectra for PEEK and S-PEEK powders treated under differing relative humidity conditions. PEEK itself in Figure 3-5(a) shows a single, broad aromatic resonance. Dried S-PEEK in Figure 3-5(b) gave a broad resonance (393 Hz) for the acidic protons at 7.6 ppm. After it was treated in RH equal to 50% for 24 hrs, the water content was slightly increased which shifted this resonance to 7.4 ppm in Figure 3-5(c). The line width narrowed slightly to 372 Hz. In figure 3-5(d), when a higher RH equal to 100% was applied for an equivalent time, a further increase in water content shifted the resonance to 5.9 ppm accompanied by line narrowing to 261 Hz. Compared with the small fluctuation of line width of aromatic proton less than 3 %, the significant decrease in the line width of the sulfonic acid proton indicates increasing proton mobility resulting from rapid proton exchange with water molecules, and thus indicates a mechanism for proton diffusion that occurs independent of polymer backbone dynamics.

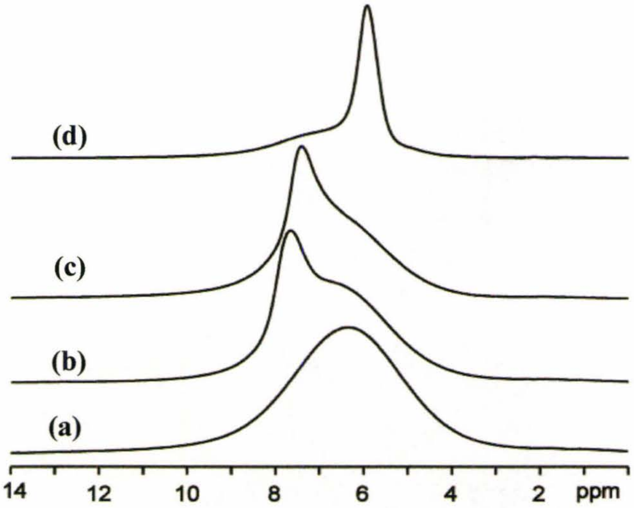

Figure 3-5. ^{1}H MAS NMR spectra at 25 kHz for PEEK and S-PEEK (DS=57%) (a) PEEK (b) dried S-PEEK (c) S-PEEK (24 hrs in RH=50%) (d) S-PEEK (24 hrs in RH=100%)

Careful comparisons of the ^{1}H solution-state NMR spectra and ^{1}H solid-state NMR spectra allow us to deduce not only the degree of sulfonation, but also the amount of water associated in the membranes. The acidic proton resonance in the solid-state spectra is consistently larger than what should be attributed to the sulfonic acid proton alone at a given degree of sulfonation. Therefore, the excess proton intensity is assigned to trapped water molecules, and is seen to increase as expected, as a function of humidification. Accurate spectral decomposition is essential to both this analysis, and the previous observations regarding the aromatic polymer backbone. Therefore, an example of spectrum decomposition is presented in Figure 3-6, showing the two resonances, their sum, and the minimal residual signal observed following subtraction of the fitted and experimental data.

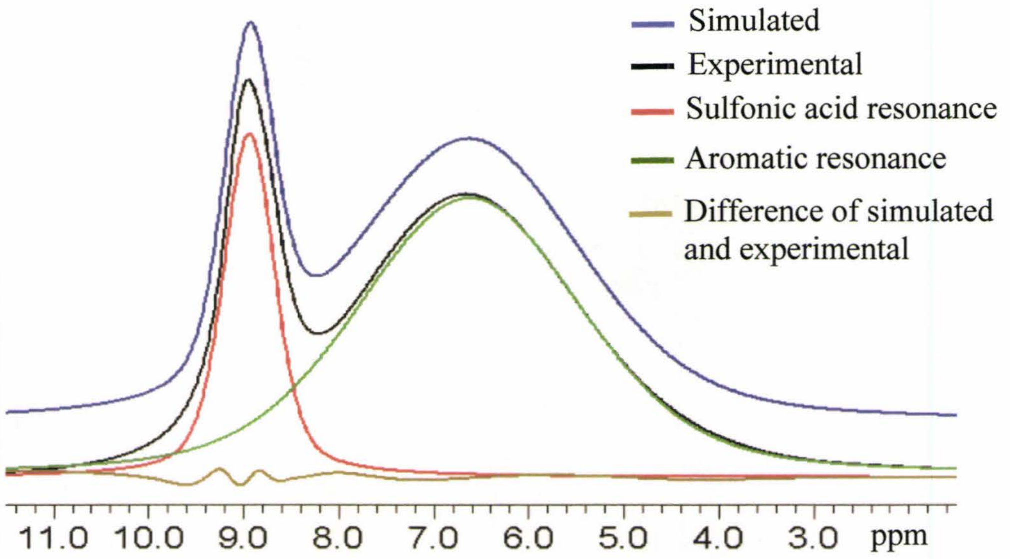

Figure 3-6. Decomposition of ^1H MAS NMR of dried S-PEEK (DS=73%) Top: simulated spectrum using NMR software MestRe-C. Below top: experimental spectrum. Bottom: difference between the simulated and the experimental. Broad single peak: aromatic proton. Narrow single peak: sulfonic acid proton

3.3.3 Activation energy for proton transport in Nafion and S-PEEK

Figure 3-7(a) shows the dependence of the proton chemical shift on temperature for a dried Nafion sample. As the temperature increases, the effective hydrogen bond strength of the sulfonic acid protons becomes weaker. This moves the chemical shift toward lower frequency. As well, higher temperature leads to a faster proton exchange rate between the sulfonic acid group and surrounding water molecules, and causes the resonance to narrow. The same trend was found for the Nafion composites of Nafion/SiO_2 in Figure 3-7(b) and Nafion/ZrP in Figure 3-7(c).

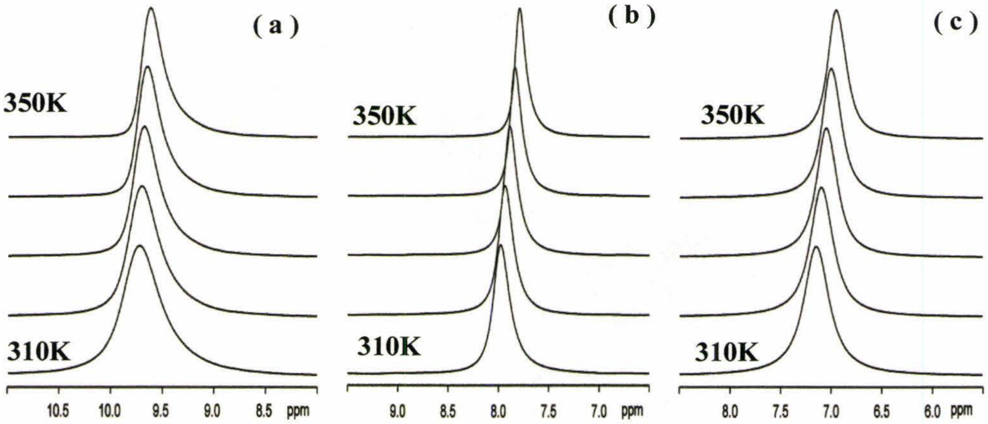

Figure 3-7. ^1H MAS NMR spectra at 5kHz for (a) dried Nafion (b) dried Nafion/SiO_2 (c) dried Nafion/ZrP

In the case of Nafion/SiO_2, there are strong hydrogen bonding sites available which may trap extra water molecules in the composite. These hydrogen bonds take the form of Si – OH groups located on the surfaces of silicon oxide nanoparticles. [29, 30] It was reported that the physi-sorbed water in silica gels, such as water molecules bound to Si – OH groups, starts to be driven off and surface silanol groups condense at around 443K. [31] Since our composite was treated at 353K, water molecules bound to surface Si–OH groups will remain. The single peak shown in Fig 3-7(b) is the resonance of sulfonic acid proton exchanging with water adsorbed on silica surface. [32]

The chemical shift of this resonance is lower than that of pure Nafion treated under equivalent conditions.

In the case of Nafion/ZrP, the inorganic component, zirconium phosphate, is a well-known proton conductor. [33] In this layered compound, the acid P-OH groups belonging to adjacent layers remain close to each other, and allow proton transport in the interlayer region even under anhydrous conditions. It has been demonstrated that Nafion/ZrP membranes can reabsorb water at 403 K from the vapor phase that was lost at 413 K. [21] This indicates that zirconium phosphate in the nanopores of the Nafion can reduce the rate of evaporation of water in Nafion. Thus, after our sample was treated at a lower temperature of 353 K, it is probable that there are still water molecules left in the membrane which move the sulfonic acid ^{1}H resonance to lower chemical shift relative to Nafion treated under equivalent conditions. It has also been confirmed by the thermo-gravimetric analysis (TGA) (not shown here) that the ZrP-Nafion composite has a higher water content per sulfonic acid group than pure Nafion.

Not surprisingly, S-PEEKs with different degrees of sulfonation in Figure 3-8 also showed dependence of both proton chemical shifts and line widths on temperature, consistent with the weakening relative strength of hydrogen bonding with increasing temperature. More interestingly, the amount of water retained in S-PEEK increases with increasing degrees of sulfonation. This is seen both in the decreasing linewidth with increasing DS shown in the Figure 3-8(a) and Figure 3-8(b) and by comparing the integrated acidic proton intensities in these materials. Compared with the linewidth of the sulfonic acid proton resonance (344 Hz at 310K) of S-PEEK

(DS=61%) in Figure 3-8(a), a narrower line width of the sulfonic acid proton resonance (256 Hz at 310K) for S-PEEK (DS=73%) in Figure 3-8(b) indicates that the sulfonic acid protons in the latter are more mobile than those in the former. The ratio of the number of water molecules per sulfonic acid proton, denoted as nH_2O/SO_3H, in both dried and hydrated S-PEEKs can be estimated from peak areas of the sulfonic acid proton peak and aromatic proton peak of solid state ^1H NMR of S-PEEKs, by comparison with the degree of sulfonation established by ^1H solution-state NMR studies above. The obtained nH_2O / SO_3H values for dried and hydrated S-PEEKs are presented in Table 3-1. It is important to note that as the DS of the polymer increases, the amount of associated water retained in the membrane will increase proportionally. Therefore, higher proton mobility would be expected from humidified S-PEEK with higher DS, consistent with the trend of macroscopic proton conductivity that higher DS gives better proton conductivity. [34, 35]

Table 3-1. Activation energy of proton transport for S-PEEK with variable DS

S-PEEKs with variable DS		DS=61%	DS=73%	DS=82%
Dried samples	E_a (kJ/mol)	20.1±0.8	20.8±0.8	27.3±1.1
	nH_2O / SO_3H	1.7±0.1	1.6±0.1	1.9±0.1
Hydrated samples	E_a (kJ/mol)	18.3±0.7	13.9±0.6	12.8±0.5
	nH_2O / SO_3H	2.6±0.1	2.6±0.1	2.8±0.1

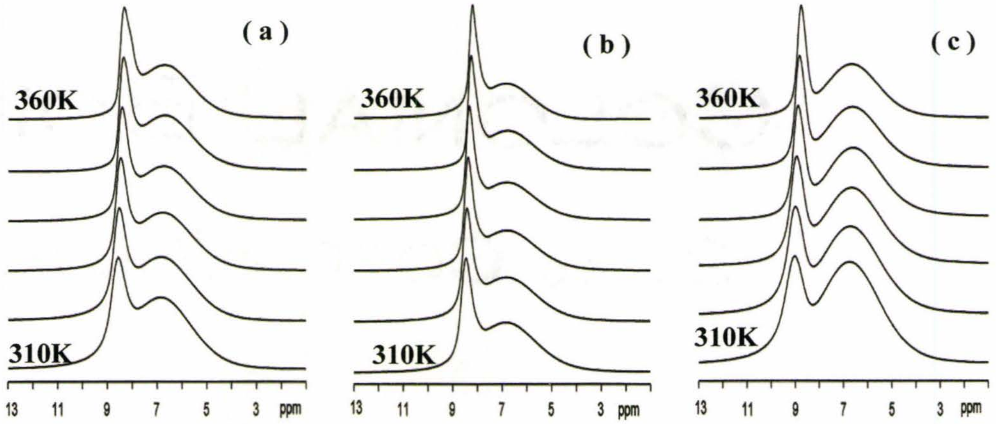

Figure 3-8. ^1H MAS NMR spectra at 25kHz for (a) humidified S-PEEK(DS=61%) (b) humidified S-PEEK(DS=73%) (c) dried S-PEEK(DS=73%)

The influence of polymer backbone motion on the sulfonic acid proton dynamics has also been considered. Since the aromatic proton resonance always shows an invariable line width for S-PEEKs with variable DS treated under different relative humidity, which is 1480 ± 40 Hz, this implies that the motions of polymer chain for measured S-PEEK samples do not change with DS and relative humidity. Thus, in this study the contribution of polymer chain motion to proton mobility can be ignored, compared with that of motion of sulfonic acid protons. A more accurate measurement of polymer chain motion can be performed by examining the influence of dynamics on the ^{13}C chemical shielding anisotropies. [36] However, in the case of S-PEEK, the ^{13}C spectrum shown in Figure 3-9 is not well resolved, which does not allow one to get the information of carbon dynamics by spin-lattice relaxation time in the rotation frame ($T_1\rho$), or center-band only detection of exchange (CODEX). [36]

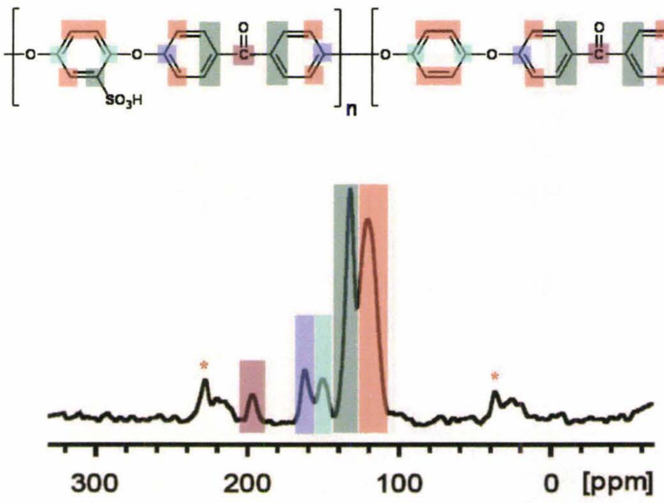

Figure 3-9. ^{13}C-^{1}H CPMAS spectrum of S-PEEK (DS=72%), MAS=12 kHz. The assignment of the spectrum is shown by the colored bars. The * indicates side bands.

The line width trends of the acidic protons can be analyzed using the Arrhenius equation. As shown in equation (3-2), the change in line width is proportional to the inverse of T_2^*, the spin-spin relaxation time. Equation (3-3) shows how activation energy can be obtained from line width, [37] where E_a is the activation energy for proton transport and τ_c is the correlation time of the motion.

$$\Delta\nu_{FWHM} = \frac{1}{\pi T_2^*} \tag{3-2}$$

$$\frac{1}{T_2^*} \approx \tau_c = \tau_\infty \exp(\frac{E_a}{RT}) \tag{3-3}$$

Figure 3-10 shows an example of an Arrhenius plot for dried S-PEEK (DS=73%). Activation energies for S-PEEKs with variable DS treated under different relative humidity are shown in Table 3-1. Those for Nafion and its composites are presented in Table 3-2.

In Table 3-2 the activation energy for hydrated pure Nafion obtained by NMR (11.0 kJ/mol) correlates very well with the macroscopic conductivity measurements (9.34 kJ/mol). [21] The dried pure Nafion shows an activation energy higher than hydrated Nafion, due to the significantly lower water content of the dried Nafion membrane. This is consistent with the presumed vehicle mechanism of proton transport in Nafion and its composites. As the number of water molecules or "vehicles" is reduced, the activation energy for proton transport increases steeply. Analogously, the connectivity of the hydrogen bonding network is reduced in the dried sample: as the domains become isolated, the probability of structural proton transport is also reduced.

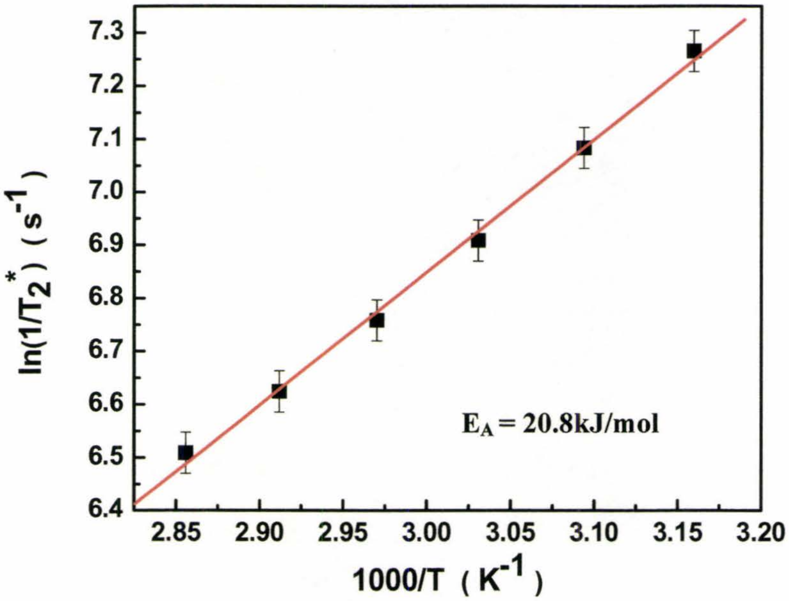

Figure 3- 10. Activation energy for proton mobility in dried S-PEEK (DS=73%) by linear fitting to the Arrhenius equation

Table 3-2. Activation energy of proton transport for Nafion and Nafion composites

Nafion and composites	Nafion (hydrated)	Nafion (dried)	Nafion/SiO_2 (dried)	Nafion/ZrP (dried)
E_a (kJ/mol)	11.0±0.4	16.4±0.7	12.2±0.5	10.3±0.4

Compared with dried pure Nafion, both dried Nafion/SiO_2 and dried Nafion/ZrP give lower activation energies for proton hopping. This is attributed to the greater number of water molecules retained in the Nafion composites, which help to enhance mobility of the sulfonic acid protons. It is important to emphasize again that these activation energies arise from NMR measurements of proton dynamics, and as such, are extremely local, molecular probes of proton mobility. This is in contrast with impedance measurements, which give macroscopic pictures, but lack molecular-level detail. Both composites show significantly reduced activation energies for proton hopping relative to pure, dried Nafion. This indicates that at the molecular level, the inorganic fillers are playing their intended roles; providing excess mobile protons to the hydrogen bonding network. Moreover, the enhancement is more substantial for Nafion/ZrP than for Nafion/SiO_2, suggesting that ZrP, a known proton conductor, contributes to proton mobility of Nafion/ZrP. This synergistic contribution of the inorganic 'filler' was part of the motivation for choosing this composite. [38]

In comparing S-PEEKs with different degrees of sulfonation, higher activation energies were determined for dried S-PEEK with higher DS in Table 3-1. As expected, the hydrated samples show decreased activation energy with increasing degree of sulfonation. To our knowledge, activation energies for pure S-PEEKs are not reported in the literature. For comparison, the activation energy determined by impedance measurements for fully hydrated composites of S-PEEK (DS=70%) is roughly 15 kJ/mol, [4] which is comparable to our results.

To compare activation energies of S-PEEKs, the residual water in these samples has to be considered. As seen in Nafion, the observed chemical shift of the sulfonic acid proton is influenced by the exchange with residual water molecules. In dried S-PEEK, the low value of nH_2O / SO_3H decreases mobility of sulfonic acid proton due to the stronger hydrogen bonding. Therefore, within the same domain size of polymer, the greater number of sulfonic acid groups in polymers with higher DS will limit proton mobility and increase the activation energy for proton transport in dried samples.

S-PEEK samples listed in Table 3-1 were hydrated at RH=50% for 24hrs, causing a slight increase in the water content of these materials. In these slightly hydrated S-PEEKs, although the value of nH_2O / SO_3H does not increase much, the number of water molecules within the same domain size of polymer will increase drastically as the degree of sulfonation increases. This facilitates the water molecules exchange among sulfonic acid groups by providing an increasingly continuous network for proton conductivity, and allowing Grotthus mechanism diffusion.

A comparison of dried Nafion with dried S-PEEKs indicates an obvious difference of proton mobility when their water content is low. This is consistent with results reported by Alberti where it is stated that Nafion is the best proton conductor at low relative humidity and differences of proton conductivity become smaller and vanish when the relative humidity is close to 100%. [33, 34]

3.3.4 Detection of immobile protons in Nafion and S-PEEK

DQF MAS NMR spectra differ from normal MAS NMR spectra in that resonances are only observed for protons having strong dipolar couplings. Thus, peaks which disappear from the DQF MAS NMR spectrum can be correlated with protons with very weak dipolar coupling. Weak or residual dipolar couplings may still be detected by extending the recoupling time for efficient excitation of double quantum coherence. In Figure 3-11(a) the resonance corresponding to protons of sulfonic acid group and associated water molecules in dried Nafion shows a strong dipolar coupling, detected most intensely when the recoupling time is short (τ_r), and decaying as the recoupling time is extended, as expected for strongly coupled spins. [17] The estimated nH_2O / SO_3H for this sample is about 1.5 ± 0.1, based on comparisons with literature values. [28] In Nafion, the flexible side chains can reorient to shorten the distance between sulfonic acid groups. Thus, strong dipolar couplings are detected for sulfonic acid proton of rigorously dried Nafion, and are attributed to strongly H-bonded acid-H_2O complexes. In Figure 3-11(b) the proton resonance in a less-rigorously dried Nafion is not observed at short recoupling times. The appearance of this peak at recoupling times of $4\tau_r$ and longer indicates that the residual dipolar coupling among these protons is nevertheless strong enough to be detected in the membrane. This is indicative of increasing proton mobility in the membrane. The nH_2O/SO_3H in this sample is estimated to be 2.0 ± 0.1 based on our TGA studies, and is consistent with values in the literature. [28] As expected, humidified Nafion did not exhibit peaks attributable to dipolar coupled protons in DQF MAS NMR spectrum even when the recoupling time was extended up to $8\tau_r$. The particularly weak dipolar coupling suggests very mobile protons which are attributed to rapid proton exchange between sulfonic acid protons and mobile water molecules. These three stages represent a three points along a continuum of increasing humidification (illustrated in Figure 3-13), corresponding with increasing proton-transport within the hydrogen-bonding network. The connectivity between domains allows for structural, or Grotthus, mechanism diffusion to participate together with vehicular proton transport.

Backbone mobility has been discounted as a significant influence on proton transport in S-PEEK in the temperature ranges considered here. Nevertheless, there are key differences between the polymer backbones in the two polyelectrolytes of interest here. The flexible backbone and long side-chains in Nafion as compared to the rigid aromatic backbone and lack of sidechains in S-PEEK play significant roles in the nature of the hydrogen bonding domains found in the two polymers. For Nafion, the distance between sulfonic acid protons on same polymer backbone or spatially adjacent ones is short, on account of the flexibility of the long side chain.

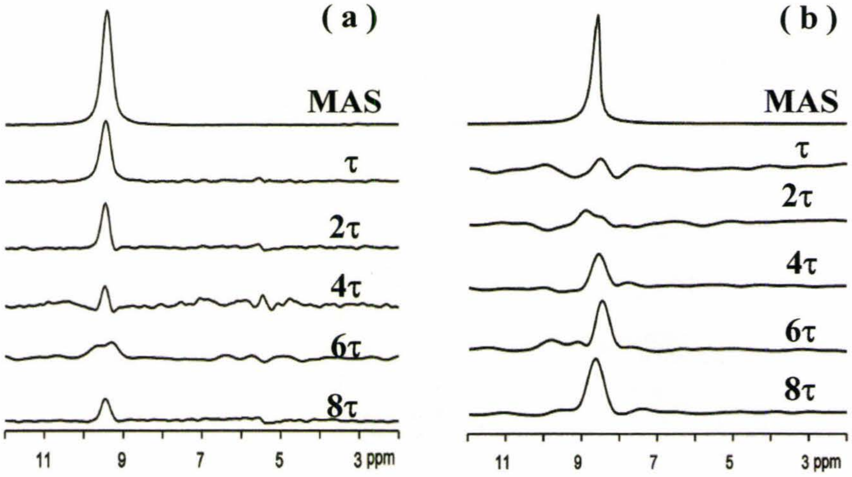

Figure 3-11. ^{1}H DQF MAS NMR of dried Nafion spun at 10kHz, $\tau = 0.1$ms
(a) dried at 353 K for 1 week (b) dried at 353 K for 2 days

Compared with dried Nafion, a clear difference has been observed for dried S-PEEK (DS=73%) as seen in Figure 3-12(a). Namely, there is no observable dipolar coupling among the sulfonic acid protons, even when the recoupling time is extended up to $8\tau_r$. The possibility of close packing between adjacent polymer chains could give short distance between sulfonic acid protons. However, since no coupling was observed in the dried sample, the protons must be either isolated or extremely mobile. Due to absence of long side chain in S-PEEK, proton distance of sulfonic acid groups in dried sample must be long irrespective of whether they are on same polymer backbone or spatially adjacent ones. Thus, the hydronium ions formed by complexing of water molecule and sulfonic acid proton are isolated. The fast rotation of these ions around any of O-H bonds greatly averages the dipolar coupling between protons of hydronium ion, and could explain the weakness of the dipolar coupling in the dried S-PEEK sample. It is important to note that the hydronium ion rotation will not contribute long-range proton transport in the absence of a continuous H-bonding network. After this sample was humidified slightly, the dipolar coupling become strong enough to be detectable when the recoupling time is $8\tau_r$ (Figure 3-12(b)). Since humidification of S-PEEK will increase the mobility of the sulfonic acid group, the dipolar coupling would be intuitively expected to decrease. The observed increase in the coupling strength is attributed to the growth of the hydrogen-bonding network beyond local SO_3H groups and their associated ~2-3 water molecules (Table 3-1), to a more extended, but still strongly H-bonded network. The formation of this network is considered to be essential to long-range proton transport, and continues to grow with increasing humidification. Again, under 100% humidification, no detectable dipolar couplings were observed in the DQF MAS spectra.

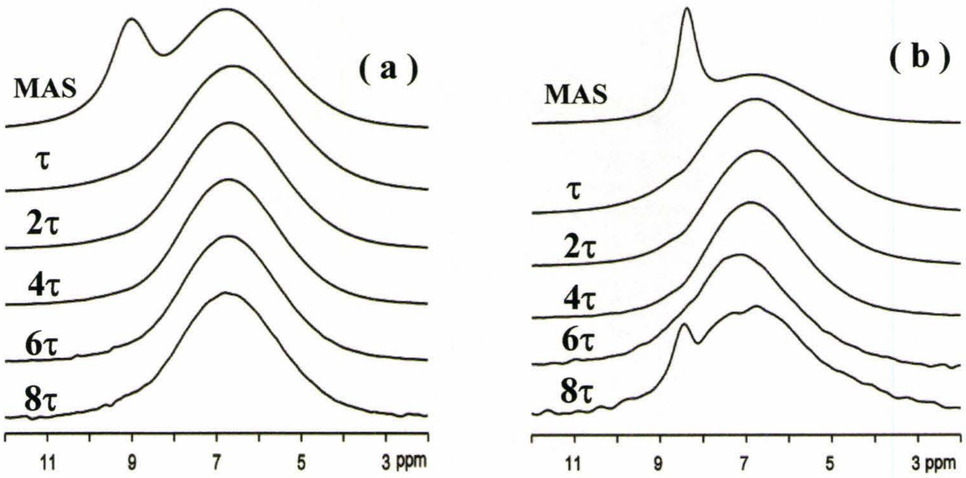

Figure 3-12. ^{1}H DQF MAS NMR of S-PEEK spun at 25kHz, τ = 0.04 ms
(a) dried S-PEEK (DS=73%) (b) humidified S-PEEK(DS=73%)

A model illustrating the hydrogen bonding between sulfonic acid protons and water molecules in Nafion and S-PEEK is shown in Figure 3-13. In Nafion, flexible side chains (blue) allow for close proximity between different sulfonic acid groups (red) and associated water molecules (green). This makes it possible to form a hydrogen bonded network when nH_2O/SO_3H is about 1~2. Higher water content, $nH_2O/SO_3H > 2$, increases proton mobility, which decreases dipolar coupling. In S-PEEK, the sulfonic acid groups (red) are too far apart, due to the lack of sidechains and the relative rigidity of the aromatic backbone (blue). When $nH_2O/SO_3H < 2$, there is no hydrogen bonded network formed, and rotation of hydronium ion (green) averages proton dipolar coupling, which makes it undetectable. When nH_2O/SO_3H is about 2~3, a hydrogen bonded network is formed. In the mean time, the increased water mobility makes the proton dipolar coupling very weak. Thus it is expected that a further increased water content $nH_2O/SO_3H > 3$ causes proton dipolar coupling undetectable due to the high mobility of the water molecules.

The model resulting from this study gives a concise differentiation between the conductivity of Nafion and S-PEEK, based on the responses of these two materials, under varying degrees of humidification, to the DQF pulse sequences. This molecular level understanding of proton conductivity has been lacking in the discussions of membrane candidates, which are more typically characterized exclusively by macroscopic conductivity measurements obtained using impedance spectroscopy.

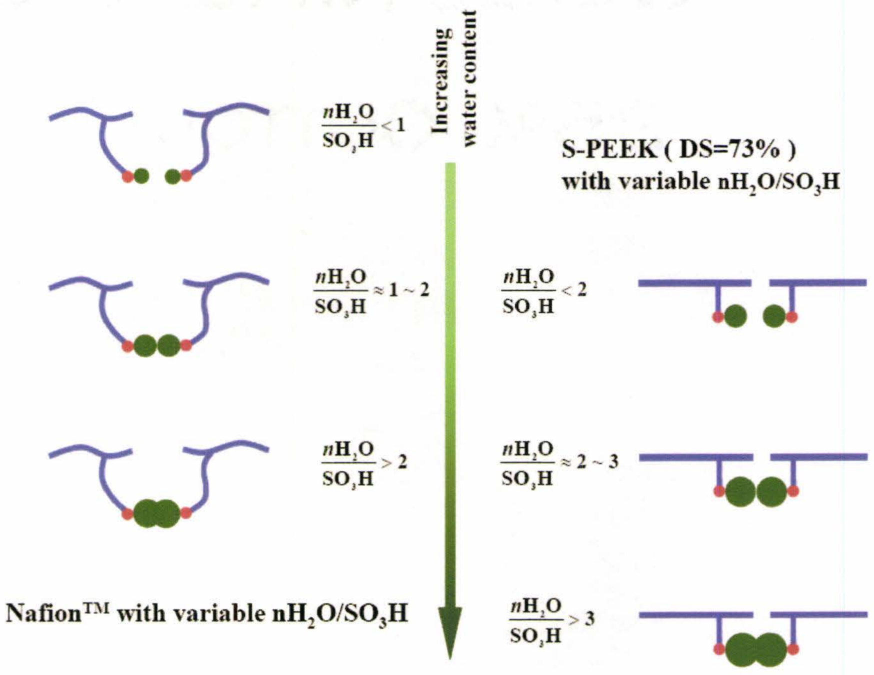

Figure 3-13. A model illustrating the hydrogen bonding between sulfonic acid protons and water molecules in Nafion and S-PEEK. The blue lines, red balls and green balls represent the polymer chains, sulfonic acid protons and water clusters in the polymers, respectively. The figures on the left represent Nafion, with a flexible polymer backbone and sidechains, whereas the figures on the right represent the more rigid S-PEEK polymer, without side-chains. From top to bottom, the relative humidity of the membranes increases, as shown schematically by the increasing size of the acidic proton/water clusters. At the highest relative humidity, these hydrogen-bonded domains overlap, and provide a conduit for long-range proton transport

3.4 Conclusions

Proton exchange between water and sulfonic acid groups has been confirmed by high-resolution solid-state NMR for both Nafion and S-PEEK. The proton mobility depends on not only water content but also temperature. Compared with dried S-PEEK, a lower activation energy for proton transport in dried Nafion suggests that S-

PEEK is a competitive proton conductor under low humidity conditions. The small difference in activation energy between dried pure Nafion and hydrated Nafion/ZrP composites indicates that ZrP is a good candidate to be an additive for Nafion composites. In dried S-PEEK, more sulfonic acid groups due to higher DS result in a greater numbers of hydrogen bonds among sulfonic acid protons, thereby lowering proton mobility. Therefore the activation energy increases with increasing the degree of sulfonation. A model is proposed for the proton-proton contacts in Nafion and S-PEEK, based on their respective ^{1}H-^{1}H dipolar couplings. These data were obtained using a homonuclear double-quantum filtered NMR sequence, which allows the molecular level structure and dynamics to be explored.

3.5 References

[1] L. Carrette, K.A. Friedrich, U. Stimming, *Fuel Cells*, **2001**, 1, 5-39.

[2] K. D. Kreuer, *Chem. Mater.*, **1996**, 8, 610-641.

[3] A. J. Appleby, *Phil. Trans. R. Soc.*, **1996**, 354, 1681.

[4] S. M. J. Zaidi, S. D. Mikhailenko, G. P. Robertson, M. D. Guiver, S. Kaliaguine, *J. Membr. Sci.*, **2000**, 173, 17-34.

[5] P. L. Antonucci, A. S. Arico, P. Creti, E. Ramunni, V. Antonucci, *Solid state Ionics*, **1999**, 125, 431-437.

[6] P. Dimitrova, K. A. Friedrich, B. Vogt, U. Stimming, *J. Electroanal. Chem.*, **2002**, 532, 75-83.

[7] T. Kobayashi, M. Rikukawa, K. Sanui, N. Ogata, *Solid State Ionics*, **1998,** 106, 219-225.

[8] K. D. Kreuer, *J. Membr. Sci.*, **2001,** 185, 29-39.

[9] J. J. Fontanella, M. G. Mclin, M. C. Wintersgill, *Solid State Ionics*, **1993**, 66, 1-4.

[10] J.J.Sumner, S. E. Creager, J. J. Ma,D. D. DesMarteau, *J. Electrochem. Soc.*, **1998**, 145, 107-110.

[11] M. C. Wintersgill, J. J. Fontanella, *Electrochim. Acta*, **1998,** 43, 1533-1538.

[12] G. Gebel, J. Lambard, *Macromolecules*, **1997**, 30, 7914-7920.

[13] G. Gebel, *Polymer*, **2000**, 41, 5829-5838.

[14] J. M. Serpico, S. G. Ehrenberg, J. J. Fontanella, X. Jiao; D. Perahia, K. A. McGrady, E. H.Sanders, G. E. Kellogg, G. E. Wnek, *Macromolecules*, **2002**, 35, 5916-5921.

[15] B. S. Hickman, M. Mascal, J. J. Titman, I. G. Wood, *J. Am. Chem. Soc.*, **1999**, 121,11486-11490.

[16] G. R. Goward, M. F. H. Schuster, D. Sebastiani, I. Schnell, H. W. Spiess, *J. Phys. Chem.* B, **2003**, *106*, 9322-9334.

[17] I. Schnell, H. W. Spiess, *J. Magn. Reson.*, **2001**, 151, 153-227.

[18] S. P. Brown, I. Schnell, J. D. Brand, K. Mullen, H. W. Spiess, J. Mol. Struct, **2000**, 521, 179-195.

[19] Q. Deng, R. B. Moore, K. A. Mauritz, *Chem. Mater.*, **1995**, *7*, 2259-2268

[20] P. Costamagna, C. Yang, A. B. Bocarsly, S. Srinivasan, *Electrochim. Acta*, **2002**, *47*, 1023-1033.

[21] S. R. Benhabbour, R. P. Chapman, G. Scharfenberger, W. H. Meyer, G. R. Goward, *Chem. Mater.*, **2005**, *17*, 1605-1612.

[22] E. D. Becker, *High resolution NMR theory and chemical applications*, 3rd edition, **2000**, p32.

[23] M. Feike, D. E. Demco, R. Graf,; J. Gottwald, S. Hafner, H. W. Spiess, *J. Magn. Reson.*, **1996** A, 122, 214-221.

[24] G. P. Robertson, S. D. Mikhailenko, K. Wang, P. Xing, M. D. Guiver, S. Kaliaguine, *J. Membr. Sci.*, **2003,** *219*, 113-121.

[25] R. Y. M. Huang, P. Shao, C. M. Burns, X. Feng, *J. App. Polym. Sci.*, **2001**, *82*, 2651-2660.

[26] Note that the water molecules associated with Na^+, have a chemical shift than the pure water chemical shift, and move from 4.8 ppm to 4.2 ppm as the sodium ions interrupt and weaken the hydrogen bonding among water molecules.

[27] S. J. Sondheimer, N. J. Bunce, M. E. Lemke, C. A. Fyfe, *Macromolecules*, **1986**, *19*, 339-343.

[28] P. Batamack, J. Fraissard, *Catal. Lett.*, **1995**, *35*, 135-142.

[29] Q. Deng, R. B. Moore, K. A. Mauritz, *J. App. Polym. Sci.*, **1998,** *68*, 747-763.

[30] C. J. Brinker, G. W. Scherer, *Sol-Gel Science: the Physics and Chemistry of Sol-Gel Processing*, acadamic press, Inc., Boston, **1990**, p.627.

[31] L. L. Hench, J. K. West, *Chem. Rev.*, **1990,** *90*, 33-72.

[32] G. Ye, C.A. Hayden, G. R. Goward, *Macromolecules*, **2007**, 40, 1529-1537.

[33] G. Alberti, M. Casciola, *Solid State Ionics*, **2001,** *145*, 3-16.

[34] G. Alberti, M. Casciola, L. Massinelli, B. Bauer, *J. Mem. Sci.*, **2001,** *185*, 73-81

[35] S. D. Mikhailenko, S. M. J. Zaidi, S. Kaliaguine, *J. Polym. Sci. Part B: Polymer Physics*, **2000,** *38*, 1386-1395.

[36] E. R. deAzevedo, W. G. Hu, T. J. Bonagamba, K. Schmidt-rohr, *J. Am. Chem. Soc.*, **1999**, 121, 8411-8412.

[37] B. R. Cherry, C. H. Fujimoto, C. J. Cornelius, T. M. Alam, *Macromolecules*, **2005**, *38*, 1201-1206.

[38] C. Yang, S. Srinivasan, A. B. Bocarsly, S. Tulyani, J. B. Benziger, *J. Membr. Sci.*, **2004**, *237*, 145-161.

Chapter 4

Proton Dynamics of Nafion/SiO_2 Composites

This chapter has been published on *Macromolecules* (**2007**, 40, 1529-1537). The co-authors are C. A. Hayden and G. R. Goward. The manuscript was initially prepared by me. Then it was revised by me and G. R. Goward for submission. My contribution to this paper includes the sample preparation, NMR experiments, conductivity measurements, and a proposed model to understand the conductivity differences between Nafion®/SiO_2 composites. In this chapter, ^1H NMR studies on Nafion/SiO_2 composites show that low concentrations of TEOS or short permeation times are necessary to allow complete hydrolysis of TEOS in Nafion. ^{29}Si NMR shows that Nafion/SiO_2 composite prepared from low concentration of TEOS has more surface hydroxyl groups. Together, these data demonstrate the role of high-surface-area SiO_2 particles in trapping water and building a pathway for structural (Grotthuss mechanism) proton diffusion. The diffusion coefficients established using PFG NMR show that the best Nafion/SiO_2 composite can be obtained from synthesis with a low concentration of TEOS in a methanol solution. A model is used to explain the different diffusion coefficients and conductivities of Nafion/SiO_2 composites.

4.1 Introduction

Studies on proton exchange membranes for the applications of fuel cells have been encouraged by the necessity to reduce pollution. As a well-known polymer electrolyte many studies have focused on, Nafion has been given much attention because of its excellent conductivity in the hydrated state. [1, 2] However, when this membrane is operated at high temperatures (above 100 °C), the conductivity of the membrane is dramatically decreased due to water loss. Since an elevated temperature has benefit to the fuel cell such as minimizing platinum poisoning and improving the electrode kinetics of the oxygen reduction reaction, [3, 4] membranes providing acceptable conductivity at high temperature and low hydration level are desirable. Although increasing the operating pressure can raise the boiling point of water to prevent water loss, this is not efficient due to the energy penalty associated with compressing the reactant gases.[5] A variety of polymer electrolytes have been developed as proton exchange membranes (PEMs).[6, 7] These membranes also show strong conductivity dependence on the state of membrane hydration. It has been demonstrated that addition of inorganic particles to polymers can enhance conductivity. [8] A composite Nafion115/zirconium phosphate membrane displayed better fuel cell performance than pure Nafion115 when the fuel cell was operated at reduced humidity conditions. [9] The proton conductivity of a Nafion/zirconium sulphophenyl phosphate (ZrSPP) composite membrane was reported to reach 0.07 S/cm at 140°C without additional humidification. [10] Nafion/SiO_2 has also shown better conductivity than pure Nafion at high temperature. [11, 12] The improved conductivity of these composites is generally attributed to the surface hydroxyl groups of dopants which retain water at high temperature. [1, 13] However, more information on how to obtain well-controlled composites with optimized amounts of dopants and particle size is needed, since these factors play a particularly important role in determining the performance of a composite as a proton exchange membrane.

Solid state nuclear magnetic resonance (NMR) can provide useful information concerning proton mobility within conducting polymers on the molecular level, [14, 15] because it is able to probe the local chemical environments. Such information is helpful to give a deeper understanding of the observed differences in proton conductivity. Magic angle spinning (MAS) is used routinely to achieve high resolution of ^{1}H NMR spectra in the solid state. Since dipolar interactions can reveal the relative mobility, methods which can retrieve information about the dipolar interaction removed by magic angle spinning are desirable. The double quantum filtering (DQF) pulse sequence, Back-to-Back (BaBa), [16, 17] has been used to recouple the dipolar coupling between protons, and thereby deduce their relative mobility. The intensity of the double quantum coherence (DQC) depends on the product of coupling strength and the excitation time, meaning a DQC based on strong dipolar coupling will be efficiently excited in a short recoupling time. Mobile protons which generate weak or no dipolar coupling will be absent from the DQF MAS NMR spectra due to inefficient excitation. Hence we can distinguish mobile and rigid protons by comparing MAS NMR with DQF MAS NMR spectra. On the other hand, a longer recoupling (excitation) time is useful to detect weak dipolar couplings which indicate either slowly mobile (i.e., less rigid) protons or dipolar couplings occurring over long distances.

Pulse Field Gradient (PFG) NMR provides a convenient and noninvasive means for measuring translational motion of protons. Although translational motion can be measured by analysis of spin-lattice relaxation data, the two methods will agree only under certain conditions since the relaxation is also sensitive to rotational diffusion, which does not necessarily lead to long range proton transport. [18] In PFG NMR, the nuclear motion can be measured by the attenuation of a spin echo signal resulting from the dephasing of the nuclear spins due to the combination of the translational motion of the spins and the imposition of spatially well-defined gradient pulses. Since this method can measure motion over millisecond to second time scales, the proton diffusion coefficient obtained by PFG NMR will reflect the proton mobility on the macroscopic level. This information can be used for comparison of various proton exchange membranes.

In this chapter, we studied proton mobility in Nafion/SiO_2 composites prepared by *in-situ* synthesis. Both the concentration of tetraethyl orthosilicate (TEOS) and the permeation time (PT) were varied to investigate how the amount of silica and particle size affects proton dynamics. Homonuclear double quantum pulse (Back-to-Back) experiments were performed to distinguish strong proton dipolar couplings from weak ones. PFG NMR measurements were obtained for Nafion and Nafion/SiO_2 composites in both the dried and hydrated states. The differences in proton mobility are compared and discussed, in combination with the results of our solid state NMR measurements.

4.2 Experimental

4.2.1 Preparation of samples

Treatment of Nafion112 was performed as follows. Nafion112 was first washed in 1M NaOH for 1 hour and then it was washed in distilled deionized water for another hour, during which time the water was refreshed four times. Subsequently, the membrane was washed in 1M HCl for 1 hour. Finally, it was washed repeatedly in distilled deionized water until a constant pH was obtained. Nafion/SiO_2 composite membranes were prepared according to the procedure reported by Deng. [19] The pretreated Nafion was first swollen in MeOH: H_2O (V/V) =5:1 for 24 hours. It was then put in the mixture of methanol, water and tetraethyl orthosilicate (TEOS) for 24 hours to allow permeation of TEOS into Nafion. The concentration of TEOS in mixture was changed to control the amount of silica in the resulting composites. Thus, in this paper Nafion/SiO_2 composites made from different mixture will be shown as Nafion/SiO_2 (a:b:c) in which the ratio is molar ratio of methanol to water to TEOS. For the mixtures in which no methanol is used, a variable permeation time (PT) was used to control the hydrolysis and condensation of TEOS. Three samples made from MeOH:H_2O:TEOS (mol:mol:mol) = 0:1:1 with permeation times of 9 minutes, 120 minutes, and 24 hours are denoted as Nafion/SiO_2 (0:1:1, PT9min), Nafion/SiO_2 (0:1:1, PT120min), and Nafion/SiO_2 (0:1:1, PT24hr), respectively. After the TEOS was allowed to permeate into Nafion, the membrane was dried at 105°C overnight to remove the excess alcohols and water. Some selected composites were further treated at 170 °C, a temperature at which water physisorbed on silica starts to be driven off. [20] This treatment allowed the study of the interaction of water and silica. The polymerization of TEOS to silica is an acid-catalyzed process. Since the sulfonic acid groups within Nafion are the only source of acid, it is assumed that the silica is formed within the Nafion membrane. For comparison, silica was also made by simply mixing TEOS with 1M sulfuric acid solution. The molar ratio of TEOS to sulfuric acid is

4.5:1. The white powder obtained from this sol-gel process was dried at 105 °C overnight to remove the excess alcohols and water.

4.2.2 ^{1}H NMR

^{1}H solid state NMR experiments were performed on a Bruker AV 500 spectrometer at a ^{1}H Larmor frequency of 500.13 MHz. Both 4 mm and 2.5 mm diameter rotors were used for Nafion samples spun at 5 kHz and 25 kHz, respectively. In both cases a recycle delay of 3 s and a pre-scan delay of 4.5 μs were used. The spectra were referenced to adamantane (1.63 ppm for ^{1}H). Solid state ^{1}H NMR spectra were acquired with a 90° pulse length of 2.5 μs. The rotor-synchronized DQF MAS spectra were recorded using the Back-to-Back (BaBa) pulse sequence, with τ_{exc} variable from half a rotor period $\tau_r / 2$ to eight rotor periods, $8\tau_r$, and 512 scans. [16]

4.2.3 ^{29}Si NMR

^{29}Si solid state NMR experiments were performed on a Bruker AV 500 spectrometer at a ^{29}Si Larmor frequency of 99.35 MHz. A 4 mm diameter rotor was used for samples spun at 5 kHz. A recycle delay of 180 s was used. It was found that this delay time is long enough since the obtained spectrum does not show observable difference from that by 420 s delay time. The ^{29}Si NMR spectra were acquired with a 90° pulse length of 3.5 μs, and referenced to tetrakis (trimethylsilyl) silane (-10.02 ppm and -135.7 ppm for ^{29}Si). 512 scans were averaged for the ^{29}Si NMR spectra.

4.2.4 PFG NMR

^1H diffusion coefficient experiments were performed on Bruker Avance 400WB spectrometer at a ^1H Larmor frequency of 400.13 MHz. Gradient pulse duration ranged from 1-2 ms and diffusion time ranged from 50-300 ms. The maximum gradient strength ranged from 50-1800 G/cm. For variable temperature measurements, the probe temperature was calibrated using ethylene glycol. A 5mm Diff30 probe was used with a 60 A (Bruker Great 1/60) amplifier. The pre-dried sample was placed directly into a 5 mm NMR tube for measurement. The uncapped NMR tube with the dried sample was placed in a humidity chamber for 8 days at 50°C and 90% relative humidity to obtain the hydrated sample. Hydrated samples were capped immediately and analyzed within a few hours of removal from the humidity chamber. The chemical shift of the sulfonic acid proton, which is sensitive to humidity, remained unchanged during measurement once the sample was in the capped NMR tube.

4.2.5 Impedance spectroscopy for proton conductivity measurements

A BekkTech four-probe conductivity cell with two platinum foil outer electrodes and two platinum wire inner electrodes, shown in Figure 2-7, was used for proton conductivity measurement. The membrane samples were cut into strips which were 0.3~0.5 cm wide and 2~3 cm long. The thickness of membranes was measured by a micrometer. An AUTOLAB PGSTAT30 impedance analyzer was used for acquisition of impedance spectroscopy. The instrument was used in potentiostatic mode with an AC potential amplitude of 0.01 V over a frequency range of 10 to 20,000 Hz. The conductivity of membrane was measured in the longitudinal direction. It is calculated using the equation (2-27). [21, 22] In order to measure the conductivity of dried samples, membranes were dried at 105 ^{o}C for several days and then equilibrated overnight at 35 ^{o}C in a sealed oven with desiccants. The hydrated samples were equilibrated overnight at 35 ^{o}C and 95% relative humidity in a humidity chamber. This equilibration time was found to be sufficiently long for the four-probe cell configuration, since the membrane is entirely exposed to the environment in the humidity chamber. The conductivity was found to be constant within 1% over several days in the controlled environment. The water content of these samples was measured to determine number of water molecules per sulfonic acid group for comparison of proton diffusion coefficients. For dried samples, the water content can be determined from the first weight loss in a thermal gravimetric analysis (TGA) study. The water content of hydrated samples was measured by the weight difference of dried samples and hydrated samples, with the weights of the dried samples normalized for their known water contents.

4.3 Results and discussion

4.3.1 Nafion/SiO_2 composites: influence of concentration of TEOS

Figure 4-1 shows ^{1}H MAS NMR spectra of SiO_2, Nafion and Nafion/SiO_2 prepared from different concentrations of TEOS and 24 hours of permeation time. The high frequency proton resonance shown in Figure 4-1(a) is assigned to the residual sulfuric acid protons. Due to the complete hydrolysis of TEOS under these conditions, no residual ethyl group signals were observed. The absence of Si-OH proton signal in this spectrum could be attributed to the insignificant amount of surface Si-OH groups, compared with the large number of sulfuric acid protons. The only peak shown in Figure 4-1 (b) is assigned to the sulfonic acid protons of Nafion. After silica was doped into Nafion, water adsorbed on the silica surface forms hydrogen bonds with Si-OH groups. This water shifts the sulfonic acid proton resonance to a lower chemical shift as shown in Figure 4-1 (c).

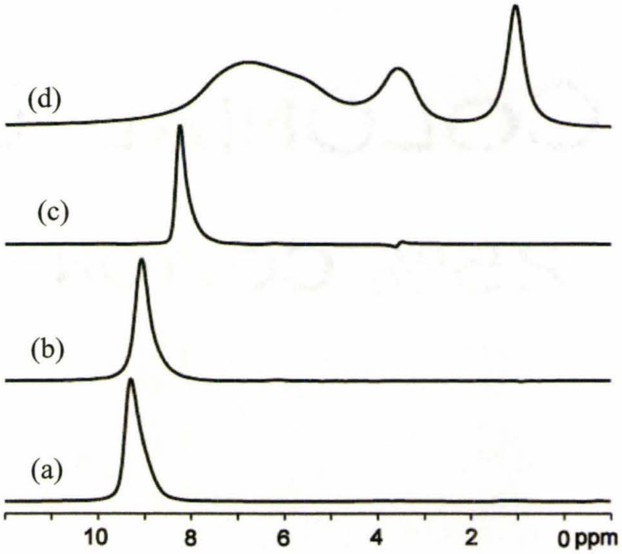

Figure 4-1. ^{1}H MAS NMR of SiO_2, Nafion and Nafion/SiO_2 composites prepared from different concentrations of TEOS and 24 hours of permeation time. All samples were treated overnight at 105°C (a) SiO_2 prepared from mixture of TEOS and 1M $H_2SO_{4\,(aq)}$, MAS=5kHz (b) Nafion, MAS=5 kHz (c) Nafion/SiO_2 (23:1:1), MAS=5 kHz (d) Nafion/SiO_2 (2.3:1:1), MAS=25 kHz

Proton resonances from Si-OH groups were not observed in this composite, as only a small amount of silica was formed from the initial low concentration of TEOS. When a higher concentration of TEOS was used to dope silica into Nafion, new peaks were observed in Figure 4-1 (d). The peaks at 1.0 ppm and 3.5 ppm are assigned to CH_3 and CH_2 groups of the residual ethyl groups of incompletely hydrolyzed TEOS, respectively. The broad resonance spanning from 5 ppm to 8 ppm in Figure 4-1 (d) is assigned to hydrogen bonded $-SO_3H$ and Si-OH protons. The wide range of local environments in the membrane causes significant spectral overlap. The broad resonance at 4 ppm is assigned to water physisorbed on silica. Similar spectra have been reported in the literature for silicates, in which a resonance at 4 ppm is assigned to physisorbed water and broad resonances ranging from 2 to 8 ppm are attributed to silanol protons in various hydrogen bonding environments. [23, 24, 25]

Comparing Figure 4-1 (a) with Figure 4-1 (c) & (d), we find that full hydrolysis of TEOS can be achieved in a mixture of sulfuric acid and TEOS without polymer, and in Nafion membranes when the concentration of TEOS is very low. When the concentration of TEOS is as high as that in Figure 4-1 (d), an incomplete hydrolysis of TEOS is observed. This is caused by the steric effect of the polymer microstructure in the Nafion/SiO_2 composite. When Nafion is immersed in methanol and water, the competing hydrolysis and condensation reactions favour the former, allowing full hydrolysis of TEOS. When the concentration of TEOS is increased, the condensation reaction dominates over full hydrolysis of TEOS, leading to a fast growth of silica particle size. Since the sulfonic acid group is restricted by the pendant side chain of Nafion, the mobility of H^+ and SO_3 in Nafion will be lower than that in free sulfuric acid. Additionally, the increasing silica particle size will decrease its mobility. Both factors inhibit the complete hydrolysis of residual ethyl groups in the membrane composites when the concentration of TEOS is high.

4.3.2 Nafion/SiO$_2$ composites: influence of permeation time

^{1}H MAS NMR spectra of Nafion/SiO$_2$ (0:1:1) prepared by varying the permeation time are shown in Figure 4-2. As expected, when the permeation time is decreased from 24 hours to either 120 or 9 minutes, the obtained composites exhibit only a sulfonic acid proton resonance. However, if we take a closer look at the two spectra, we can still observe the proton signal of Si-OH as shown in the expanded plots in Figure 4-2 (a) and Figure 4-2 (b). In addition, Figure 4-2 (b) also shows weak proton signals for the residual ethyl group from TEOS (near 1.0 and 3.5 ppm). Since these signals are not observed in Figure 4-2 (a), this means that there are virtually no residual ethyl groups of TEOS in Nafion/SiO$_2$ (0:1:1, PT9min), compared with the Si-OH groups. The presence of residual ethyl groups from TEOS will have two negative effects on proton conductivity of the composites. One is to reduce the number of surface hydroxyl groups by occupying the surface of the silica. This ultimately decreases the amount of water adsorbed by the silica particles, thereby minimizing the targeted water-binding action of the composite. The other is to block the proton channels of the composite due to the larger volume occupied by ethyl groups compared with hydroxyl groups. This result demonstrates that a short permeation time is preferable to allow hydrolysis of TEOS to form silica, while maintaining a high surface area, ensuring that ethyl groups are fully hydrolyzed and can escape from the membrane. These conditions will positively influence proton mobility within Nafion/SiO$_2$ composite.

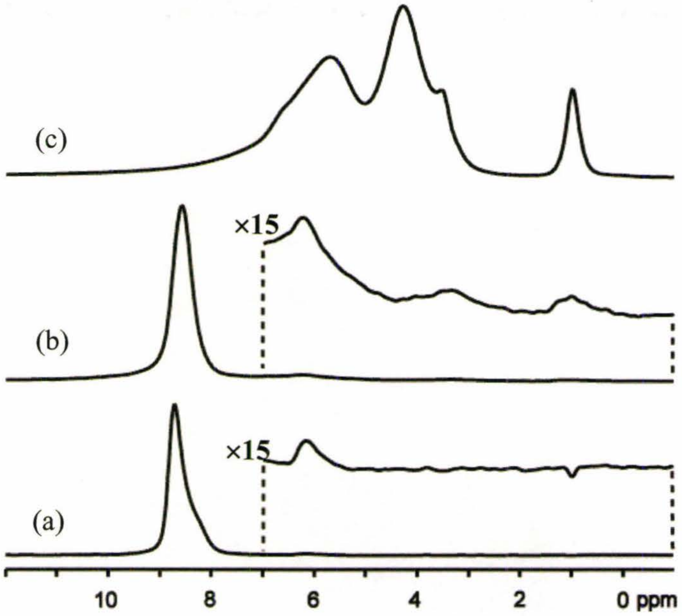

Figure 4-2. ^1H MAS NMR of Nafion/SiO_2 (0:1:1) composites prepared using different permeation times. All samples were treated overnight at 105°C (a) Nafion/SiO_2 (PT9min), MAS=5 kHz (b) Nafion/SiO_2 (PT120min), MAS=5 kHz (c) Nafion/SiO_2 (PT24hrs), MAS=25 kHz

4.3.3 Nafion/SiO_2 composites: influence of relative humidity

The unambiguous assignment of ^1H resonances for $H_2O/OH/H^+$ groups in these systems is difficult. With reference to literature studies of related SiO_2-based materials, and using our knowledge of the treatment conditions of the composites, we attempt a logical interpretation of the observed changes as a function of temperature/humidity. Figure 4-3 shows spectra of Nafion/SiO_2 (0:1:1, PT24hr) treated by drying or hydration. Comparing with Figure 4-2 (c), two new peaks at 1.6 ppm and 3.0 ppm are readily observed in Figure 4-3 (a), and the resonance assigned to physisorbed water (4.3 ppm) has disappeared from the spectrum. The peak at 1.6 ppm is assigned to isolated (non-hydrogen bonded) Si-OH groups. [26, 27] The other peak at

3.0 ppm is assigned to rapidly exchanging, weakly hydrogen bonded hydroxyls (including those of both water and silanols).[28, 29] Other studies have attributed the resonances at 3 ppm to water on significantly dehydrated surfaces and those at 4.5-5.0 ppm to water on strongly hydrated surfaces, as reviewed by Turov *et al.* [30] It has been reported that, for silica gels, physisorbed water starts to be driven off at about 170-175 °C. [20, 31] Since this composite was dried at 170 °C for 24 hours before NMR measurement, loss of physisorbed water is expected, which accounts for the absence of a physisorbed water signal. On the other hand, physisorbed water must be very immobile at room temperature because it was not removed even when the drying temperature was as high as 105 °C, as seen in Figure 4-2 (c). At 170°C, not only is the physisorbed water eliminated, but water strongly hydrogen bonded with Si-OH is also partially removed. This causes some isolated Si-OH groups to appear with a peak at 1.6 ppm. At the same time, the percentage of hydrogen bonded Si-OH groups decreases, which results in a smaller but broader peak.

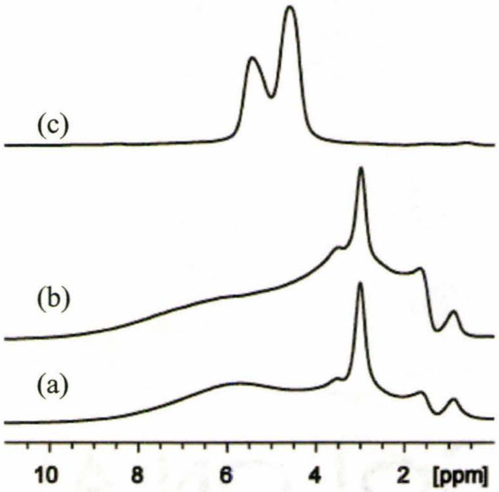

Figure 4-3. ^{1}H MAS NMR of Nafion/SiO$_2$ (0:1:1) composites with PT=24 hrs at 25 kHz (a) treated at 105 °C for 24hrs, then 170 °C for 24hrs (b) The sample from (a) treated at 170 °C for another 24hrs (c) The sample from (b) in oven for 96hrs at 50 °C and relative humidity =90%

The weakly hydrogen bonded hydroxyls at 3.0 ppm could be due to protons which are rapidly exchanging with water trapped within tiny cavities formed in silica particles. In an analogous study, the improved water retention of Nafion/zirconium phosphate composites was attributed to capillary condensation effects induced by zirconium phosphate doped in Nafion. [5] In the present case, the strong capillary condensation effect prevented the weakly bonded water from being eliminated even at temperatures as high as 170 °C. After this composite was treated for another 24 hours at the same temperature, the NMR spectrum shown in Figure 4-3 (b) indicates that the percentages of both strongly and weakly hydrogen bonded Si-OH groups decrease, while the percentage of isolated Si-OH groups increases. This also supports the hypothesis that hydrogen bonded Si-OH groups changed into isolated Si-OH groups after the loss of water. The hydrated sample shown in Figure 4-3 (c) only presented two peaks which should be assigned to hydrogen bonded Si-OH groups and physisorbed water, respectively. Since a large amount of water is present in the sample treated at 50% relative humidity, the residual ethyl groups cannot be observed from this sample due to their very low relative concentration. However, once the sample is dried again, the resonance of ethyl groups become observable in the ^{1}H NMR spectrum, confirming therefore the loss of this signal under hydration is simply an issue of relative intensity, and not a completion of the hydrolysis reaction.

4.3.4 Immobile protons detected by DQ MAS NMR of Nafion/SiO_2

Since DQF MAS NMR measurements provide information on the relative mobility of protons, it is used to distinguish immobile protons from mobile ones in

Nafion/SiO_2 composites. Results of Nafion/SiO_2 (2.3:1:1) composite prepared from an intermediate concentration of TEOS are chosen to represent this information. Figure 4-4 and Figure 4-5 show the 1D and 2D ^1H DQF MAS NMR spectra of Nafion/SiO_2 (2.3:1:1), respectively. It is clear that the residual ethyl group of TEOS is not mobile since it did not disappear from the DQF MAS spectra when the recoupling time was increased from τ_r to $8\tau_r$ in Figure 4-4. This proves that the ethyl group is from incompletely hydrolysed TEOS rather than from free TEOS, since the ethyl group of free TEOS would be mobile even if the TEOS was trapped in silica. In DQF MAS NMR spectra, the presence of the Si-OH resonance indicates that some of these hydroxyl groups are not mobile, which is consistent with ^1H CRAMPS dipolar dephasing experiments in which silanol groups show strong dipolar interactions. [25, 26] Not surprisingly, the strong dipolar coupling between ethyl protons was observed in the 2D DQF MAS spectrum as well, shown in Figure 4-5. Strong dipolar coupling between protons of the ethyl group and Si-OH was also observed. This implies that the residual ethyl groups are spatially close to Si-OH groups. Since these Si-OH groups always are on the surface of silica, some of the residual ethyl groups have to be on the silica surface. Those residual ethyl groups located on the silica surface can still be hydrolyzed once an acid catalyst is available. Thus, acidifying the composite can finally complete the hydrolysis of these residual ethyl groups. Figure 4-5 also shows strong proton dipolar coupling between Si-OH groups. The strong proton dipolar coupling between Si-OH groups suggests that Si-OH groups are spatially close to each other as well. This proximity is important for allowing a hopping mechanism of proton transport. Water molecules hydrogen bonded with these Si-OH groups will be able to have proton exchange with each other because of the short distance between these bonding sites. Nevertheless, since this composite was treated at 105 °C for 24 hours before NMR measurement, water molecules left in the composite would not be expected to undergo proton exchange with each other at room temperature. The reduced intensity of the Si-OH resonance relative to the CH_2/CH_3 resonances in the DQF spectrum as compared to the MAS spectrum indicates a weaker coupling, possibly attributable to local mobility. If the composite is subjected to an operating temperature above 105 °C, proton exchange among water would be expected. This is also the motivation for doping silica to improve proton conductivity of Nafion.

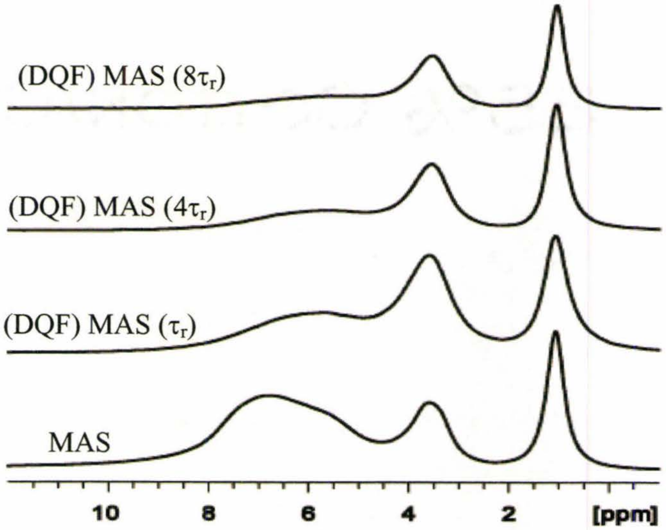

Figure 4-4 ^1H MAS & DQF MAS NMR spectra of $Nafion/SiO_2$ (2.3:1:1) composite dried at 105 °C for 24hrs, MAS = 25 kHz. τ_r indicates the number of rotor periods of recoupling used in the DQF sequence.

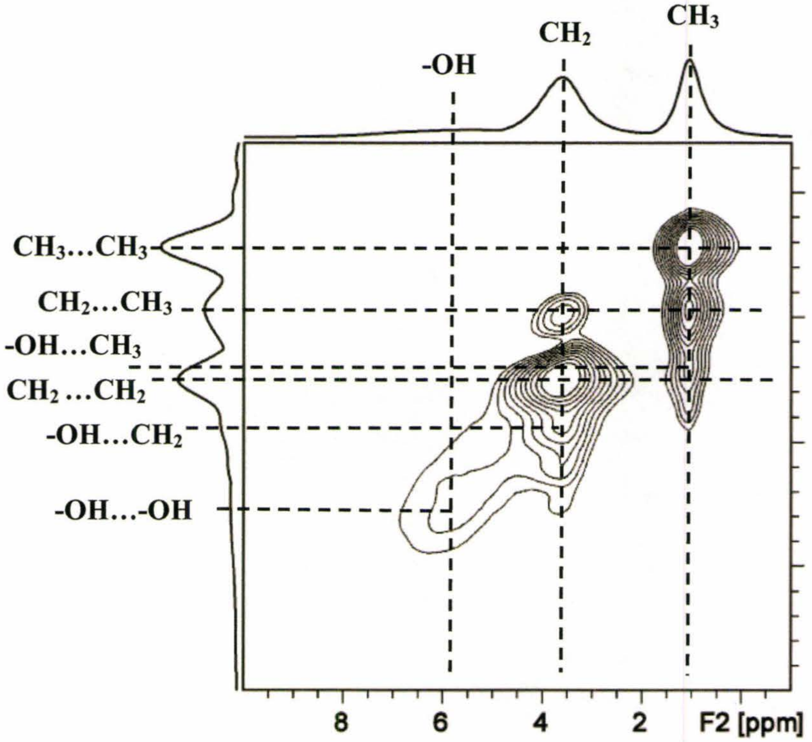

Figure 4-5. ^{1}H 2D DQ MAS NMR of Nafion/SiO$_2$ (2.3:1:1) composite dried at 105 °C for 24hrs, MAS = 25 kHz, $\tau_{exc} = \tau_r$

4.3.5 ^{29}Si MAS NMR

^{29}Si solid state NMR is a well-established means of determining the coordination environments of ^{29}Si nuclei. From this information, we can deduce the number of surface hydroxyl groups in the various samples, and optimize the synthetic conditions to favour high surface area materials. A silicon atom which is bonded to 3 other silicon atoms through oxygen can be shown as HO-Si-(O-Si)$_3$ and is generally denoted as Q$_3$, giving a chemical shift of ~ −100 ppm. Similarly, Si-(O-Si)$_4$ is denoted as Q$_4$ and has a chemical shift of ~ −110 ppm. [32, 33, 34] It is clear that the higher ratio of Q_3 to Q_4 indicates a higher surface area, therefore smaller average size of silica particles for the same total amount of SiO_2. Thus, ^{29}Si MAS NMR of Nafion/SiO_2 composites can provide qualitative information regarding the silica particle size.

^{29}Si MAS NMR of SiO_2 and Nafion/SiO_2 composites are shown in Figure 4-6. There is no silicon resonance observed at -80 ppm in all ^{29}Si spectra, confirming that there is no unreacted TEOS in these samples. Based upon the data shown in Figure 4-6 (a), the majority of silicon nuclei in the silica made from TEOS and sulfuric acid are in the form of Q_4. This indicates that a full condensation reaction has occurred among the hydrolyzed TEOS molecules and that the average silica particle size is large. The Nafion/SiO_2 composite prepared using a short permeation time (120 minutes) gives an increased ratio of Q_3 to Q_4 as shown in Figure 4-6 (b), which suggests smaller silica particles in the composite compared with neat SiO_2. This is likely due to the restricted motion of silica in water channels of Nafion. It has been reported that the diameter of water channels in hydrated Nafion is as large as 5 nm. [35] Compared with silica made from a mixture of TEOS and sulfuric acid, such a narrow channel will certainly restrict the motion of the precursor units within the membrane. Therefore, the condensation reaction among these silica units will be limited. This maintains a large number of surface hydroxyl groups of silica. Thus, more silicon atoms have the Q_3 coordination environment in the composite. Nevertheless, when a longer permeation time is allowed (24 hours), the ratio of Q_3 to Q_4 decreases slightly as shown in Figure 4-6 (c). This may be attributed to the condensation reaction dominating over the hydrolysis reaction of TEOS. Interestingly, this composite also shows a peak at –90ppm which is attributed to silicon in the form of $(HO)_2$-Si-$(O$-$Si)_2$ denoted as Q_2.

The Q_2 sites of silicon could be also due to the restricted condensation reaction between newly formed small silica particles, since the initially formed silica particles would be large and further prevent the fast motion of the subsequently formed small particles. As expected, due to the reduced concentration of TEOS, the composite Nafion/SiO_2 (2.3:1:1) shows an even higher ratio of Q_3 to Q_4, as shown in Figure 4-6 (d), which suggests a further decrease in the condensation among silica particles. This is desirable because silica with more surface hydroxyl groups will provide more sites to retain water. Ramani reported that an enhanced conductivity of Nafion/phosphotungstic acid composite membrane by up to 35% was obtained when the additive particle size was reduced by nearly two orders of magnitude from 1 to 2 μm to 30 nm. [36] The ratios of Q_3 to Q_4 calculated from the deconvoluted spectra for these samples are shown in Table 4-1 for reference.

Table 4-1. Ratio of Q_3 to Q_4 in SiO_2 and Nafion/SiO_2 composites

Samples	SiO_2 (TEOS and H_2SO_4)	Nafion/SiO_2 (0:1:1) PT=120min	Nafion/SiO_2 (0:1:1) PT=24hrs	Nafion/SiO_2 (2.3:1:1) PT=24hrs
Q_3: Q_4	1: 4.2	1: 1.2	1: 1.6	1: 0.7

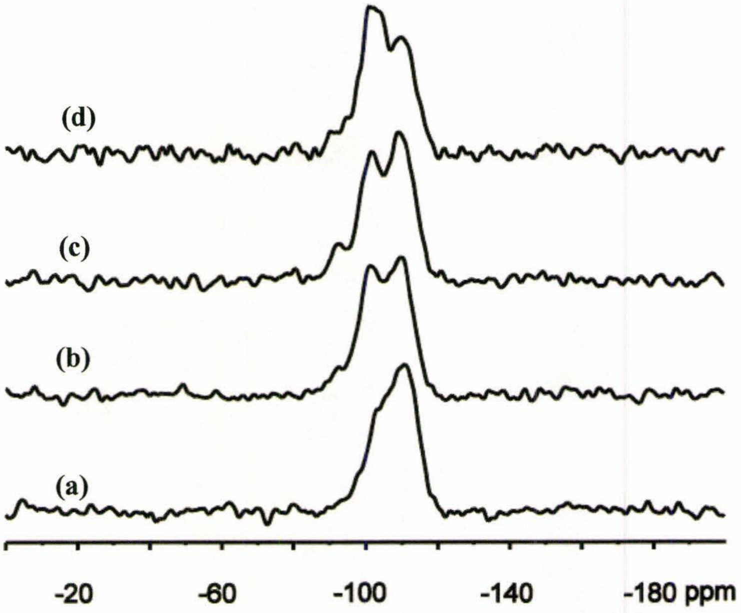

Figure 4-6. ^{29}Si MAS NMR of SiO_2 and Nafion/SiO_2 composites dried at 105 °C for 24hrs, MAS = 5 kHz (a) SiO_2 from TEOS and $H_2SO_{4\ (aq)}$ (b) Nafion/SiO_2 (0:1:1, PT=120min) (c) Nafion/SiO_2 (0:1:1, PT=24hrs) (d) Nafion/SiO_2 (2.3:1:1, PT=24hrs)

Based on the ^{29}Si NMR results, we target samples which have the maximum number of Q_3 sites, or equivalently, a high concentration of surface OH groups. We also note that samples with even lower concentrations of silicate gave very weak ^{29}Si NMR signals, but did not provide quantifiable spectra. Nevertheless, the same trend is expected.

4.3.6 PFG NMR for proton diffusion coefficient measurement

The pulse field gradient NMR experiment provides a measure of the translational motion of protons in the membrane. By comparing a select set of samples, where high numbers of surface hydroxyl groups are present (i.e. those with low permeation times or low concentrations of TEOS used in the sample preparation), we can determine the influence of those surface hydroxyl groups on water retention and proton transport within the dried versus humidified membranes. These data are compared to the performance of Nafion itself under equivalent conditions.

The pulse sequence applied for PFG NMR measurement in this study is shown in Figure 2-4. A pair of symmetrically spaced field gradient pulses is superimposed onto a standard spin-echo sequence. This is known as the stimulated echo (STE) pulse sequence. The predicted dependence of the observed signal attenuation on gradient strength is [18]

$$E(2\tau) = \frac{S(2\tau)}{S(2\tau)_{g=0}} = \exp(-\gamma^2 g^2 D\delta^2(\Delta - \delta/3)) \tag{4-1}$$

where $S(2\tau)$ is the observed signal intensity with applied gradient pulse g, $S(2\tau)_{g=0}$ is the signal intensity observed in the absence of an applied gradient, γ is the nuclear gyromagnetic ratio, D is the self-diffusion coefficient, δ is a pulse width of applied gradient, and Δ is the separation in time between the leading edges of the two gradient pulses (also referred to as the "diffusion time"). In this study, a series of spectra are obtained at increasing gradient strengths holding all other parameters constant. The diffusion coefficient is obtained by fitting the peak intensity data vs. the applied gradient strength as shown in Figure 4-7.

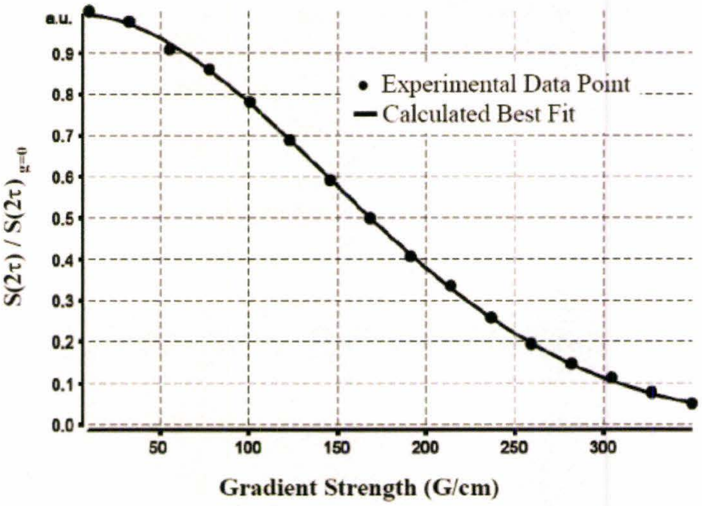

Figure 4-7. An example of fitted PFG NMR data. The sample is dried Nafion/SiO_2 (23:1:1). The fitted diffusion coefficient is 2.55×10^{-7} cm^2/s at 305K

A fundamental requirement of a PFG NMR experiment is that the diffusional attenuation must be significant relative to attenuation caused by relaxation of the observed nuclei. Determination of diffusion coefficients by PFG NMR measurement will be difficult or infeasible if relaxation is too rapid. Boyle [37] reported that iron contamination in Nafion caused significantly shortened relaxation time (T_1 on the order of 10ms for 1100 EW Nafion), which made the PFG NMR experiment of Nafion impractical in their studies. Based on well-purified, protonic forms of Nafion, T.A. Zawodzinski found that T_1 relaxation times vary from 80 to 200 ms for Nafion 117 membranes and reduce with decreasing water content in the membrane.[38] In our experiments, the T_1 relaxation times ranged from 130 to 580 ms, and the hydrated samples showed longer T_1 relaxation times than dried samples as well.

The proton diffusion coefficients obtained by PFG NMR are shown in Table 4-2. For pure Nafion, the hydrated sample shows a proton diffusion coefficient around

37 times higher than the dried ones. T.A. Zawodzinski reported proton diffusion coefficients for Nafion117 4.4×10^{-6} cm^2/s and 5.8×10^{-6} cm^2/s when H_2O/SO_3H is 9 and 14, respectively. [38] By comparison, H_2O/SO_3H in our hydrated Nafion is likely to be in the range between 9 and 14 since the proton diffusion coefficient we measured is intermediate (4.83×10^{-6} cm^2/s). In Table 4-2, the dried Nafion/SiO_2 composites made from high concentration of TEOS (such as MeOH:H2O:TEOS = 0:1:1) have lower diffusion coefficients than pure Nafion, but composites made from low concentrations of TEOS (such as MeOH:H2O:TEOS = 23:1:1, 1:0.5:0.005 and 1:0.26:0.026) show higher diffusion coefficients than pure Nafion.

Doping silica in Nafion will have two opposing effects on proton mobility of Nafion/SiO_2. The first effect is to help Nafion to retain water by forming hydrogen bonds between water and hydroxyl groups of silica. This is desirable. The second is to block the pathway of proton transportation by silica. This is undesirable. The diffusion coefficients of Nafion/SiO_2 listed in Table 4-2 imply competition of the two effects. A sketch shown in Figure 4-8 is used to display the difference in Nafion/SiO_2 prepared from low and high concentrations of TEOS. For composites prepared from high concentrations of TEOS, the silica particles are relatively large since the condensation reaction of silica is facile, which has been proven by our ^{29}Si MAS NMR data (see section 4.3.5). In such a case, the negative effect will play a dominant role in changing the proton diffusion coefficient. Moreover, for the a composite prepared from a high concentration of TEOS with a permeation time of 120 minutes, the very low diffusion coefficient could be due to not only the increased silica particle size but also the residual ethyl groups which have been shown by our ^1H NMR spectra. In this case, the negative effect will be overwhelming. Since the Nafion/SiO_2 composites prepared from low concentrations of TEOS have been shown to have smaller silica particle size and no residual ethyl groups, the positive effect will be dominant in these composites. This composite would have well connected pathway for proton hopping, which contributes to higher proton diffusion coefficient.

Table 4-2. Proton diffusion coefficients of Nafion and Nafion/SiO_2

Samples	Dried ($\times 10^{-7} cm^2/s$)	Hydrated ($\times 10^{-7} cm^2/s$)
Nafion	1.32 ± 0.02	48.3 ± 0.2
Nafion/SiO_2 (0:1:1, PT9min)	0.96 ± 0.02	41.7 ± 0.2
Nafion/SiO_2 (0:1:1, PT120min)	0.097 ± 0.002	43.8 ± 0.2
Nafion/SiO_2 (23:1:1)	2.15 ± 0.02	46.7 ± 0.2
Nafion/SiO_2 (1:0.5:0.005)	1.82 ± 0.02	47.4 ± 0.2
Nafion/SiO_2 (1:0.26:0.026)	1.65 ± 0.02	48.3 ± 0.2

(Error bars reported here are based upon repeat measurements with different diffusion times.)

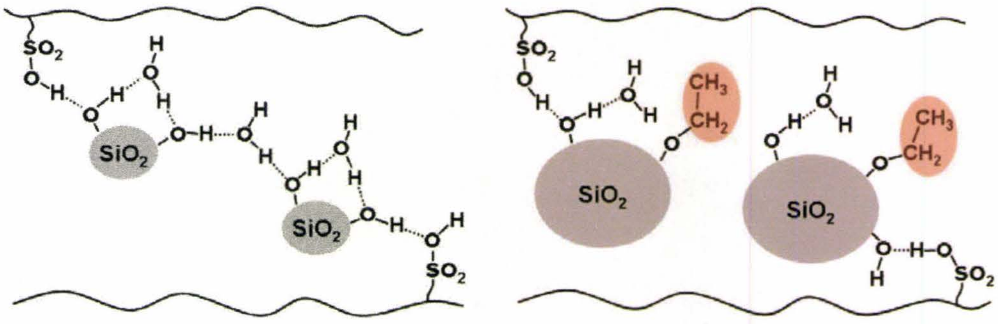

Figure 4-8. Schematic representation of the structure of dried Nafion/SiO_2 composites prepared from low concentration TEOS (the left) and high concentration TEOS (the right). The residual ethyl groups are highlighted.

TGA measurements shown in Figure 4-9 provide information about the total amount of silica in the composites. Nafion/SiO_2 (0:1:1, PT120min), Nafion/SiO_2 (0:1:1, PT9min) and Nafion/SiO_2 (23:1:1) have 2.8%, 1.2% and 1.0% mass percentage of silica, respectively, after taking into account of residual mass percentage of Nafion (1.7%). Clearly, Nafion/SiO_2 (0:1:1, PT120min) has the highest weight percentage of silica. Shortening the permeation time reduces the total amount of silica in Nafion/SiO_2 (0:1:1, PT9min), but still slightly exceeds the amount of silica prepared with a long permeation time and a low concentration of TEOS, as in Nafion/SiO_2 (23:1:1). Based on the TGA results and diffusion coefficient data, the composite prepared from the lower concentration of TEOS should have the smallest silica particle size, which should minimize the effect of blocking pathways for proton transportation. The number of surface hydroxyl groups in dried Nafion/SiO_2 composite has a significant influence on the proton diffusion coefficient. Therefore, minimizing the concentration of SiO_2, while maximizing the number of surface OH sites, as in sample Nafion/SiO_2 (23:1:1), provides the best pathway for proton conductivity.

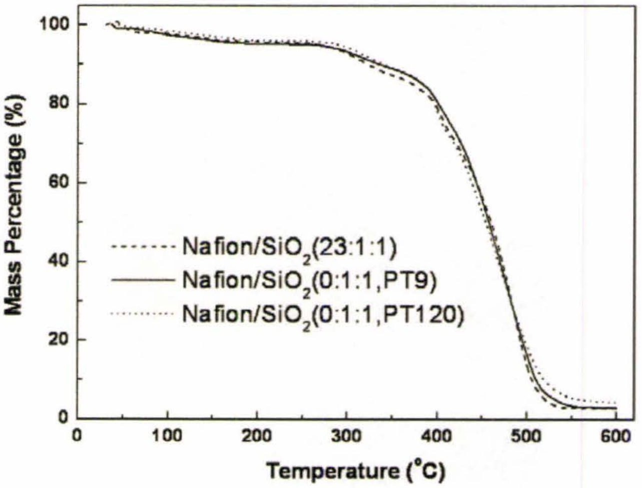

Figure 4-9. TGA analysis of Nafion/SiO_2 composites, acquired under dry in N_2

In contrast, no significant difference can be seen between hydrated Nafion and hydrated Nafion/SiO_2 composites. This is attributed to the high proton mobility in expanded water channels in hydrated samples. Compared with water added by hydration, under high relative humidity, water adsorbed on silica surface will not contribute much to the proton mobility of Nafion/SiO_2 composites since the proton diffusion coefficient in this instance is determined primarily by the water from hydration. Under this condition, the silica dopant in Nafion will merely be an obstacle for proton transportation, leading to decreased diffusion coefficients of Nafion/SiO_2. However, due to rapid vehicle transport in the fluid phase of the expanded water channels and the relatively small filled silica particles, the dopant cannot lower the diffusion coefficient significantly, even for the composite prepared with 120 minutes of permeation time. From this behaviour, we infer that proton transport in dried Nafion/SiO_2 composite has Grotthuss hopping mechanism different from that in the hydrated composite. In the dried composites, the proton transport is achieved by proton hopping on the surface of silica. Thus, well-distributed small silica particles can enhance the efficiency of proton hopping. In the hydrated composite, the proton transport is dominated by vehicle transport and completed by reorganization of hydrogen bonds between H^+ and water molecules. Kreuer points out that the Grotthuss mechanism is increasingly dominated by the vehicle mechanism as temperature increases. [39] Similarly here, the vehicle mechanism becomes increasingly important with increasing relative humidity. The existence of silica particles changes the pathway of proton migration and makes it somewhat longer, but does not significantly influence transport. The length scale of proton diffusion (d) can be given by

$$\mathrm{d} = \sqrt{2D\Delta} \qquad (4\text{-}2)$$

where D is the diffusion coefficient and Δ is the diffusion time shown in the STE pulse sequence. For the dried samples, the d is between 0.4 and 1.9 μm. Due to similar diffusion time, the sample with higher diffusion coefficient shows longer length scale of motion. For the hydrated samples, the d is between 9 and 17 μm. The difference of length scale of motion for the hydrated samples results from different diffusion time. Nevertheless, no obvious difference of diffusion coefficients is observed for the same sample when the diffusion time changes in our experiments. The above d values for both dried and hydrated samples are apparently much greater than the size of water channels in the hydrated Nafion which can be up to 5 nm. [35] This implies that proton diffusion is not constrained by the diameter of the channels even under dried conditions, but rather that the protons move readily along the channels, or from particle to channel wall, in the presence of silica particles with hydrophilic surfaces.

Since the diffusion coefficient is temperature dependent, variable temperature measurements with PFG NMR can demonstrate how the diffusion coefficients changes with temperature. The corresponding activation energy of proton diffusion can then be obtained by fitting the equation $D=D_0 \exp(-Ea/RT)$, where D is the diffusion coefficient, D_0 is a pre-exponential factor, Ea is the activation energy, R is the ideal gas constant and T is the temperature. Figure 4-10 shows the natural log plot from which the activation energies were derived for Nafion and Nafion/SiO_2 (23:1:1), which are 22.6 kJ/mol and 18.0 kJ/mol, respectively. The lower activation energy shown by the Nafion/SiO_2 (23:1:1) composite indicates that proton mobility of these composites is less sensitive to temperature change. The activation energies determined by PFG NMR are summarized in Table 4-3, along with some of the data obtained from variable solid state NMR line width calculations. The composite made from a low concentration of TEOS gives a lower E_a than that made from a high concentration of TEOS, although the difference is not very large. An interesting observation is that the composite made from a high concentration of TEOS shows a lower activation energy than pure Nafion, even though pure Nafion exhibits higher diffusion coefficients at all temperatures measured. The lower activation energy shown by both Nafion/SiO_2 (0:1:1, PT9min) and Nafion/SiO_2 (23:1:1) composites indicates that proton mobility of these composites is less sensitive to temperature. In the previous chapter, an activation energy for proton transport has been obtained by linear fitting of the change of ^1H line width with temperature in solid state NMR.[40] These solid state NMR-derived activation energies are also included in Table 4-3. The large difference between the values derived from the two different methods is attributed to the fact that PFG NMR measures the proton motion over the millisecond to second timescale; where as solid state NMR does so over the microsecond time scale. In the case of motion over long time scale (i.e. PFG NMR), the activation energy obtained will include the energy of proton motion used for crossing longer length scales in the membrane, i.e. in and out of channels, similar to grain boundary effects in microcrystalline solids. Therefore, it is reasonable that PFG NMR measures a higher E_a than solid state NMR.

Table 4-3. Activation energy of proton transport for Nafion and Nafion composites

Fully Dried Samples	PFG NMR Derived E_a Values (kJ/mol)	Solid State NMR Derived E_a Values (kJ/mol)
Nafion	22.6	15.7±0.6
Nafion/SiO_2 (0:1:1, PT9min)	20.9	12.2±0.5
Nafion/SiO_2 (23:1:1)	18.0	N/A

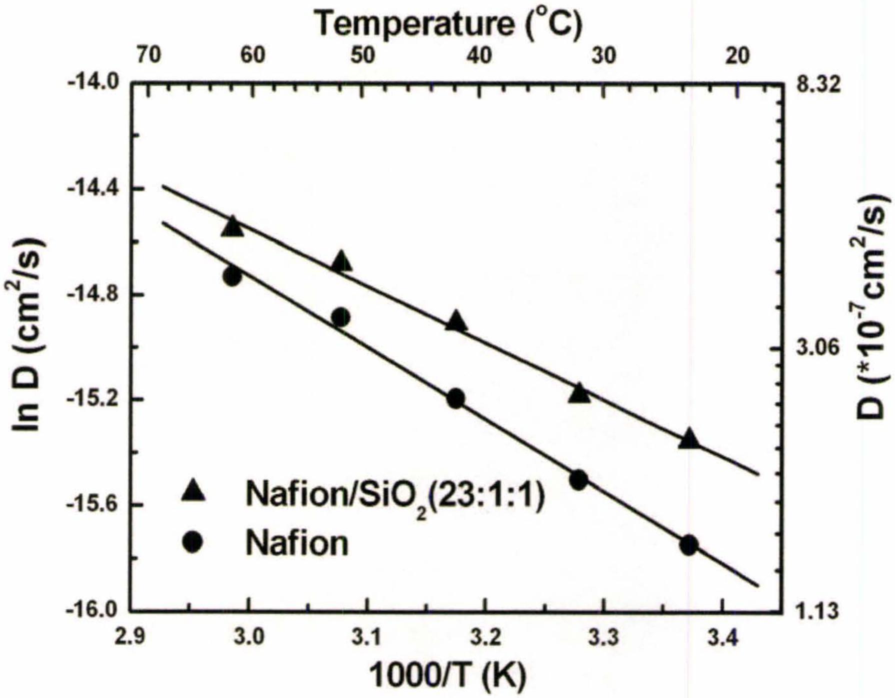

Figure 4-10. Arrhenius plot of proton diffusion for Nafion and Nafion/SiO_2

4.3.7 Proton conductivity of Nafion and Nafion/SiO_2 composites

Although PFG NMR experiments can provide information of proton translation motion in the electrolyte, this technique is not able to distinguish protons dissociated from sulfonic acid groups from those associated with sulfonic acid groups which do not contribute to proton conductivity, according to Nernst-Einstein equation.[41] Proton conductivity data measured by impedance spectroscopy is the industrially accepted method for evaluation of the conductivity of Nafion and Nafion/SiO_2 composites. The obtained results are shown in Table 4-4. The measured number of water molecules per sulfonic acid group is shown in this table for comparison as well.

Table 4-4. Conductivity of Nafion and Nafion/SiO_2 at 35 °C

Samples	Dried		Hydrated	
	σ (S/cm)	H_2O/-SO_3H	σ (S/cm)	H_2O/-SO_3H
Nafion	3.7×10^{-4}	3.1	6.0×10^{-2}	12.6
Nafion/SiO_2 (0:1:1, PT9min)	2.4×10^{-5}	3.1	5.7×10^{-2}	12.7
Nafion/SiO_2 (0:1:1, PT120min)	1.1×10^{-5}	2.6	4.9×10^{-2}	10.5
Nafion/SiO_2 (23:1:1)	4.9×10^{-4}	2.8	5.1×10^{-2}	11.8

The proton conductivity of hydrated Nafion is in good agreement with values reported by others. [21, 42] Similar to PFG NMR results, the hydrated samples do not show much conductivity difference which may be attributed to the similar, high, number of water molecules per sulfonic acid group. In contrast, the dried samples present significant conductivity differences, of as much as one order of magnitude, although the number of water molecules per sulfonic acid group in dried samples is very similar. The conductivity data is consistent with interpretation of NMR and PFG data above, where the enhancement of performance upon introduction of the silica is achieved under dry conditions for the composites formed with dilute concentrations of TEOS, and short permeation times. Higher concentrations of TEOS in the preparation give rise to more blocked channels, as reflected in the lower conductivity values for composites formed without methanol ((0:1:1, PT9min) and (0:1:1, PT120min)). This is a confirmation of observed trends, in which bulk conductivity measurements indicate impediments to long-range transport, such as blocked channels (this case), or grain boundaries, as observed in polymers with a propensity to form crystalline regions. [43] Thus, the combination of PFG NMR and impedance spectroscopy, allow us to derive a complete picture of the processes governing the function of the materials.

4.4 Conclusion

Solid state NMR measurements show that increasing the concentration of TEOS or extending the permeation time for synthesis of Nafion/SiO_2 composites will cause incomplete hydrolysis of the ethyl groups of TEOS. The residual ethyl groups are located on the surface of silica, which blocks the pathway for proton transportation and therefore lowers the proton conductivity. For synthesis with a high concentration of TEOS, a short permeation time needs to be used to avoid the issue of residual ethyl groups from TEOS. Diffusion coefficient data obtained by PFG NMR show that the best Nafion/SiO_2 composite can be obtained from synthesis with a low concentration of TEOS in methanol solution. Although all Nafion/SiO_2 composites in this study give the same or slightly lower diffusion coefficients than pure Nafion in the hydrated state, composites made from low concentrations of TEOS display higher diffusion coefficient than pure Nafion in the dried state. The same trend has been observed from conductivity measurements. This result suggests that Nafion/SiO_2 composites synthesized using the right procedures may hold promise for use as proton exchange membranes working at elevated temperature and reduced relative humidity.

4.5 References

[1] G. Alberti, M. Casciola, *Solid State Ionics*, **2001,** 145, (1-4), 3-16.

[2] R. C. T. Slade, A. Hardwick, P. G. Dickens, *Solid State Ionics*, **1983,** 9-10, 1093-1098.

[3] G. Alberti, M. Casciola, L. Massinelli, B. Bauer, *J. Membr. Sci.*, **2001,** 185, 73-81.

[4] Q. Li, R. He, J. O. Jensen, N. J. Bjerrum, *Chem. Mater.*, **2003,** 15, 4896-4915.

[5] P. Costamagna, C. Yang, A. B. Bocarsly, S. Srinivasan, *Electrochimi. Acta*, **2002,** 47, 1023-1033.

[6] M. J. Sumner, W. L. Harrison, R. M. Weyers, Y. S. Kim, J. E. McGrath, J. S. Riffle, A. Brink, M. H. Brink, *J. Membr. Sci.*, **2004**, 239, 199-211.

[7] S. M. J. Zaidi, S. D. Mikhailenko, G. P. Robertson, M. D. Guiver, S. Kaliaguine, *J. Membr. Sci.*, **2000,** 173, 17-34.

[8] E. Coronado, J. R. Galan-Mascaros, C. J. Gomez-Garcia, V. Laukhin, *Nature*, **2000,** 408, 447-449.

[9] C. Yang, S. Srinivasan, A. B. Bocarsly, S. Tulyani, J. B. Benziger, *J. Membr. Sci.*, **2004,** 237, 145-161.

[10] Y. T. Kim, M. K. Song, K. H. Kim, S. B. Park, S. K. Min, H. W. Rhee, *Electrochim. Acta*, **2004,** 50, 645-648.

[11] H. Wang, B. A. Holmberg, L. Huang, Z. Wang, A. Mitra, J. M. Norbeck, Y. Yan, *J. Mater. Chem.*, **2002,** 12, 834-837.

[12] P. L. Antonucci, A. S. Arico, P. Creti, E. Ramunni, V. Antonucci, *Solid State Ionics*, **1999,** 125, 431-437.

[13] K. A. Mauritz, J. T. Payne, *J. Membr. Sci.*, **2000,** 168, 39-51.

[14] R. Graf, D. E. Demco, S. Hafner, H. W. Spiess, *Solid State Nucl. Magn. Reson.*, **1998,** 12, 139-152.

[15] B. S. Hickman, M. Mascal, J. J. Titman, I. G. Wood, *J. Am. Chem. Soc.*, **1999,** 121, 11486-11490.

[16] I. Schnell, H. W. Spiess, *J. Magn. Reson.*, **2001,** 151, 153-227.

[17] S. P. Brown, I. Schnell, J. D. Brand, K. Mullen, H. W. Spiess, *J. Mol. Struct.*, **2000,** 521, 179-195.

[18] W. S. Price, *Concepts Magn. Reson.*, **1997,** 9, 299-336.

[19] Q. Deng, R. B. Moore, K. A. Mauritz, *Chem. Mater.*, **1995,** 7, 2259-2268.

[20] L. L. Hench, J. K. West, *Chem. Rev.*, **1990,** 90, 33-72.

[21] J. J. Sumner, S. E. Creager, J. J. Ma, D. D. DesMarteau, *J. Electrochem. Soc.*, **1998**, 145, 107-110.

[22] Y. Sone, P. Ekdunge, D. Simonsson, *J.Electrochem. Soc.*, **1996**, 143, 1254-1259.

[23] I. S. Chuang, D. R. Kinney, G. E. Maciel, *J. Am. Chem. Soc.*, **1993,** 115, 8695-705.

[24] D. R. Kinney, I. S. Chuang, G. E. Maciel, *J. Am. Chem. Soc.*, **1993,** 115, 6786-6794.

[25] C. C. Liu, G. E. Maciel, *J. Am. Chem. Soc.*, **1996,** 118, 5103-5119.

[26] C. E. Bronnimann, R. C. Zeigler, G. E. Maciel, *J. Am. Chem. Soc.*, **1988,** 110, 2023-2026.

[27] S. J. Hwang, D. O. Uner, T. S. King, M. Pruski, B. C. Gerstein, *J. Phys. Chem.*, **1995,** 99,, 3697-703.

[28] J. Trebosc, J. W. Wiench, S. Huh, V. S. Y. Lin, M. Pruski, *J. Am. Chem. Soc.*, **2005,** 127, 3057-3068.

[29] B. Grunberg, T. Emmler, E. Gedat, I. Shenderovich, H. Findenegg Gerhard, H. H. Limbach, G. Buntkowsky, *Chem. Eur. J.*, **2004,** 10, 5689-5696.

[30] V. V. Turov, R. Leboda, *Adv. Colloid Interface Sci.*, **1999,** 79, 173-211.

[31] Q. Deng, R. B. Moore, K. A. Mauritz, *J. Appl. Polymer Sci.*, **1998,** 68, 747-763.

[32] F. Babonneau, K. Thorne, J. D. Mackenzie, *Chem. Mater.*, **1989,** 1, 554-558.

[33] C. G. Wu, D. C. DeGroot, H. O. Marcy, J. L. Schindler, C. R. Kannewurf, Y. J. Liu, W. Hirpo, M. G. Kanatzidis, *Chem. Mater.*, **1996,** 8, 1992-2004.

[34] S. K. Young, W. L. Jarrett, K. A. Mauritz, *Polymer*, **2002,** 43, 2311-2320.

[35] K. A. Mauritz, R. B. Moore, *Chem. Rev.*, **2004,** 104, 4535-4585.

[36] V. Ramani, H. R. Kunz, J. M. Fenton, *J. Membr. Sci.*, **2005,** 266, 110-114.

[37] N. G. Boyle, V. J. McBrierty, D. C. Douglass, *Macromolecules*, **1983,** 16, 75-80.

[38] T. A. Zawodzinski, M. Neeman, L. O. Sillerud, S. Gottesfeld, *J. Phys. Chem.*, **1991,** 95, 6040-6044.

[39] K. D. Kreuer, *Chem. Mater.*, **1996,** 8, 610-641.

[40] G. Ye, N. Janzen, G. R. Goward, *Macromolecules*, **2006,** 39, 3283-3290.

[41] P. Atkins, *Physical Chemistry*, sixth edition, Oxford university press, **1999.**

[42] H. Wang, B. A. Holmberg, L. Huang, Z. Wang, A. Mitra, J. M. Norbeck, Y. Yan, *J. Mater. Chem.*, **2002**, 12, 834-837.

[43] G. R. Goward, M. F. H. Schuster, D. Sebastiani, I. Schnell, H. W. Spiess, *J. Phys. Chem.* B, **2003**, *106*, 9322-9334.

Chapter 5

Solid State NMR Spectroscopic Characterization of Zirconium Phosphate

This chapter is being prepared for submission. The co-author is G. R. Goward. I have initially prepared the manuscript. G. R. Goward and I are revising it for submission. My contribution to this chapter includes the sample preparation, NMR experiments, the proton conductivity measurements, and the understanding of the formation of pyrophosphate in ZrP under different conditions, as well as of the conductivity difference between α-ZrP, anhydrous α-ZrP and amorphous ZrP. In this chapter, our ^{1}H NMR studies demonstrated that both the acid proton and the water proton in α-ZrP are not mobile at room temperature. Compared with the α-ZrP, the anhydrous α-ZrP presented an even stronger dipolar coupling with the acid proton, which may be one of the reasons for its much lower proton conductivity. In contrast, the amorphous ZrP displayed a much higher conductivity than α-ZrP, which could be due to the proton exchange between the acid group and the residual water. The formation of pyrophosphate by condensing monohydrogen phosphate generally takes place at a temperature above ~ 400 °C. However, with the presence of strong acid, this can occur even at 160 °C.

5.1 Introduction

The acid phosphates of tetravalent metals have been extensively investigated over the past decades because of their ion-exchange properties. [1, 2, 3] Among many tetravalent metal phosphates, the zirconium phosphate (ZrP) received much attention, regarding its synthesis, [4-7] intercalation chemistry, [8-11] and ion-exchange properties. [12, 13] Compared with the SiO_2, the ZrP itself is a proton conductor, which makes it even more promising for the preparation of Nafion® composites. Thus, it is used as a dopant in this thesis to prepare Nafion/ZrP composites.

The conductivities of crystalline zirconium phosphate (α-ZrP ($Zr(HPO_4)_2 \cdot H_2O$)) with different degree of crystallinity have been invesigated. [14] The reported conductance of α-ZrP decreases with increase in the structural order. This is believed to be due to the significant conduction of surface protons relative to those in the interior. Thus, the fully hydrated glassy ZrP prepared via a sol-gel process presents a conductivity of 10^{-2} S/cm at room temperature. [15] However, detailed information regarding the proton dynamics of ZrP is still needed in order to fully understand the conductivity of both the α-ZrP and the glassy ZrP.

Solid state NMR can provide valuable information concerning proton mobility of proton conductors on the molecular level. The Back-to-Back (BaBa) pulse sequence, [16, 17] which creates double quantum coherence (DQC) to recouple the proton dipolar coupling removed in a regular single pulse MAS experiment, can be used to study proton mobility of the ZrP. In the case of presence of multiple rigid proton sites, the rotor-synchronized 2D DQ MAS experiment can be used to achieve the information regarding the correlation of dipolar couplings between proton sites. [18] More importantly, quantitative information regarding these dipolar couplings can be obtained using a non-rotor synchronized 2D DQ MAS experiment. [19] By fitting the sideband patterns extracted from the obtained 2D spectrum, dipolar coupling constants can be obtained. These dipolar coupling constants can then be used to analyze the mobility of protons by comparing them with the calculated dipolar coupling constants based on available crystallographic data.

In this chapter, ^{1}H NMR was used to study the proton dynamics of the ZrP. The dependence of proton mobility on temperature was investigated using variable temperature experiments. The proton mobility of ZrP is studied by rotor-synchronized BaBa experiments. A non-rotor-synchronized BaBa experiment was used to achieve the dipolar coupling contants of proton pairs. The changes of phosphorus environments in ZrP treated under different temperatures were studied using ^{31}P NMR. The obtained NMR results were discussed to understand the conductivities of ZrP. The studies of ZrP in this chapter will provide important information for the investigation of Nafion/ZrP composites (in Chapter 6).

5.2 Experimental

5.2.1 Preparation of ZrP

The α-ZrP was prepared according to the literature. [20] The 1M $ZrOCl_2$ was dropwise added into the 1M H_3PO_4 solution. The mixture was then filtered to obtain the precipitate of amorphous ZrP. The residual H_3PO_4 in the ZrP was removed by repeatedly washing the precipitate in water until no phosphorus signal for free acid was observed in the solid state ^{31}P NMR. The obtained amorphous ZrP were then refluxed for ten days in ~ 12M H_3PO_4. Some small flakes of α-ZrP were obtained after the refluxing. The excess acid in the α-ZrP was also removed by washing in water until no phosphorus signal for the free acid was observed in the solid state ^{31}P NMR. Both the amorphous ZrP and the α-ZrP were first dried in vacuum at room temperature. Then some of these samples were treated at 800 °C and 1100 °C for 6 hrs under N_2, respectively. To study the interaction of strong acid with the amorphous ZrP, 1M H_2SO_4 was added in the ZrP. The mixture was then dried under 160 °C for 1 day. For comparison, the amorphous ZrP without H_2SO_4 was also treated under same conditions.

5.2.2 X-ray powder diffraction

Powder x-ray diffraction measurements were performed on a Bruker D8 Advance powder diffractometer. The step was 0.04° and the step time was 3 s.

5.2.3 Thermal analysis

A Netzsch STA 409 thermogravimetric analyzer was used for the thermal analysis between room temperature and 1100 °C, with a heating rate of 5 °C/min and in an Argon flow. The samples had been dried in vacuum at room temperature before the thermal studies.

5.2.4 Infrared spectroscopy

The infrared absorption spectra were recorded on Bio-Rad FTS-40 Fourier transform IR spectrometer with a spectral resolution of 4 cm^{-1} between 4000 and 400 cm^{-1}. The powders were pressed into KBr pellets.

5.2.5 ^{1}H NMR

^{1}H solid state NMR experiments were performed on a Bruker AV 500 spectrometer at a ^{1}H Larmor frequency of 500.13 MHz. A 2.5 mm diameter rotor was used for ZrP samples spun at 25 kHz. The recycle delay varies with samples from 5 to 10 s. The spectra were referenced to adamantane (1.63 ppm for ^{1}H). Solid state ^{1}H

NMR spectra were acquired with a 90° pulse length of 2.5 μs. The rotor-synchronized DQF MAS spectra were recorded using the Back-to-Back (BaBa) pulse sequence, with τ_{exc} equal to one rotor period, τ_r and 512 scans. For the rotor-synchronized 2D DQ MAS experiment, the t_1 increment was equal to one rotor period. In the non-rotor-synchronized 2D DQ MAS experiment, the t_1 increment was 1.5 us. Four rotor periods were used for excitation/reconversion of DQ coherence. [19] The sideband patterns were obtained by extracting the columns for each proton resonance at F_2 dimension. Subsequently, they were fitted using a MATLAB program to achieve dipolar coupling constants.

5.2.6 ^{31}P NMR

^{31}P solid state NMR experiments were performed on a Bruker AV 500 spectrometer at a ^{31}P Larmor frequency of 202.48 MHz. The spectra were referenced to 85% H_3PO_4 (0 ppm for ^{31}P). The recycle delay varies with samples from 60 to 300 s. Both a 2.5 mm rotor and a 4 mm rotor were used to spin samples at 25 kHz and 10 kHz, respectively. The spectra were acquired with a 90° pulse length of 4 μs. In the cross polarization (CP) experiments, the contact time varies from 0.5 ms to 6 ms. A recycle delay of 8 s was used and 2560 scans were used to average the signal. The ^{31}P-^{1}H heteronuclear correlation (HETCOR) NMR experiments were performed to study the correlation between the phosphorus and the proton. The number of slices is

96 and the signal for each slice was average by 80 scans.

5.2.7 Conductivity measurement

The conductivity was measured by impedance spectroscopy. The ZrP powders, which were dried under vacuum at room temperature, were pressed into pellets with a diameter of ~ 13 mm and a thickness of 1~2 mm. An AUTOLAB PGSTAT30 impedance analyzer was used for acquisition of impedance spectra. The instrument was used in potentiostatic mode with an AC potential amplitude of 0.01 V over a frequency range of 10 to 500,000 Hz. The conductivity was measured with two stainless steel electrodes in a sealed oven with desiccants under different temperatures. The conductivity (σ) was calculated as follows:

$$\sigma = l / A \cdot R \tag{5-1}$$

Where l, A and R are the thickness, the area and the measured resistance of the ZrP pellet, respectively.

5.3 Results and discussion

5.3.1 Thermal analysis of α-ZrP

Figure 5-1 shows the thermogravimetric analysis of α-ZrP and amorphous ZrP.

The first weight loss for α-ZrP starting at ~110 °C is due to the removal of the crystallization water. The second weight loss starting at ~ 450 °C corresponds to the condensation of monohydrogen phosphates which produces the pyrophosphate ($P_2O_7^{4-}$) and water. In the TGA plot, the total weigh loss of 12.5% for α-ZrP matches the theoretical value of 12% very well. In addition, the X-ray powder diffraction of α-ZrP in Figure 5-2 also shows a good agreement with the literature. [15] Therefore, a well crystallized α-ZrP is obtained in this study.

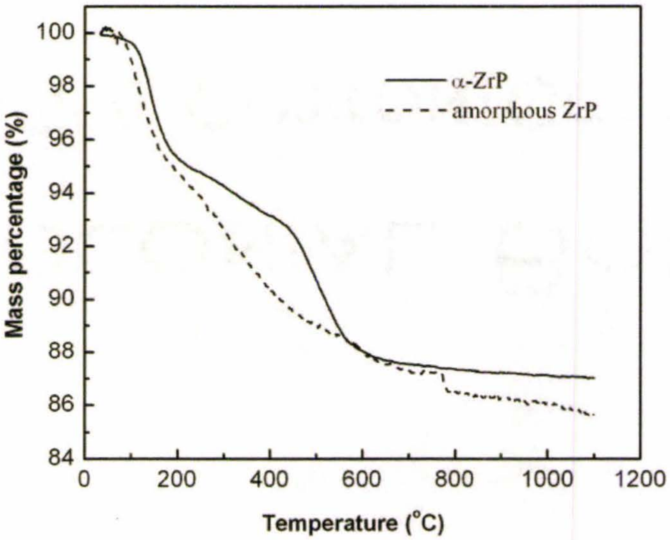

Figure 5-1. Thermogravimetric analysis of α-ZrP and amorphous ZrP under nitrogen atmosphere. The samples have been dried in vacuum at room temperature before the TGA tests.

Compared with the α-ZrP, the amorphous ZrP shows very similar weight loss up to 600 °C, although the two processes for the loss of water and the condensation of monohydrogen phosphates are poorly separated in Figure 5-1. Alberti reported that the condensation of surface acid –POH groups takes place at a temperature above 850 °C. [21] Since the amorphous ZrP is expected to have more surface acid –POH groups than the α-ZrP, the observed weight loss above 800 °C for amorphous ZrP is the result of an analogous condensation.

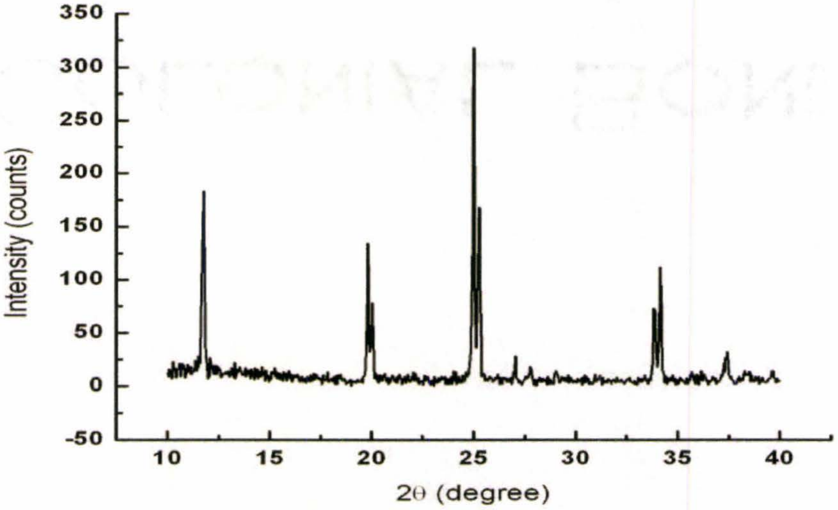

Figure 5-2. XRD patterns of α-ZrP

5.3.2 Proton studies by single pulse ^{1}H NMR experiments

^{1}H NMR is a good probe for the investigation of proton dynamics of ZrP. Using variable temperature ^{1}H NMR experiments, the dependence of proton mobility on temperature can be studied. Figure 5-3 shows the variable temperature ^{1}H NMR spectra of the α-ZrP. It can be seen from the spectrum acquired at room temperature that there are two well resolved proton resonances. The resonance at 8.2 ppm is attributed to the acid proton (P-OH) and the resonance at 3.4 ppm is attributed to the water proton. The resonance with very weak intensity at ~ 0 ppm could result from impurities in the sample. With increasing temperature, the acid proton and the water proton show increased mobility, as indicated by the coalescence at 370 K, clearly indicating an exchange between these protons. This implies that an enhanced temperature improves the proton conductivity of α-ZrP by allowing the exchange between the acid proton and the water proton, not only by increasing their individual proton mobility. It should be also noticed that the spectrum at 374 K in Figure 5-3 still shows intensity for the resonance of the crystallization water. This suggests that the exchange between the acid proton and the water proton is not significant and not all water molecules are involved in the exchange. Moreover, the peak for the coalesced resonance is still broad. According to the frequency difference of the two resonances, the exchange rate may be just slightly above 2400 Hz at this temperature. However, a further enhanced temperature for increasing proton exchange, therefore proton conductivity, is not feasible, since this temperature is near to the temperature at which the crystallization water of α-ZrP starts to be removed.

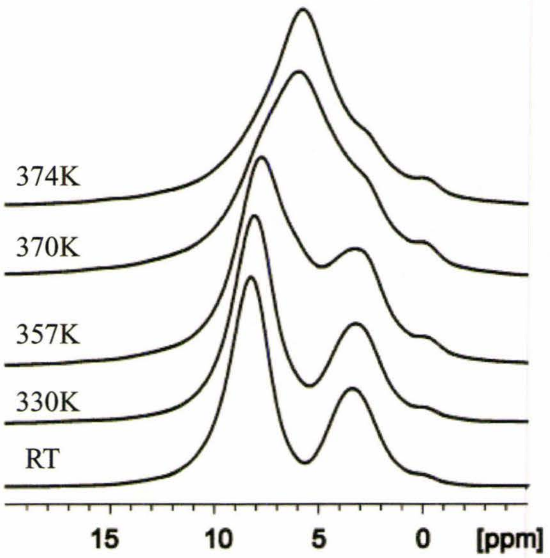

Figure 5-3. ^{1}H MAS NMR of α-ZrP at variable temperature, MAS=25 kHz

Although the removal of crystallization water in α-ZrP starts at the temperature of ~ 110 °C as shown by the TGA data in Figure 5-1, the crystallization water was still observed in the ^{1}H NMR of α-ZrP which was treated at 200 °C. Thus, in this work the α-ZrP was treated at 250 °C to fully remove the crystallization water for the preparation of the anhydrous α-ZrP. The obtained ^{1}H NMR spectrum for this compound is shown in Figure 5-4 (b). It is clear that the resonance for the crystallization water has been completely removed. The remaining resonance is attributed to the acid proton. This proton is comparatively immobile since it was observed in the DQF MAS NMR spectra (not shown here). The spectrum shown in Figure 5-4 (a) is for the sample of amorphous ZrP dried at 160 °C. Since this treatment was not sufficient to entirely remove all water molecules in the amorphous ZrP, as shown by the TGA plot in Figure 5-1, many hydrogen bonds will form between the acid proton and the residual water, which broadens the spectrum dramatically. Therefore, the observed resonance includes both the acid proton and the water proton, as opposed to only acid proton in the case of anhydrous α-ZrP. This proton resonance becomes very narrow when the amorphous ZrP is hydrated, due to fast exchange between the acid proton and the water proton.

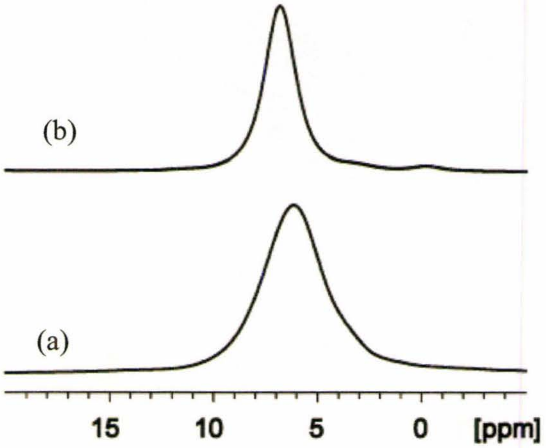

Figure 5-4. ^{1}H MAS NMR of (a) amorphous ZrP treated at 160 °C and (b) α-ZrP treated at 250 °C, MAS=25 kHz

5.3.3 Proton studies by double quantum coherence ^{1}H NMR experiments

The proton mobility in ZrP was also studied using the Back-to-Back pulse sequence. The ^{1}H DQF MAS NMR spectrum for α-ZrP was shown in Figure 5-5 (b). Compared with the spectrum by a regular single pulse experiment in Figure 5-5 (a), the DQF MAS NMR spectrum shows both the acid proton and the water proton, which indicates that these protons do not have high mobility at room temperature.

This is consistent with the above variable temperature experiments in which proton exchange between them are only observed at temperatures above 370 K. The correlation of dipolar coupling between protons was then studied by a rotor-synchronized 2D DQ MAS experiment. The spectrum was displayed in Figure 5-6. The peaks on the diagonal line indicate the dipolar coupling between the same types of protons. Thus, in the α-ZrP both the acid proton and the water proton dipolar couple with themselves. The off diagonal peaks indicate the dipolar coupling between the acid proton and the water proton. This is consistent with crystal structure in which the acid proton forms hydrogen bonds with water. [22]

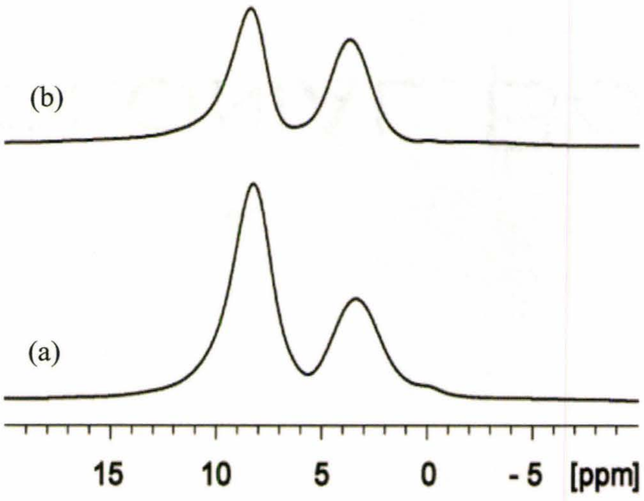

Figure 5-5. ^{1}H NMR of α-ZrP (a) MAS (b) DQF MAS $\tau=\tau_r$, MAS=25 kHz

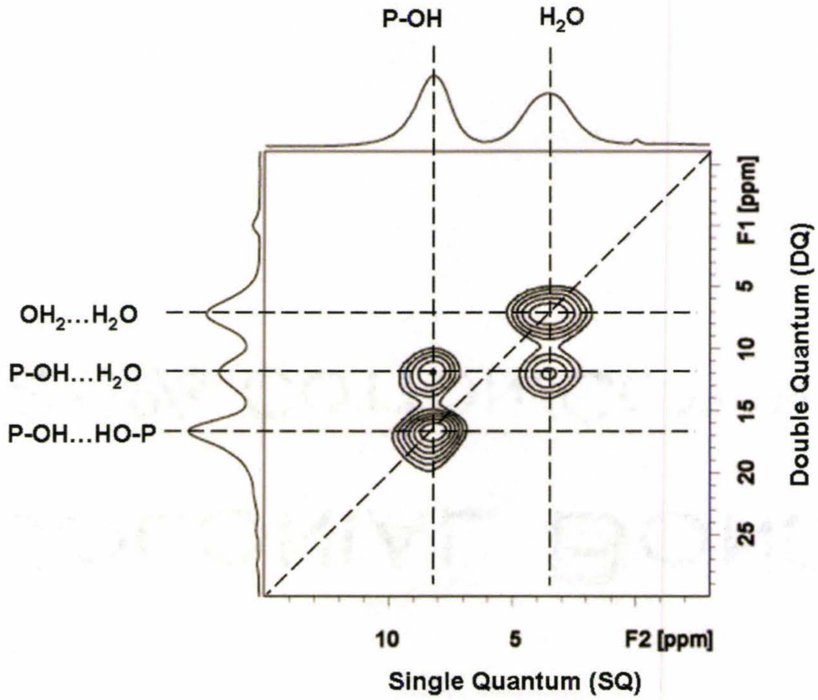

Figure 5-6. ^{1}H 2D DQ MAS NMR of α-ZrP, $\tau=\tau_r$, MAS=25 kHz

Since quantitative information about the proton dipolar coupling in α-ZrP is very helpful to understand the proton dynamics, this information is desired. Using a non-rotor-synchronized 2D DQ MAS experiment, the DQ spinning sideband patterns, which are extracted columns from the resulting 2D DQ MAS spectrum, were obtained for the protons in α-ZrP. They are shown in Figure 5-7. Generally, if a spin pair is not coupled to other spins, the MAS sideband patterns should consist of only odd-order sidebands. In real systems, perturbing interactions with other spins are often present, which results in weak intensities at the centerband and the even-order sidebands in the sideband patterns. [23] The weak intensities do not cause significant uncertainty for the fitted dipolar coupling constants. [19, 24] Therefore, the obtained dipolar coupling constants shown in Table 5-1 can be used to analysis the proton dynamics in α-ZrP.

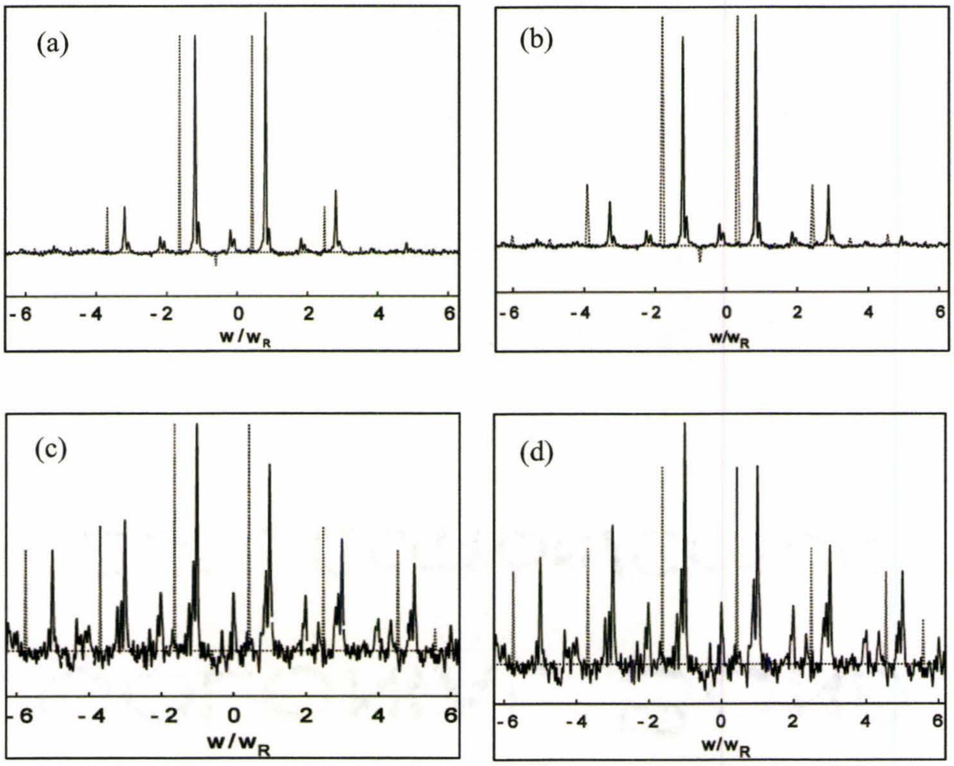

Figure 5-7. Extracted columns from non-rotor-synchronized ^1H 2D DQ MAS spectrum of α-ZrP under MAS=25 kHz, showing the DQ spinning sideband patterns. (a) and (b) are both for the acid protons at 8.2 ppm. They fit the negative and positive odd sidebands, respectively. The obtained dipolar coupling constants are 4650 Hz and 4450 Hz, respectively. (c) and (d) are both for the resonance of water proton at 3.4 ppm. They fit the negative and positive odd sidebands, respectively. The obtained dipolar coupling constants are 8800 Hz and 9000 Hz, respectively. In both cases for different proton sites, the fitting for negative and positive sidebands allows the estimation of errors, since the fitting itself is very sensitive to the change of dipolar coupling constant.

The data in Table 5-1 compares the dipolar coupling determined from solid state NMR experiments to the calculated couplings determined based on H-H distance in the known X-ray structure. By comparing these values, the impact of local dynamics on the coupling can be determined. A ratio of the D_{ij} obtained by the two methods is used as a measure of proton dynamics in the α-ZrP. The very low ratio of 0.22 for water protons implies that the two protons of the water molecule are moving rapidly, which dramatically decreases the measured dipolar coupling constant. In contrast, the high ratio of 0.86 for acid protons indicates that they have slower dynamics. The overall effect of the fast dynamics of water proton and the slow dynamics of acid proton results in the observed moderate ratio of 0.67 for the ratio of dipolar coupling constants of the water proton and the acid proton.

Table 5-1. The proton dipolar coupling constants of α-ZrP and anhydrous α-ZrP

Proton pairs	α-ZrP			Anhydrous α-ZrP
	H_2O / H_2O	P–OH / H_2O	P–OH / P–OH	P–OH / P–OH
D_{ij} (Hz) by SSNMR	8900±100	5000±150	4550±100	8400±100
D_{ij} (Hz) calculated from X-ray data [22]	39600	7410	5320	—
Ratio of D_{ij} (SSNMR) to D_{ij} (X-ray)	0.22	0.67	0.86	—

Interestingly, the dipolar coupling constant between acid protons in anhydrous α-ZrP is even stronger than that in the α-ZrP. This suggests a decrease in acid proton mobility and/or distance between the layers of anhydrous α-ZrP. It has been reported that the layer spacing for anhydrous α-ZrP is shorter by about 1.5 ~ 2 % than the α-ZrP. [25, 26] Obviously, this small difference in the distance between layers is not enough to result in the large difference in proton dipolar coupling constants. This implied a decrease in acid proton mobility in the anhydrous α-ZrP, which is consistent with a lower proton conductivity under same condition for the anhydrous α-ZrP as compared to the α-ZrP itself.

5.3.4 Infrared spectra of α-ZrP

Figure 5-8 shows the infrared absorption spectra of α-ZrP treated at different temperatures. It can be seen clearly that the bands at 3595 cm^{-1}, 3512 cm^{-1} and 3158 cm^{-1}, which are assigned to the H-O-H stretching in Figure 5-8(a), disappear from Figure 5-8(b) and Figure 5-8(c). This is due to the complete removal of crystallization water from α-ZrP. It can also be seen that the band at 3374 cm^{-1} assigned to the stretching of PO-H in Figure 5-8(a) [27] dramatically decreased and shifted to 3457 cm^{-1} in Figure 5-8(b), which is attributed to the condensation of monohydrogen phosphates, producing pyrophosphate. As a result, the bands at 747 cm^{-1} and 980 cm^{-1}, assigned to the bending and the stretching vibration of P-O-P respectively, [28] were observed clearly in Figure 5-8(c). The weak intensity for the band of the P-O-P bending vibration and the unresolved band for stretching vibration in Figure 5-8(b) indicate that the zirconium pyrophosphate formed at 800 °C has very low degree of crystallinity. The IR spectra of amorphous ZrP treated under same temperature were also measured (not shown here). It was found that the amorphous ZrP treated at temperatures of 800 °C and 1100 °C showed spectra very similar to those of α-ZrP treated under the same temperatures. This indicates a similar structure of the resulting pyrophosphates. However, compared with the well resolved stretching vibration of O-H in the α-ZrP in Figure 5-8(a), the amorphous ZrP dried in vacuum at room temperature presented a very broad and unresolved band for the stretching of O-H. As indicated by the ^1H NMR in Figure 5-4(a), this is due to the existence of many different hydrogen bonds between acid protons and the residual waters.

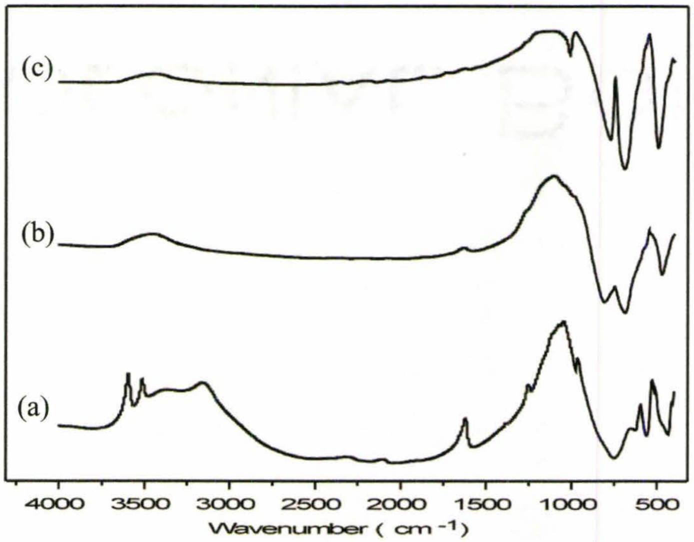

Figure 5-8. IR of α-ZrP treated at different temperatures (a) vacuum dried at room temperature (b) treated at 800 °C (c) treated at 1100 °C

5.3.5 ^{31}P NMR of ZrP

^{31}P NMR can be used as a probe to study the ZrP, since the structural change of ZrP will result in different phosphorus environments. The investigation of phosphorus environments in ZrP will also help the studies of phosphorus environments in Nafion/ZrP composites in Chapter 6. Figure 5-9 shows the ^{31}P NMR spectra of α-ZrP treated under different temperatures. The α-ZrP dried at room temperature only shows a single phosphorus resonance at -18.8 ppm in Figure 5-9(a), which is consistent with the literature. [29, 30] Since two crystallographically inequivalent phosphorus atoms have been observed, this is believed to be due to the sufficient similarity of the electronic environments of the two phosphorus nuclei. [23] When the crystallization water is fully removed from the α-ZrP at 250 °C, the resulting anhydrous α-ZrP shows a lower phosphorus resonance at -21.4 ppm in Figure 5-9(b), due to the deletion of hydrogen bonds between the phosphates and the crystallization water. A further enhanced temperature for treating the α-ZrP results in the formation of pyrophosphate by condensation of monohydrogen phosphtates, showing a very broad resonance centered at ~ -33 ppm in Figure 5-9(c). However, under this temperature only a small amount of the resulting pyrophosphate starts to show ordered structure indicated by a less broad resonance at -38.7ppm. This is in good agreement with the above IR spectra shown in Figure 5-8(b), in which the low degree of crystallinity was indicated by the weak intensity of the band for the P-O-P bending vibration. For the α-ZrP treated at the higher temperature of 1100 °C, the peaks in Figure 5-9(d) are well resolved. These sharp peaks are consistent with the literature, [31] indicating that the zirconium pyrophosphate has a highly order structure. The conversion of monohydrogen phosphate into pyrophosphate can take place at much lower temperature with the presence of strong acid (see below).

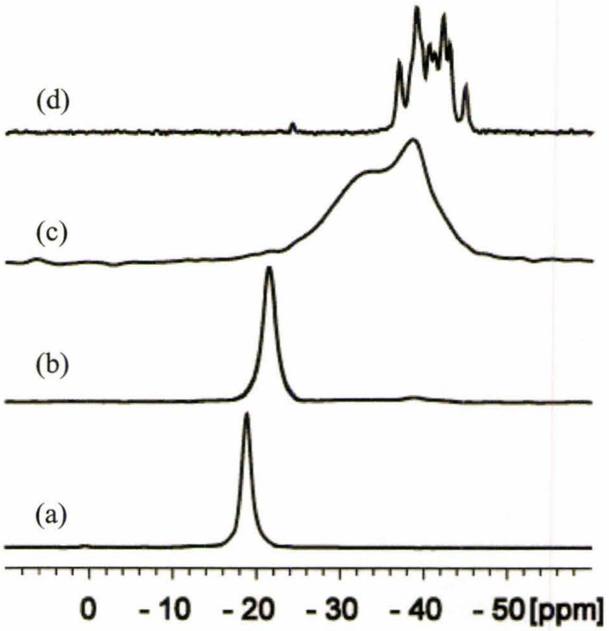

Figure 5-9. ^{31}P MAS NMR of α-ZrP treated at different temperatures (a) room temperature, MAS=10 kHz (b) 250 °C, MAS=25 kHz (c) 800 °C, MAS=25 kHz (d) 1100 °C, MAS=25 kHz

Similarly, the ^{31}P NMR was also used to study the amorphous ZrP treated at different temperatures. The spectra are shown in Figure 5-10. The amorphous ZrP dried in vacuum at room temperature shows clearly three phosphorus resonances in Figure 5-10(a). The peak with the strongest intensity at -21.7 ppm is assigned to the phosphorus atom bonded with one hydrogen atom and three zirconium atoms through oxygen atoms (denoted as $HOP(OZr)_3$). This phosphorus site has the similar structure as α-ZrP. The other two resonances at -13.3 ppm and -27.4 ppm are assigned to the phosphorus atoms bonded with two and four zirconium atoms through oxygen, respectively. Thus, they are denoted as $(HO)_2P(OZr)_2$ and $P(OZr)_4$, respectively. The two phosphorus sites could result from the γ-ZrP in which the zirconium is octahedrally coordinated with four oxygen atoms of a phosphate group and two oxygen atoms of a dihydrogen phosphate group. [1, 20, 32] As indicated by the Figure 5-9(b), the treatment of amorphous ZrP at 160 °C only broadens the phosphorus resonances, which could be mainly due to the increased dipolar coupling from protons with decreased mobilities ascribed to much reduced water in the ZrP. Similar to α-ZrP, the amorphous ZrP treated at 800 °C shows a very broad resonance centered at -31.7 ppm in Figure 5-10(c), indicating the formation of zirconium pyrophosphate. Nevertheless, the zirconium pyrophosphate with ordered structure is not observed in Figure 5-10(c), which is different from the spectrum for α-ZrP sample treated under same temperature. As discussed above, this is due to the amorphous ZrP having more surface –POH groups which generally condense at temperature above 800 °C. However, the amorphous ZrP treated at a temperature of 1100 °C exhibits almost the same spectrum as the α-ZrP treated under same temperature, which suggests that both samples completely converted into the zirconium pyrophosphate with highly ordered structure at this temperature.

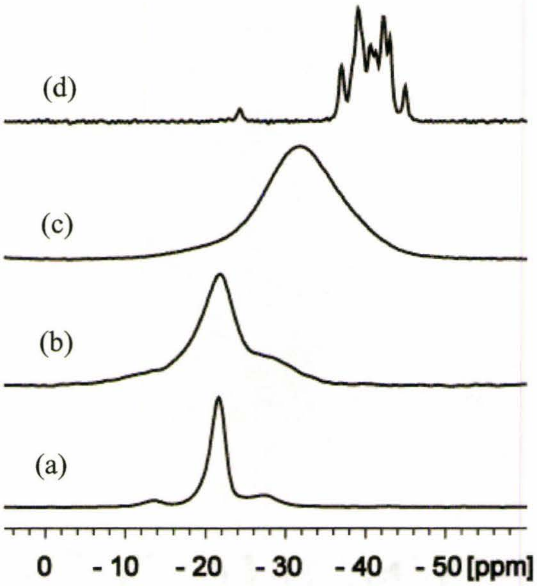

Figure 5-10. ^{31}P MAS NMR of the amorphous ZrP treated at different temperature (a) room temperature, MAS=10kHz (b)160 °C, MAS=10 kHz (c) 800 °C, MAS= 10 kHz (d)1100 °C, MAS=25 kHz

Since the ZrP is used as a dopant in the Nafion/ZrP composite and the Nafion has high acidity, it is necessary to understand the properties of ZrP in strong acid environment. Therefore, the ZrP was treated with the presence of sulfuric acid solution. Surprisingly, the conversion of monohydrogen phosphate into pyrophosphate can take place at a much lower temperature with the existence of the strong acid. The Figure 5-11 shows the ^{31}P spectra of the amorphous ZrP which has been dried at 160 °C after mixed with the 1M sulfuric acid. Compared with the amorphous ZrP treated under same temperature without sulfuric acid in Figure 5-10(b), the amorphous ZrP with

H_2SO_4 dried at 160 °C shows a very strong resonance at -41.2 ppm. This resonance, which does not show any intensity in the CPMAS spectra in Figure 5-11(a) and Figure 5-11(b), should be attributed to the zirconium pyrophosphate with ordered structure. Similar to amorphous ZrP treated at 800 °C, this sample also shows a resonance at -32 ppm in Figure 5-11(a). The weak intensity for this resonance in CPMAS spectra in Figure 5-11(b) and Figure 5-11(c) could indicate that this phosphorus site from pyrophosphate is near to some surface –POH groups which were not condensed. Clearly, the strong intensity for the resonance at -25 ppm in Figure 5-11(b) and Figure 5-11(c) suggests that the phosphorus site should be from the phosphate in which the phosphorus bonds with three zirconium atoms and one hydrogen atom through oxygen ($HOP(OZr)_3$). The other two resonances at -16.3 ppm and -7.1 ppm can be respectively assigned to the singly and doubly protonated phosphorus which has the structure of $HOP(OZr)_3$. The weak intensity of the peak at -16.3 ppm in Figure 5-11(b) and Figure 5-11(c) suggests that the proton which protonates the phosphate could be relatively more mobile and/or further away from the phosphorus, compared with the acid proton in $HOP(OZr)_3$. Therefore, the resonance at -7.1 ppm was not observed.

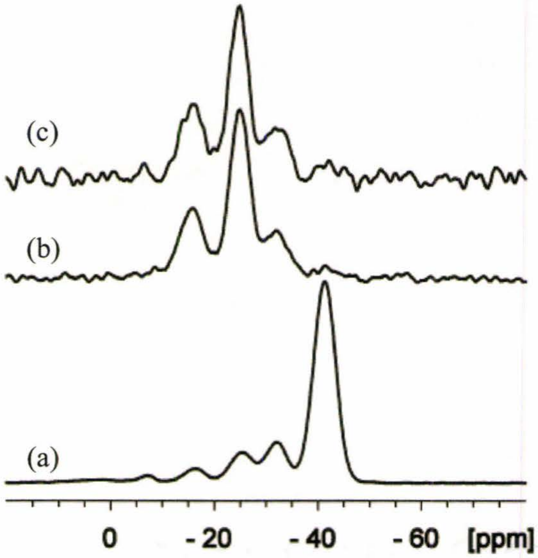

Figure 5-11. ^{31}P NMR of ZrP-gel with 1M H_2SO_4 treated at 160 °C, MAS=25 kHz (a) ^{31}P MAS (b) ^{31}P-^{1}H CPMAS, contact time= 0.5 ms (c) ^{31}P-^{1}H CPMAS, contact time= 6 ms.

5.3.6 ^{31}P-^{1}H HETCOR of α-ZrP

Since there are two proton sites in the α-ZrP, it is useful to achieve the information regarding the dipolar coupling between the proton and the phosphorus. This information can be obtained from ^{31}P-^{1}H HETCOR NMR experiments. The spectrum is shown in Figure 5-12. It can be seen that the acid proton has strong dipolar coupling with the only phosphorus in the α-ZrP, which is consistent with the observed rigidity of acid proton. Nevertheless, the dipolar coupling between the water proton and the phosphorus is weaker, as shown by the weak intensity in the ^{31}P-^{1}H HETCOR NMR spectrum. This weak dipolar coupling could be due to both the higher mobility of water proton but also the longer distance between the phosphorus and the water proton.

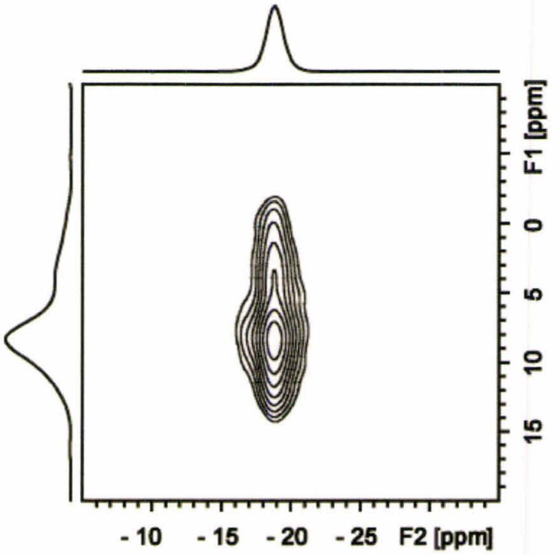

Figure 5-12. ^{31}P-^{1}H HETCOR NMR of α-ZrP, MAS=10 kHz, contact time =3ms

5.3.7 Conductivity of ZrP

Since the information regarding proton dynamics of ZrP provided by solid state NMR is more suitable for describing short range proton motion, other information for describing the long range proton motion, such as proton conductivity, is needed. The proton conductivity of ZrP can be measured using impedance spectroscopy. Figure 5-13 shows the impedance spectra of amorphous ZrP and α-ZrP at 20 °C. The fitting of the spectrum of α-ZrP is presented in Figure 5-14, which gives the resistance of this sample, from which the conductivity was obtained. The conductivities for α-ZrP, anhydrous α-ZrP and amorphous ZrP at different temperatures are presented in Figure 5-13. At 100 °C, the α-ZrP has a conductivity of 5.4×10^{-7} S/cm. According to the

TGA results in Figure 5-1, the α-ZrP under investigation has ~ 0.83 water molecules per formula weight. Thus, this conductivity is comparable with the result reported in the literature, in which the α-ZrP with 0.67 water molecules per formula weight has a conductivity of 1×10^{-7} S/cm at the same temperature. [33] An increase in conductivity with increasing surface hydration has been observed in literature. [34, 35] However, the conductivity of α-ZrP reported here would not have significant contribution from water on its surface, since the water on the surface has been minimized by treating the α-ZrP in vacuum and the ^{1}H NMR spectra clearly show resonances only for the acid proton and the proton of crystallization water.

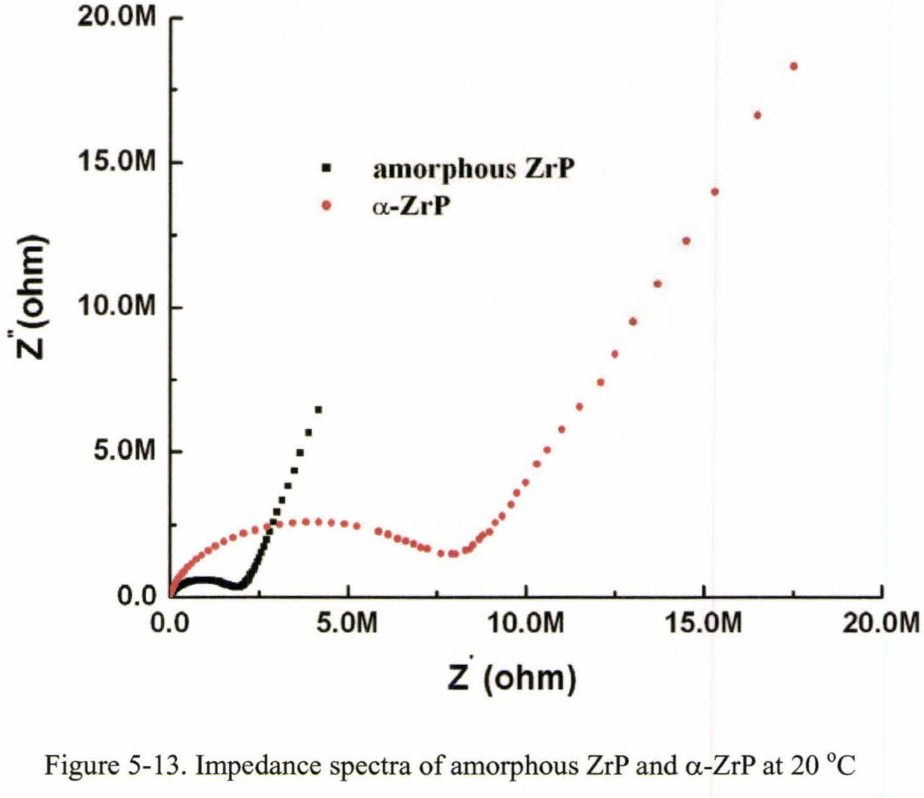

Figure 5-13. Impedance spectra of amorphous ZrP and α-ZrP at 20 °C

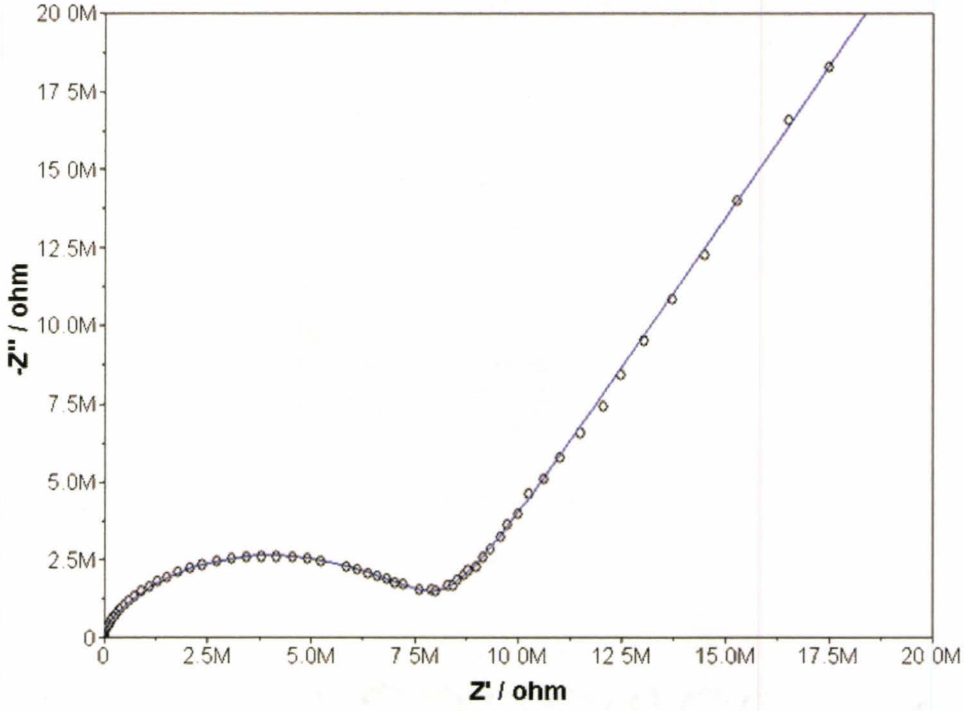

Figure 5-14. An example of fitting the impedance spectrum of α-ZrP to obtain its resistance. The spectrum was acquired at 20 °C. The obtained resistance is 7.3 MΩ.

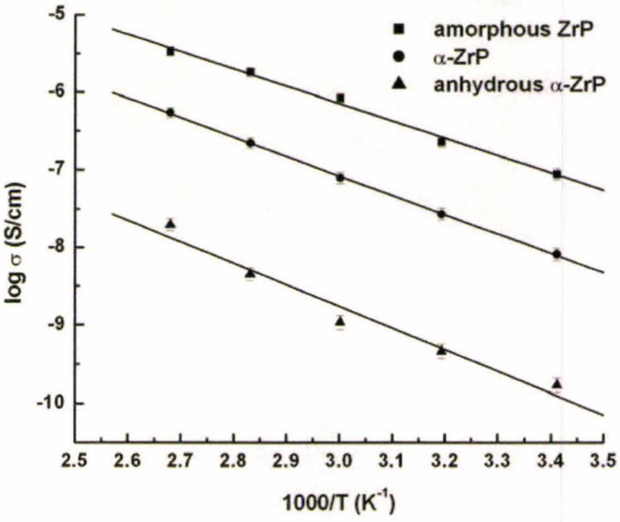

Figure 5-15. Conductivity of ZrP at different temperatures. The α-ZrP and amorphous ZrP were dried in vacuum at room temperature before measured. The anhydrous α-ZrP was measured after it was prepared by treating the α-ZrP at 250 °C for 24 hrs.

Compared with α-ZrP, the amorphous ZrP presents almost one order of magnitude higher proton conductivity, although they showed similar weight loss of water below 200 °C in Figure 5-1. It has been reported that the conductivity of α-ZrP decreases with increasing the structural order. [14] Since the amorphous ZrP would be expected to have much lower structural order, and consequent higher number of surface acid –POH groups, its proton conductivity is much higher than that of α-ZrP. Interestingly, the anhydrous α-ZrP shows one order of magnitude lower proton conductivity than α-ZrP. This is again consistent with the literature in which the dehydrated α-ZrP has much lower conductivity than α-ZrP. [25] The very low conductivity for anhydrous α-ZrP may be also explained by our obtained proton dipolar coupling constants. As discuss above, the acid proton in anhydrous α-ZrP was found to have lower mobility, based on its strong D_{ij}. Consistently, its proton conductivity is lower than that of α-ZrP. In Figure 5-15, the fitted activation energy shows the same trend as the conductivity. The amorphous ZrP presents an activation energy of 42.5 kJ/mol, which is lower than 47.9 kJ/mol for α-ZrP and 53.1 kJ/mol for anhydrous α-ZrP. Nevertheless, unlike the amorphous ZrP and the α-ZrP which lose water near 100 °C, the anhydrous α-ZrP could be better for a proton conductor at higher temperature since it is stable up to 250 °C.

5.4 Conclusions

The ^1H NMR studies indicate that both the acid proton and the water proton in α-ZrP are not mobile at room temperature. These protons start to exchange at temperatures near to 100 °C. Due to the insignificant and/or the slow exchange, its conductivity does not show a fast increase near this temperature. Compared with the α-ZrP, the anhydrous α-ZrP presented an even stronger dipolar coupling for the acid proton, which may be one of the reasons for that the anhydrous α-ZrP has much lower proton conductivity. In contrast, the amorphous ZrP displayed a much higher conductivity than α-ZrP. This is due to the network of hydrogen bonds between the acid proton and the residual water, which allows proton hopping on the surface of amorphous ZrP. The production of pyrophosphate by condensing monohydrogen phosphate generally takes place at a temperature above ~ 400 °C. However, with the presence of strong acid, the pyrophosphate can be obtained even at 160 °C.

The ^{1}H NMR studies of ZrP in this chapter will be helpful for the preparation of Nafion/ZrP composites by choosing the ZrP with faster proton dynamics. It will also help the understanding of proton mobilities of the composites in the next chapter. In addition, the information from ^{31}P NMR of ZrP will be useful for understanding the phosphorus environments in Nafion/ZrP composites.

5.5 References

[1] H. Benhamza, P. Barboux, A. Bouhaouss, F. A. Josien, J. Livage, *J. Mater. Chem.*, **1991**, 1, 681-684.

[2] A. Ahrland, J. Albertson, *Acta Chem. Scand.*, **1969**, 23, 1446.

[3] A. Clearfield, Ann. *Rev. Mater. Sci.*, **1984**, 14, 205-229.

[4] A. M. K. Andersen, P. Norby, J. C. Hanson, T. Vogt, *Inorg. Chem.*, **1998**, 37, 876-881.

[5] C. Trobajo, S. A. Khainakov, A. Espina, J. R. Garcia, *Chem. Mater.*, **2000**, 12, 1787-1790.

[6] G. Alberti, U. Costantino, R. Millini, G. Perego, R. Vivani, *J. Solid State Chem.*, **1994**, 113, 289-295.

[7] J. Jimenez-Jimenez, P. Maireles-Torres, P. Plivera-Pastor, E. Rodriguez-Castellon, A. jimenez-Lopez, D. J. Jones, J. Roziere, *Adv. Mater.*, **1998**, 10(10), 812-814.

[8] N. Bestaoui, N. A. Spurr, A. Clearfield, *J. Mater. Chem.*, **2006**, 16, 759-764.

[9] A. Hayashi, Y. Fujimoto, Y. Ogawa, H. Nakayama, M. Tsuhako, *J. Colloid Interface Sci.*, **2005**, 283, 57-63.

[10] M. Kaneno, S. Yamaguchi, H. Nakayama, K. Miyakubo, T. Ueda, T. Eguchi, N. Nakamura, *Inter. J. Inorg. Mater.*, **1999**, 1, 379-384.

[11] D. J. Maclachlan, K. R. Morgan, *J. Phys. Chem.*, **1992**, 96, 3458-3464.

[12] J. Albertsson, A. Oskarsson, R. Tellgren, J. O. Thomas, *J. Phys. Chem.*, **1977**, 81, 1574-1578.

[13] A. Clearfield, W. L. Duax, J. M. A. S. Medina, G. D. Smith, J. R. Thomas, *J. Phys. Chem.*, **1969**, 73, 3424-3430.

[14] G. Alberti, M. Casciola, U. Costantino, G. Levi, G. Ricciardi, *J. Inorg. Nucl. Chem.*, **1978**, 40, 533.

[15] Y. Abe, G. Li, M. Nogami, T. Kasuga, L. L. Hench, *J. Electrochem. Soc.*, **1996**,

143, 144-147.

[16] M. Feike, D. E. Demco, R. Graf, J. Gottwald, S. Hafner, H. W. Spiess, *J. Magn. Reson. A.* , **1996**, 122, 214-221.

[17] I. Schnell, H. W. Spiess, *J. Magn. Reson.*, **2001**, 151, 153-227.

[18] I. Schnell, *Prog. Nucl. Magn. Reson. Spectrosc.*, **2001**, 39, 191-267.

[19] S. P. Brown, I. Schnell, J. D. Brand, K. Mullen, H. W. Spiess, *J. Am. Chem. Soc.*, **1999**, 121, 6712-6718.

[20] N. J. Clayden, *J. Chem. Soc. Dalton Trans.*, **1987**, 1877-1881.

[21] G. Alberti, M. Casciola, F. Marmottini, R. Vivani, *J. Porous Mater.*, **1999**, 6, 299-305.

[22] J. M. Troup, A. Clearfield, *Inorg. Chem.*, **1977**, 16, 3311-3314.

[23] I. Schnell, H. W. Spiess, *J. Magn. Reson.*, **2001**, 151, 153-227.

[24] T. M. Alam, M. Nyman, B. R. Cherry, J. M. Segall, L. E. Lybarger, *J. Am. Chem. Soc.*, **2004**, 126, 5610-5620.

[25] G. Schuck, R. Melzer, R. Sonntag, R. E. Lechner, A. Bohn, K. Langer, M. Casciola, *Solid State Ionics*, **1995**, 77, 55-62.

[26] G. Alberti, M. Casciola, *Solid State Ionics*, **2001**, 145, 3-16.

[27] K. Segawa, Y. Kurusu, Y. Nakajima, M. Kinoshita, *J. Catal.*, **1985**, 94, 491-500.

[28] K. Segawa, *Mater. Chem. Phys.*, **1987**, 17, 181-200.

[29] D. J. Maclachlan, K. R. Morgan, *J. Phys. Chem.*, **1990**, 94, 7656-7661.

[30] N. Bestaoui, N. A. Spurr, A. Clearfield, *J. Mater. Chem.*, **2006**, 16, 759-764.

[31] I. J. King, F. Fayon, D. Massiot, R. K. Harris, J. S. O. Evans, *Chem. Commun.*, **2001**, 1766-1767.

[32] D. M. Poojary, B. Shpeizer, A. Clearfield, *J. Chem. Soc. Dalton Trans.*, **1995**,

111-113.

[33] M. Casciola, F. Marmottini, *Solid State Ionics*, **1993**, 61, 125-129.

[34] S. Yde-Andersen, J. S. Lundsgarrd, J. Malling, J. Jensen, *Solid State Ionics*, **1984**, 13, 81-85.

[35] M. Casciola, D. Bianchi, *Solid State Ionics*, **1985**, 17, 287-293

Chapter 6

Solid State NMR Spectroscopic Characterization of Nafion/ZrP Composites

This chapter is being prepared for submission to the Journal of Physical Chemistry C. The co-author is G. R. Goward. My contribution to this chapter includes writing the initial draft of the manuscript, and all aspects of the experimental work, including sample preparation of Nafion®/ZrP composites, NMR experiments, conductivity measurements, and the understanding of changes taken place in the composites when dried at 160 °C. In this chapter, the NMR experiments show that the reduced water content in the dried composites results not only in the decreased proton mobility but also changes in phosphorus environments. Both the conversion of monohydrogen phosphate into pyrophosphate and the protonation of monohydrogen phosphate have been observed in composites dried at 160 °C. This resulted in a significant change in the interaction of Nafion112 and ZrP, which is found here to be the reason that the composite presented clearly decreased proton conductivity after it was rehydrated again.

6.1 Introduction

Among many polymer electrolyte membranes (PEMs), Nafion is the one of the most popular PEMs because of excellent chemical and thermal stability, and proton conductivity. [1-4] However, the conductivity decreases dramatically at temperatures above 100 °C due to the dehydration of the PEM. [5] Moreover, a working temperature greater than the glass transition temperature of Nafion (~ 110 °C) will result in the PEM with a poor stability and performance. [6-8] Since a polymer electrolyte membrane fuel cell (PEMFC) working at a high temperature has benefits to both minimizing the catalyst poisoning and improving the electrode kinetics of the oxygen reduction reaction, [9, 10] PEMs which can provide acceptable conductivity at high temperature and low hydration level are desired.

A very promising way to improve the conductivities of PEMs at high temperatures has been demonstrated by the addition of inorganic proton conductors to polymer. For example, it has also been reported that the Nafion/ZrP composites showed a better ionic conductivity than the unmodified Nafion at temperatures greater than 100 °C. [11,12] Compared with the dopant of SiO_2, the ZrP itself is a proton conductor. Its acid proton can participate in proton conduction. Therefore, it is expected to have more contribution to proton conductivity in the resulting composite.

It is believed that the enhanced conductivity could be due to some modifications of polymer microstructure induced by the filled nano-particles of ZrP, instead of their intrinsic proton conductivity. [13] Other authors attributed the difference of performance between the Nafion and the Nafion/ZrP composite to the stronger ionic interaction in the composite, [14, 15] rather than to the additional water adsorbed at the surface of ZrP. Obviously, these interpretations suggested that more detailed information regarding the interaction between the polymer and the ZrP is needed in order to fully understand the observed difference. Solid state NMR can provide us with this type of information, since it can measure the chemical environments of nuclei under investigation on the molecular level. For example, the change in the interaction between protons from both the polymer and the ZrP will result in distinct ^{1}H NMR spectra from which the information regarding the interaction between them can be extracted.

It has been shown in Chapter 5 that amorphous ZrP has better conductivity than the α-ZrP and anhydrous α-ZrP. Therefore, in this chapter the amorphous ZrP is synthesized *in-situ* in Nafion membranes to prepare Nafion/ZrP composites, rather than adding α-ZrP in Nafion solution to prepare the composites. Subsequently, the proton and the phosphorus environments in composites were characterized using ^{1}H NMR and ^{31}P NMR, respectively.

6.2 Experimental

6.2.1 Preparation of Nafion112/ZrP

Treatment of Nafion112 was performed as follows. Nafion112 was first washed in

3% H_2O_2 for 1 hour and then washed in distilled deionized water for another hour, during which time change the water several times. Subsequently, it was washed in 1M H_2SO_4 for 1 hour. Finally, it was again washed in distilled deionized water until a constant pH was obtained. Nafion112/ZrP composite membranes were prepared following the procedure reported by Costamagna. [16] The pretreated Nafion112 was first swollen in MeOH: H_2O (V/V) = 1:1 for 2~3 hours. Subsequently the material was washed in 1M zirconyl chloride solution at 80 °C for variable time, ranging from 2 minutes, to 300 minutes, to control the loading of ZrP. In order to remove excess zirconium chloride, the membrane was quickly rinsed in distilled deionized water and then put in 1M H_3PO_4 at 80 °C overnight. Finally, it was washed in distilled deionized water to remove the excess phosphoric acid. The obtained Nafion112/ZrP composites are denoted as Nafion112/ZrP-2, Nafion112/ZrP-10 and Nafion112/ZrP-300 in this work.

The water content (wt.%) of Nafion112/ZrP composites were determined by the mass difference of the hydrated sample and the dried sample. Thermogravimetric analysis was used to determine the mass percentage of ZrP (wt.%) in the dried composite. It was also used to obtain the mass of residual water to correct the mass of the dried sample in the determination of water content. For solid state NMR studies, the composites were dried at temperatures of 105 and 160 °C. The Nafion112/ZrP-300, which has the highest loading of ZrP in this work, was dried at 160 °C and then rehydrated to investigate the stability of this composite. This sample was denoted as Nafion/ZrP-300 (dried then rehydrated).

6.2.2 ^{1}H NMR

^{1}H solid state NMR experiments were performed on a Bruker AV 500 spectrometer at a ^{1}H Larmor frequency of 500.13 MHz. Both 4 mm and 2.5 mm diameter rotors were used for Nafion112/ZrP samples spun at 10 kHz and 25 kHz, respectively. A recycle delay of 3 s was used. The spectra were referenced to adamantane (1.63 ppm for ^{1}H). Solid state ^{1}H NMR spectra were acquired with a 90° pulse length of 2.5 μs. Variable temperature experiments were performed in the range of 300-360K, with the sample temperature corrected to include heating effect arising from the high-speed MAS. [17]

6.2.3 ^{31}P NMR

^{31}P solid state NMR experiments were performed on a Bruker AV 500 spectrometer at a ^{31}P Larmor frequency of 202.48 MHz. The spectra were referenced to 85% H_3PO_4 (0 ppm for ^{31}P). The recycle delay varies with samples from 60 to 180 s. A 4 mm rotor was used to spin samples at 10 kHz. The spectra were acquired with a 90° pulse length of 4 μs. In the cross polarization (CP) experiments, the contact time varies from 0.5 ms to 6 ms. A recycle delay of 3 s was used. 5120 scans were used to average the signal.

The separation of undistorted powder patterns by effortless recoupling (SUPER) experiment was performed at MAS=5 kHz, with a scaling factor χ'=0.155. [18, 19] This results in an effective spectral width in the indirect dimension of ω_R/χ'=32 kHz. For the ^{31}P 2π pulses, the pulse strength was set to 60.6 kHz, according to $\omega(^{31}P) = 12.12\ \omega_R$. Proton decoupling during 2π ^{31}P pulses was set to ~ 90 kHz. 1 ms contact time was chosen for the ^{31}P-^{1}H cross polarization.

6.2.4 Conductivity measurement

An AUTOLAB PGSTAT30 impedance analyzer was used for impedance spectroscopy. The instrument was used in potentiostatic mode with an AC potential amplitude of 0.01 V over a frequency range of 10 to 20,000 Hz. The impedance was measured over a BekkTech four-probe conductivity cell with two platinum foil outer electrodes and two platinum wire inner electrodes. The membrane sample in the cell was cut into a strip which was 0.3~0.5 cm wide and 2~3 cm long. The conductivity of membrane was measured in the longitudinal direction. It can be calculated using the following equation

$$\sigma = d \ / \ R \cdot l \cdot h \qquad (6\text{-}1)$$

where σ, *d*, R, *l*, *h* denote the ionic conductivity, distance between the two inner electrodes, the measured resistance of the membrane, the width of the membrane, and the thickness of the membrane, respectively. [20, 21] The samples were equilibrated for several hours in a humidity chamber before conductivity measurement. This equilibration time was found to be sufficiently long for the four-probe cell configuration, since the membrane is entirely exposed to the environment in the humidity chamber.

6.3 Results and discussion

6.3.1 Water content in Nafion112 and Nafion112/ZrP composites

Although the water content of polymer electrolyte membranes is generally not directly correlated to their proton conductivities, especially for polymer electrolyte membranes from different families, [22, 23] the water content indeed strongly influence their conductivities. Thus, the water content of fully hydrated Nafion112 and Nafion112/ZrP composites were measured and presented in Table 6-1 as this is essential for a correct comparison of their conductivities. It can be seen from this table that the 9.2% loading of ZrP results in the Nafion112/ZrP composites with water content higher than that of the unmodified Nafion112. However, the composite with 4.1% loading of ZrP presents water content lower than the unmodified Nafion112.

Since adding ZrP in Nafion112 will change the interactions of polymer chains, these results suggest that the higher loading of ZrP could cause the larger change in their interactions which allows higher water uptake for the composite. In contrast, the lower loading of ZrP may minimally influence the interaction, in which case the added ZrP will fill some of the free volume in Nafion112. Therefore, the water content is lower for composites with low loading of ZrP. Surprisingly, the Nafion112/ZrP-300 (dried then rehydrated) sample shows much lower water content, although the loading of ZrP is almost same. This should be also ascribed to the change in the interaction of polymer chains, resulting from the change induced in ZrP by the heat treatment, which forms a compact structure (see below ^{31}P NMR results).

Table 6-1. The water content in Nafion112 and Nafion112/ZrP composites at room temperature. The mass percentage of ZrP was determined for the dried composites

Sample	Nafion112	Nafion112 /ZrP-2	Nafion112 /ZrP-10	Nafion112 /ZrP-300	Nafion112/ZrP-300 (dried then rehydrated)
H_2O (%)	19%	15%	21%	27%	12%
ZrP (%)	–	4.1%	6.8%	9.2%	8.7%

(The error bars for H_2O (%) and ZrP (%) are about 1% and 0.2%, respectively.)

6.3.2 ^{1}H NMR of Nafion/ZrP composites

As shown by equations (3-2) and (3-3) in Chapter 3, the dependence of proton linewidth on temperature can be used to fit the activation energy for proton transport in polymer electrolyte membranes. This dependence of linewidth on temperature was also observed for the hydrated Nafion112/ZrP composites. Figure 6-1 shows ln T_2^* as a function of 1000/T for hydrated Nafion112 and Nafion112/ZrP composites. The fitted activation energies are presented in Table 6-2. The linewidths of Nafion112/ZrP-2 were not obtained as the proton resonance presented as several partially overlapped proton resonances which do not allow to be fitted as a single proton resonance. This could be due to distinct proton environments caused by the low loading of ZrP in the composite.

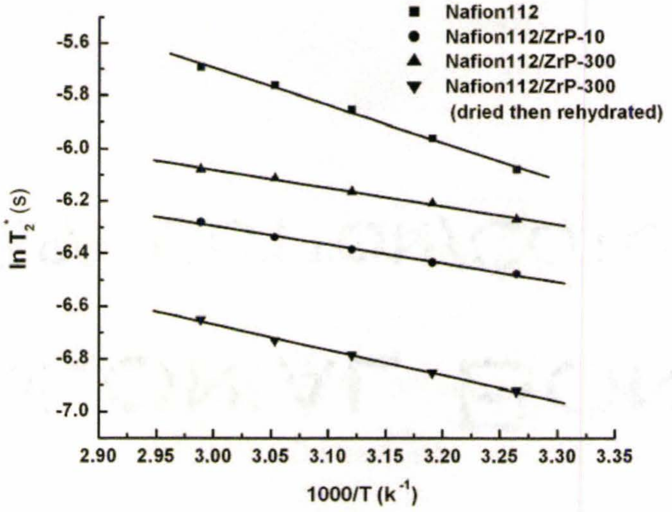

Figure 6-1. Dependence of T_2^* on temperature for fitting activation energy of Nafion112 and Nafion112/ZrP composites. The T_2^* was calculated from spectra under MAS=10 kHz.

Table 6-2. The activation energy for proton transport in hydrated Nafion112 and Nafion112/ZrP composites with different loadings of ZrP

Sample	Nafion112	Nafion112 /ZrP-10	Nafion112 /ZrP-300	Nafion112/ZrP-300 (dried then rehydrated)
Ea (kJ/mol)	11.7±0.5	6.2±0.2	6.1±0.2	8.6±0.3

The Ea for hydrated Nafion112 in Table 6-2 is quite similar to that in Chapter 3. The small difference is attributed to different errors for temperature corrections of rotor at different spinning speeds (The linewidth in Chapter 3 for Nafion112 was at MAS = 5 kHz). It can be seen clearly that all the composites present lower activation energy than unmodified Nafion112. This suggests a weaker dependence of proton mobility on temperature. Interestingly, the Nafion112/ZrP-10 and Nafion112/ZrP-300 have almost same activation energy, despite the fact that they have different water content and loadings of ZrP. However, a clear difference was observed for the Nafion112/ZrP-300 including samples that underwent subsequent drying and rehydration. Since the phosphorus environment in the composites was changed after treatment (see ^{31}P NMR below), this could be related to the changed in structure of ZrP.

In the dried composites, residual water plays an important role in influencing the linewidth of the proton resonance. Figure 6-2 shows the ^{1}H NMR of Nafion112/ZrP-300 which was dried at 105 °C. The linewidth, which is greater than 400 Hz at MAS=25 kHz, results from strong dipolar coupling between the acid proton of Nafion, the acid proton of ZrP and the residual water (observed from TGA experiments), indicating much reduced proton mobility. For composites treated at higher temperature, such as 160 °C, even broader linewidths were observed and the proton resonances shifted to higher frequency due to further reduction of water content. However, since the maximum working temperature for the NMR probe in this project is limited to 380 K, the information regarding proton dynamics of Nafion/ZrP at higher temperatures was not obtained. That information would be very helpful for understanding the better proton conductivity of the composites than the unmodified Nafion under high temperatures, and is planned in future work, which will require use of a probe and spectrometer outside McMaster.

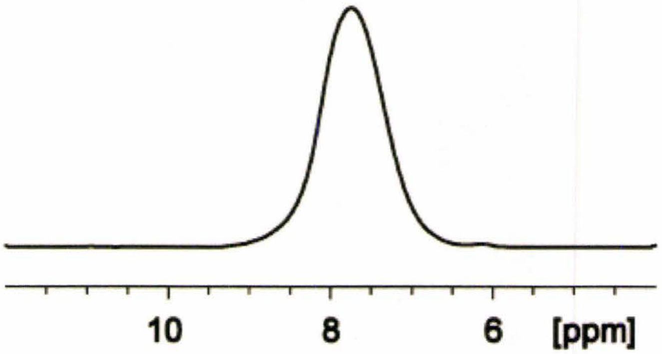

Figure 6-2. ^{1}H NMR of Nafion112/ZrP-300 dried at 105 °C, MAS=25 kHz

6.3.3 ^{31}P NMR of the Nafion/ZrP composites treated at variable temperatures

Although the NMR probe does not allow the measurement of proton dynamics at higher temperatures, it can still measure the altered phosphorus environments for composites treated at higher temperatures. Figure 6-3 shows the ^{31}P NMR of Nafion112/ZrP-300 composites, which have been treated under different temperatures. The spectrum in Figure 6-3(a) is very similar to the spectrum of amorphous ZrP shown in Figure 5-9(a). Therefore, the assignment of the resonances is straightforward. The peak at ~ -22 ppm is attributed to the phosphorus which bonds with three zirconium atoms and one hydrogen atom through oxygen (denoted as $HOP(OZr)_3$). This phosphorus site has the similar structure to α-ZrP. The other two resonances with much weaker intensities at ~ -14 ppm and ~ -28 ppm are assigned to phosphorus bonding with two and four zirconium atoms through oxygen, respectively. Thus, they are denoted as $(HO)_2P(OZr)_2$ and $P(OZr)_4$, respectively. The two phosphorus sites could result from the γ-ZrP in which the zirconium is octahedrally coordinated with four oxygen atoms of a phosphate group and two oxygen atoms of a dihydrogen phosphate group. [24, 25]

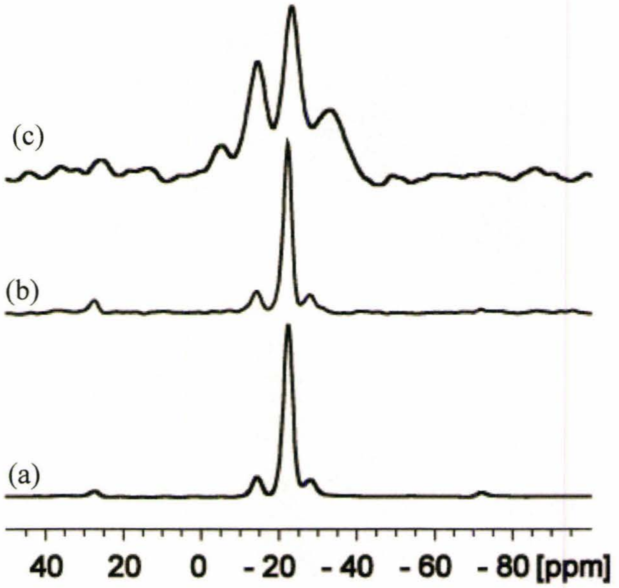

Figure 6-3. ^{31}P NMR of Nafion112/ZrP (5hrs) treated at (a) room temperature (b) 105 °C (c) 160 °C, MAS=10 kHz

Clearly, the amorphous ZrP (in Figure 5-9(a)), the hydrated Nafion112/ZrP and the Nafion112/ZrP treated at 105 °C (in Figure 6-3(b)) showed very similar ^{31}P NMR spectra, suggesting that they have very similar phosphorus environments. However, after the composite was treated at a temperature of 160 °C, a large change of phosphorus environments was observed, as shown in Figure 6-3(c). In Chapter 5, it was observed that the sulfuric acid treated amorphous ZrP showed both the conversion of $HOP(OZr)_3$ into pyrophosphate and the protonation of $HOP(OZr)_3$ after it was dried at 160 °C. Since the Nafion112 also has strong acidity, [26, 27] the observed large change in phosphorus environments is attributed to the role of these sulfonic acid groups. Namely, in the dried Nafion112/ZrP composite, the acid proton of Nafion112 helps the conversion of $HOP(OZr)_3$ into pyrophosphate and protonates the $HOP(OZr)_3$.

Therefore, the resonance at ~ -33 ppm is assigned to the pyrophosphate. The resonance at ~ -14 ppm and ~ -5 ppm are attributed to the singly and the doubly protonated monohydrogen phosphates (denoted as protonated $(HO)P(OZr)_3$) by the acid proton of Nafion112, respectively. However, the protonation of monohydrogen phosphate did not take place in the composite which dried at 105 °C. This is due to the higher concentration of residual water molecules which hydrate the acid proton of Nafion112.

The above assignment is further confirmed by the ^{31}P-^{1}H CPMAS NMR experiments. The spectra are shown in Figure 6-4, together with the ^{31}P NMR spectrum as a comparison. It can be seen that the resonance assigned to pyrophosphate did not show intensity in the spectra with both short and long contact times, indicating that the phosphorus is far from the protons. The resonance at ~ -14 ppm presented stronger and weaker intensity than the one at ~ - 23 ppm in the spectrum with short and long contact time, respectively. This implies that the phosphorus at ~ -14 ppm could have stronger dipolar coupling with the proton than the one at ~ - 23 ppm, which should be attributed to the protonation by the acid proton of Nafion112. Nevertheless, the similar trend is not clear for the resonance at ~ - 5 ppm, due to its very weak intensity and low ratio of signal to noise in Figure 6-4(a).

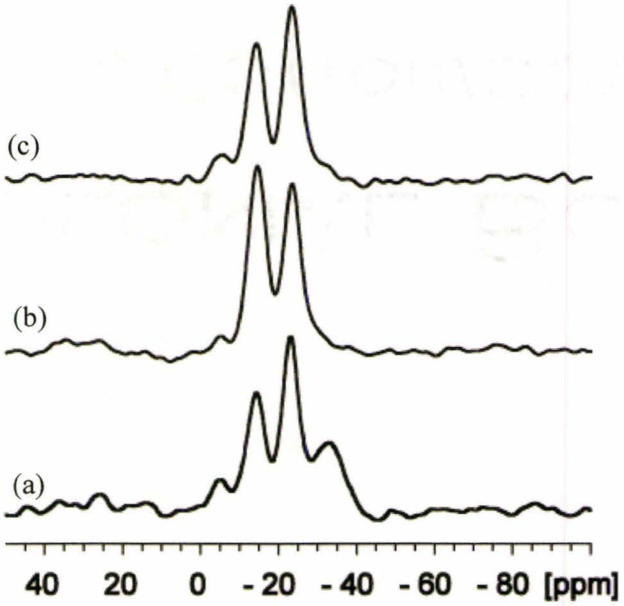

Figure 6-4. ^{31}P NMR of Nafion/ZrP treated at 160 °C, MAS=10 kHz. (a) ^{31}P NMR (b) ^{31}P-^{1}H CPMAS, contact time =1ms, (c) ^{31}P-^{1}H CPMAS, contact time=6ms

Surprisingly, after the Nafion112/ZrP composite, which has been dried at 160 °C, was rehydrated, only a single phosphorus resonance was observed. From Table 6-1, it can be seen that the ZrP % in the dried Nafion112/ZrP (5hrs) composite before and after rehydration remains almost unchanged. Therefore, the disappearance of some phosphorus sites indicates some conversion between them and the other phosphorus site rather than loss by hydration. The phosphorus sites, which have been assigned to the protonated monohydrogen phosphate, converted into monohydrogen phosphate due to the rehydrated acid proton of Nafion112 which is unable to protonate the phosphate group. This is similar to the absence of protonated monohydrogen phosphate in the composites which was dried at 105 °C. However, the disappearance of the resonance at ~ -33 ppm is due to the hydrolysis of pyrophosphate which produces the monohydrogen phosphate. [28] Interestingly, after this rehydrated sample was subjected to be dried at 160 °C again, the resonances for the protonated monohydrogen phosphate and the pyrophosphate were not seen clearly in Figure 6-5(b), which is consistent with a possible morphology change which took place during the rehydration of the dried composite. This is consistent with the literature in which the surface area of the rehydrated ZrP has reduced significantly and is more compact. [28] Therefore, the protonation and the conversion of monohydrogen phosphate were restricted in the Nafion112/ZrP-300(dried then rehydrated) when it was redried again, due to the reduced accessibility of the acid proton of Nafion112 to the surface of ZrP.

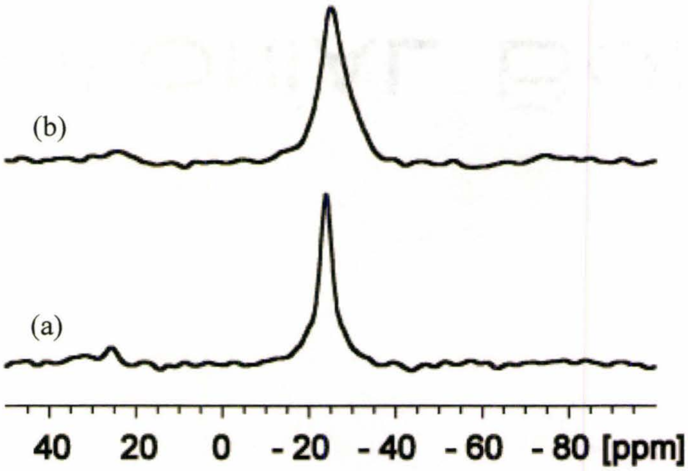

Figure 6-5. ^{31}P NMR of Nafion/ZrP-300, MAS=10 kHz, (a) dried then rehydrated (b) dried then rehydrated and redried

The phosphorus environments in the composite were also investigated using a 2D ^{31}P SUPER NMR experiment. The spectrum is shown in Figure 6-6. The chemical shift anisotropy (CSA) of different phosphorus sites in the composite can be achieved by extracting the columns at their isotropic chemical shifts in the F2 dimension. Subsequently, the CSA spectra can be fitted to give chemical shift tensors for these different phosphorus sites. However, since no intensity was observed for the resonance at ~ - 5 ppm at ~ - 33 ppm in this spectrum, the spectra for fitting CSA were only extracted for the resonances at ~ - 14 ppm and ~ - 22 ppm. They are shown in Figure 6-7, together with the ^{31}P-^{1}H static CP spectrum of α-ZrP. The CSA information for these phosphorus sites, which was obtained by fitting these spectra, is presented in Table 6-3. The amorphous ZrP was not measured here. Since the amorphous ZrP shows the very similar ^{31}P spectrum in Figure 5-10(a) (both chemical shifts and relative ratio of different phosphorus sites) to that of ZrP in Nafion/ZrP composites, they should have very similar CSA parameters as well. It can be seen in Table 6-3 that the phosphorus with the structure of $HOP(OZr)_3$ in the composite has CSA parameters similar to those of α-ZrP, which suggests a similar structure. However, the phosphorus of the protonated $HOP(OZr)_3$ in the composite has quite different CSA parameters. This indicates that the acid proton of Nafion112 has significantly changed the phosphorus environment of $HOP(OZr)_3$ by protonation.

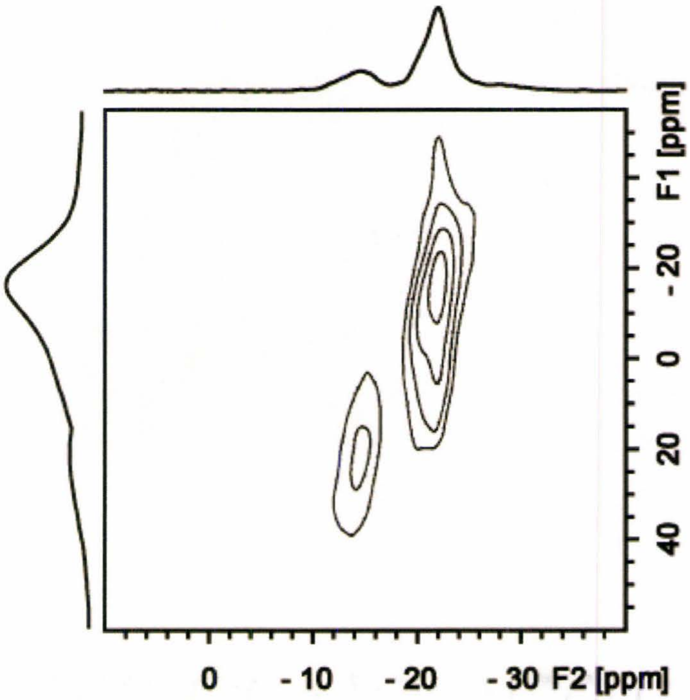

Figure 6-6. the unsheared SUPER spectrum of Nafion/ZrP-300 under MAS=10 kHz and with contact time = 1.5 ms.

Table 6-3. The CSA parameters of phosphorus in α-ZrP and Nafion112/ZrP-300

Samples	Types of Phosphorus	Asymmetry η	δ_{iso} (ppm)	δ_{11} (ppm)	δ_{22} (ppm)	δ_{33} (ppm)
Nafion112/ ZrP -300	Protonated $HOP(OZr)_3$	0.58	-14.7	4.9	-18.8	-30.1
	$HOP(OZr)_3$	0.25	-22.0	6.8	-32.8	-40.0
α-ZrP	$HOP(OZr)_3$	0.23	-18.8	6.5	-28.6	-34.4

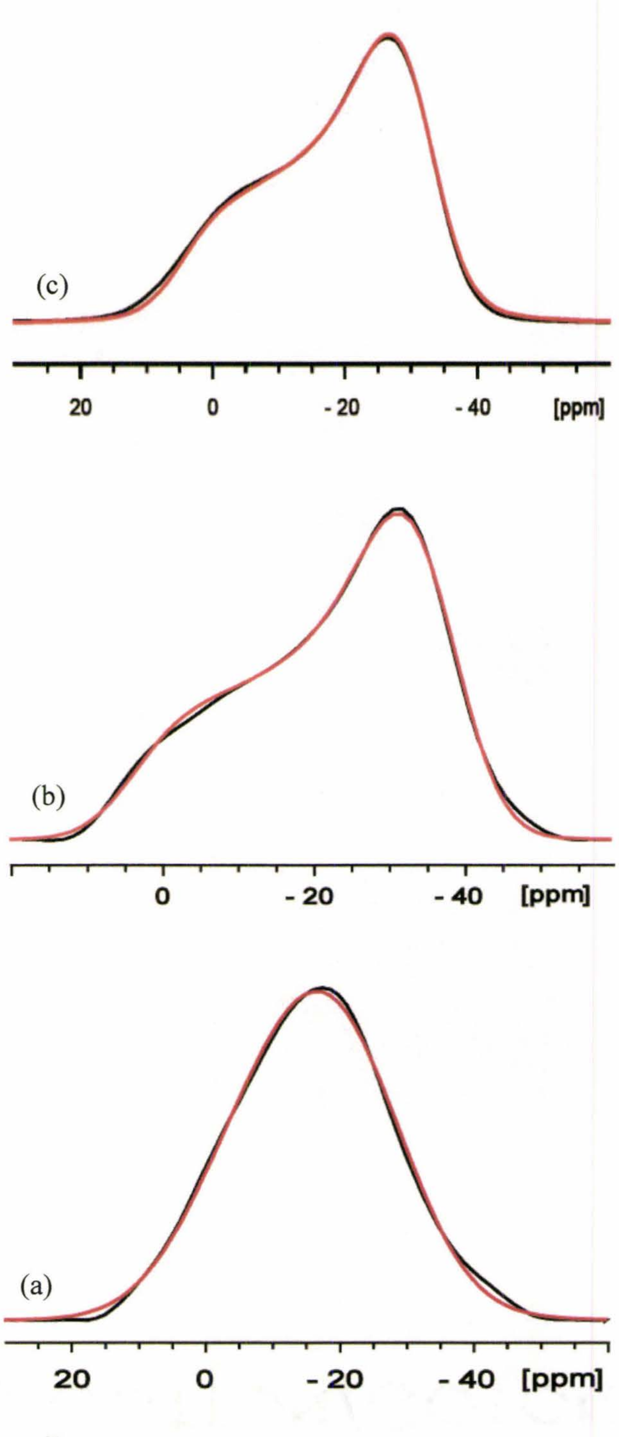

Figure 6-7. ^{31}P chemical shift anisotropy of ZrP for (a) the resonance at ~ -14 ppm in Nafion112/ZrP-300, MAS= 5 kHz (b) the resonance at ~ -22 ppm in Nafion112/ZrP-300, MAS=5 kHz (c) α-ZrP, the spectrum was acquired from a static ^{31}P-^{1}H CP experiment.

6.3.4 Conductivity of Nafion112 and Nafion112/ZrP composites

The conductivity data of Nafion and Nafion/ZrP composites have been reported elsewhere. [15, 16] Their conductivities were also measured in this work to correlate to the above NMR information. The data is shown in Figure 6-8. It can be seen clearly that all the composites have lower proton conductivity than the unmodified Nafion112 under different relative humidity at 35 °C, although some of these composites exhibited higher water content in Table 6-1. Among the composites with different loadings of ZrP, the Nafion112/ZrP-300, which has displayed the highest water content, does not show the highest conductivity. Clearly the observed difference in water content does not explain their difference in conductivity. Moreover, the lower activation energy for proton transport in composites determined by solid state NMR does not help for understanding their conductivity differences. However, in the case of Nafion112/ZrP-300 (dried then rehydrated), the lower conductivity, compared with that of Nafion112/ZrP-300, could be interpreted by the altered structure of ZrP which results in different interactions between Nafion112 and ZrP.

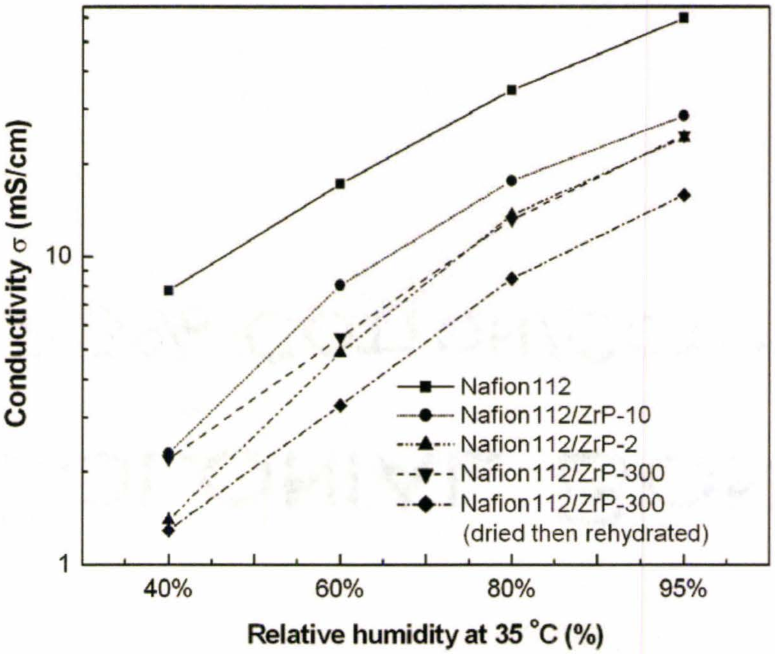

Figure 6-8. Conductivity of Nafion112 and Nafion112/ZrP composites under different relative humidity at 35 °C

6.4 Summary

The studies in this chapter demonstrated that in dried composites, the reduced water content in the composites results in not only the decreased proton mobility but also significant changes in phosphorus environments. For composites dried at 160 °C, both the conversion of monohydrogen phosphate into pyrophosphate and the protonation of monohydrogen phosphate have been observed. This caused a significant change in the interaction of Nafion112 and ZrP, which is one of reasons that the composite presented clearly decreased proton conductivity after it was rehydrated again.

Compared with the hydrated Nafion112, all hydrated Nafion112/ZrP composites show lower proton conductivity at 35 °C. This difference can neither be explained by their water content nor the activation energy for proton transport. In the future, further experiments for studying the Nafion112 and Nafion112/ZrP composites by both solid state NMR and impedance spectroscopy at high temperatures will be helpful to have an overall understanding these observations.

6.5 References

[1] O. Savadogo, *J. Power Sources*, **2004**, 127, 135-161.

[2] G. Alberti, M. Casciola, *Solid State Ionics*, **2001**, 145, 3-16.

[3] K. A. Mauritz, R. B. Moore, *Chem. Rev.,* **2004**, 104, 4535-4585.

[4] K. D. Kreuer, *J. Membr. Sci.*, **2001**, 185, 29-39.

[5] Q. Li, R. He, J. O. Jensen, N. J. Bjerrum, *Chem. Mater.*, **2003**, 15, 4896-4915.

[6] C. Yang, S. Srinivasan, A. B. Bocarsly, S. Tulyani, J. B. Benziger, *J. Membr. Sci.*, **2004**, 237, 145-161.

[7] S. C. Yeo, A. Eisenberg, *J. Appl. Polm. Sci.*, **1977**, 21, 875-898.

[8] L. A. Zook, J. Leddy, *Anal. Chem.*, **1996**, 68, 3793-3796.

[9] G. Alberti, M. Casiola, L. Massinelli, B. Bauer, *J. Membr. Sci.*, **2001**, 185, 73-81.

[10] Q. Li, R. He, J. O. Jensen, N. J. Bjerrum, *Chem. Mater.*, **2003**, 15, 4896-4915.

[11] F. Bauer, M. Willert-Porada, *Fuel Cells*, **2006**, 3-4, 261-269.

[12] M. K. Song, Y. T. Kim, J. S. Hwang, H. Y. Ha, H. W. Rhee, *Electrochem. Solid State Lett.*, **2004**, 7, A127-A130.

[13] G. Alberti, M. Casciola, *Annu. Rev. Mater. Res.*, **2003**, 33, 129-154.

[14] T. A. Zawodzinski, C. Derouin, S. Radzinski, R. J. Sherman, V. T. Smith, T. E. Springer, S. Gottesfeld, *J. Electrochem. Soc.*, **1993**, 140, 1041-1047.

[15] F. Bauer, M. Willert-Porada, *Solid State Ionics*, **2006**, 177, 2391-2396.

[16] P. Costamagna, C. Yang, A. B. Bocarsly, S. Srinivasan, *Electrochim. Acta*, **2002**, 47, 1023-1033.

[17] S. R. Benhabbour, R. P. Chapman, G. Scharfenberger, W. H. Meyer, G. R. Goward, *Chem. Mater.*, **2005**, *17*, 1605-1612.

[18] S-F. Liu, J-D. Mao, K. Schmidt-Rohr, *J. Magn. Reson.*, **2002**, 155, 15-28.

[19] S. Wi, H. S. E. Oldfield, M. Hong, *J. Am. Chem. Soc.*, **2005**, 127, 6451-6458.

[20] J. J. Sumner, S. E. Creager, J. J. Ma, D. D. DesMarteau, *J. Electrochem. Soc.* **1998**, 145, 107-110.

[21] Y. Sone, P. Ekdunge, D. Simonsson, *J. Electrochem. Soc.*, **1996**, 143, 1254-1259.

[22] S. M. J. Zaidi, *Electrochimica, Acta,* **2005**, 50, 4771-4777.

[23] T. J. Peckham, J. Schmeisser, M. Rodgers, S. Holdcroft, *J. Mater. Chem.*, **2007**, 17, 3255-3268.

[24] N. J. Clayden, *J. Chem. Soc. Dalton Trans.*, **1987**, 1877-1881.

[25] D. M. Poojary, B. Shpeizer, A. Clearfield, *J. Chem. Soc. Dalton Trans.*, **1995**, 111-113.

[26] K. D. Kreuer, *J. Membr. Sci.*, **2001**, 185, 29-39.

[27] M. A. Harmer, W. E. Farneth, Q. Sun, *J. Am. Chem. Soc.*, **1996**, 118, 7708-7715.

[28] G. Alberti, M. Casciola, F. Marmottini, R. Vivani, *J. Porous Mater.*, **1998**, 6, 299-305.

Chapter 7

Proton Dynamics of S-PEEKs

This chapter has been published on J. Membr. Sci. (2008, 319, 238-243). The co-authors are C. M. Mills and G. R. Goward. The manuscript was initially prepared by me. Then it was revised by me and G. R. Goward for submission. My contribution to this paper includes the sample preparation, NMR experiments, conductivity measurements, and the understanding of conductivity difference of S-PEEKs. In this chapter, Proton mobilities of S-PEEK membranes with variable degrees of sulfonation (DS), and of S-PEEK membranes cast from different solvents were studied using high resolution solid state ^{1}H MAS NMR. Both single and multiple proton resonances were observed in hydrated S-PEEKs with different DS. This suggests distinct acid proton environments resulting from an uneven distribution of water to sulfonic acid protons in these S-PEEK membranes. For S-PEEK membranes cast from different solvents, stronger polymer chain interactions were observed in S-PEEK from N,N-dimethylformamide (DMF) than in those from N,N-dimethylacetamide (DMAc) and dimethylsulfoxide (DMSO). The NMR results were used to understand the conductivity difference of these S-PEEKs, combining with their water content data.

7.1 Introduction

The studies of polymer electrolyte membrane fuel cells (PEMFC) are being given global attention because of increasing environmental concerns. As a commercial product, Nafion® is a very popular polymer electrolyte membrane because of its excellent conductivity and chemical stability. [1, 2] However, Nafion also has some drawbacks, such as high cost, limited working temperature, and methanol cross over. [3-5] These problems can be reduced with hydrophilic additives, such as silica [6, 7] superacid zirconium [8] and zirconium phosphate, [9] which provide hydrogen-bonding sites for water retention and proton transportation in the resulting composites. An alternative way to deal with the drawbacks of Nafion is to use fluorine-free or partially fluorinated membranes as substitutes for Nafion or Nafion-like membranes. [10-12] Among many fluorine-free polymers, the sulfonated aromatic polymer polyether ether ketone (PEEK) has received much attention since it has good chemical stability and mechanical properties, and the conductivity improves with increasing degree of sulfonation (DS). [13, 14] Although Sulfonated PEEK (S-PEEK) with a very high DS is desirable because of its high proton conductivity, this causes deteriorated mechanical strength due to the high water content and consequent high swelling of the membrane. This implies that a proper degree of sulfonation is crucial for both good proton conductivity and favorable membrane strength. Consequently, it is necessary to have a detailed understanding of the dependence of proton conductivity on the degree of sulfonation.

The conductivities of S-PEEKs have been reported. [15-19] The water content of S-PEEKs is usually presented in these studies to discuss proton conductivity differences. Generally, the proton conductivity of different families of polymers does not directly correlate with either water content or ion exchange capacity. [20-22] Moreover, even in the same polymer family, the proton exchange membranes prepared by different methods, such as using different casting solvents, present large conductivity differences For example, the S-PEEK (DS=79%) cast from DMAc presents conductivity one order of magnitude higher than that of the S-PEEK with same DS but cast from DMF, although they both have similar water content. [23] Such an effect cannot be explained by water content in the samples. Therefore, we investigate here the influence of different casting solvents on the solid-state proton NMR spectra of the S-PEEK membranes

Solid state NMR of proton exchange membranes provides useful information on local proton environments at the molecular level and provides a better understanding of their conductivity differences. In this chapter, we studied S-PEEK membranes with variable degrees of sulfonation and membranes cast from different solvents by solid state ^{1}H MAS NMR. Variable temperature NMR experiments were performed to investigate the mobilities of sulfonic acid protons and polymer backbones. The proton conductivities of these samples measured by AC impedance spectroscopy are discussed in the context of the NMR results.

7.2 Experimental

7.2.1 Preparation of S-PEEK membranes

Commercial PEEK (Grade 450P, Victrec Company) was dissolved in 98% H_2SO_4 at room temperature. In intervals of tens of hours, samples were taken periodically from the mixture and dropwise added to ice water with strong agitation. The residual acid in the polymer precipitates was removed by washing in ice water until constant pH was obtained. After drying, the polymer appeared as beads. Determination of the DS of S-PEEK was performed by solution-state NMR of the materials dissolved in DMSO-d_6. [24] The S-PEEKs with sulfonation time of 73hrs, 120hrs, 144hrs, 263hrs and 577 hrs were determined to have DS of 58%, 68%, 72%, 86% and 95%, respectively. S-PEEK membranes were prepared by dissolving the S-PEEK beads in solvents including N,N-dimethylformamide (DMF), N,N-dimethylacetamide (DMAc) and dimethylsulfoxide (DMSO), and then casting the solutions onto glass. In this paper, all S-PEEK membranes were prepared using DMSO unless a different solvent is indicated. After drying, the membranes were first washed in distilled water to remove the solvent. Then for the sake of comparison, the S-PEEK membranes were purified using an analogous method to that reported for Nafion. [24] Due to the high solubility of S-PEEK in water at high temperature, the heating step was excluded. The S-PEEK was first washed in 3% H_2O_2 for 1hr at room temperature, while stirring.

Subsequently, it was rinsed with distilled water every 15 minutes for 1hr. It was then washed in 1M H_2SO_4 for 1hr at room temperature. Finally it was washed with distilled water at room temperature until constant pH was obtained. The membrane was stirred throughout the entire process. The water content of the hydrated membrane was measured by the weight difference of the hydrated sample and the dried sample. The weight of the dried samples was corrected to remove the contribution of the mass of residual water by using the peak areas of the sulfonic acid protons and the aromatic protons obtained from the decomposition of the ^1H NMR spectra. [24] This correction of mass of residual water in the dried sample can be done based on integration of spectra acquired at variable temperatures, which was used to calculate the error bar of water content. Samples for solid-state NMR measurements were first hydrated by soaking in water, and then surface-dried using a Kimwipe, before packing in the NMR rotors. The NMR rotors are well sealed, as observed in the constant chemical shift (which is highly sensitive to relative humidity) during the measurements. [24]

7.2.2 ^1H NMR

Solid-state ^1H NMR experiments were performed on a Bruker AV 500 spectrometer at a ^1H Larmor frequency of 500.13 MHz. A 2.5 mm rotor was used to spin the samples at 25 kHz. A recycle delay of 3 s was used. The spectra were referenced to adamantane (1.63 ppm for ^1H). The spectra were acquired with a 90°

pulse length of 2.5 μs. Variable temperature experiments were performed in the range of 300-370K, with the sample temperature corrected to include the heating effect arising from the high-speed MAS. [25] The decomposition of the S-PEEK ^{1}H MAS NMR spectra was performed by DMFIT software to determine the peak areas of the sulfonic acid protons and the aromatic protons. [26]

7.2.3 Conductivity measurements

The proton conductivity of the membranes was measured by AC impedance spectroscopy using a BekkTech four-probe conductivity cell with two platinum foil outer electrodes and two platinum wire inner electrodes. [27] The membrane samples were cut into strips 0.3~0.5 cm wide and 2~3 cm long. An AUTOLAB PGSTAT30 impedance analyzer was used for impedance spectroscopy. The instrument was used in the potentiostatic mode with an AC potential amplitude of 0.01 V over a frequency range of 10 to 20,000 Hz. The conductivity is calculated using the following equation

$$\sigma = d \ / \ \mathrm{R} \cdot l \cdot h \qquad (7\text{-}1)$$

where σ, d, R, l, h denote the ionic conductivity, distance between the two inner electrodes, the measured resistance of the membrane, the width of the membrane, and the thickness of the membrane, respectively. The samples were equilibrated overnight at 35 °C (the lowest stable temperature) in a humidity chamber (model 9000, VWR) with variable relative humidity and then measured in the chamber. This equilibration time was found to be sufficiently long for the four-probe cell configuration, since the membrane is entirely exposed to the environment in the humidity chamber.

7.3 Results and discussion

7.3.1 S-PEEK membranes with variable DS prepared using DMSO

In order to compare and understand the mobility of sulfonic acid protons in S-PEEKs, it is necessary to eliminate the solvent used for membrane preparation. The existence of residual solvent can be easily identified by ^{1}H MAS NMR. In Figure 7-1(a) the methyl protons of the DMSO solvent are clearly observed at 2.3 ppm for the dried S-PEEK which was not washed with water after casting from DMSO. The other two resonances at ~ 8.5 ppm and ~ 6.9 ppm are assigned to sulfonic acid protons and aromatic protons, respectively. The residual methyl proton signal suggests that drying S-PEEK at 105 °C, the usual way to prepare membranes for conductivity measurements as seen in literature although the temperature may vary, [19, 23] can not efficiently remove the DMSO solvent. In Figure 7-1(b) the dried sample which has been washed in H_2O does not show any DMSO signal. These results are not surprising since the DMSO solvent has a high boiling point of 189 °C and is miscible with water. These results indicate that water-washing is an efficient way to remove the casting solvent. Nevertheless, this is not a standard step in membrane preparation for conductivity analysis. Residual solvent was also observed for membranes cast from DMF and DMAc that were analyzed unwashed, as these solvents both have high boiling points and are miscible with water. Therefore, all membranes in this study, after preparation, were washed in water to remove residual solvent.

It has been reported that the proton conductivity of S-PEEK improves with increasing degree of sulfonation. This is generally attributed to the direct increase in the sulfonic acid protons, which allows higher water content for proton transportation. By measuring the water content of hydrated S-PEEK membranes, we can calculate the molar ratio of H_2O/-SO_3H (denoted as $N_{\text{water / acid proton}}$) in the samples. The results are shown in Table 7-1. The S-PEEK membranes prepared using DMSO show increased $N_{\text{water / acid proton}}$ with increasing DS, which is consistent with literature. [19, 23] The water content of the S-PEEK (DS=95%) was not measured because the large degree of swelling prevented water on the surface of the membrane from being adequately removed, such that an accurate mass could not be obtained. It is expected that S-PEEK (DS=95%) has a higher $N_{\text{water / acid proton}}$ value than S-PEEK (DS=85%) as it is a highly swollen membrane. Unfortunately, these measured ratios by weight indicate only an average value of $N_{\text{water / acid proton}}$ over the entire sample. They do not provide any information on the distribution of water to acid proton sites at the molecular level in the membrane, which is very important in determining morphology and the pathways of proton conductivity.

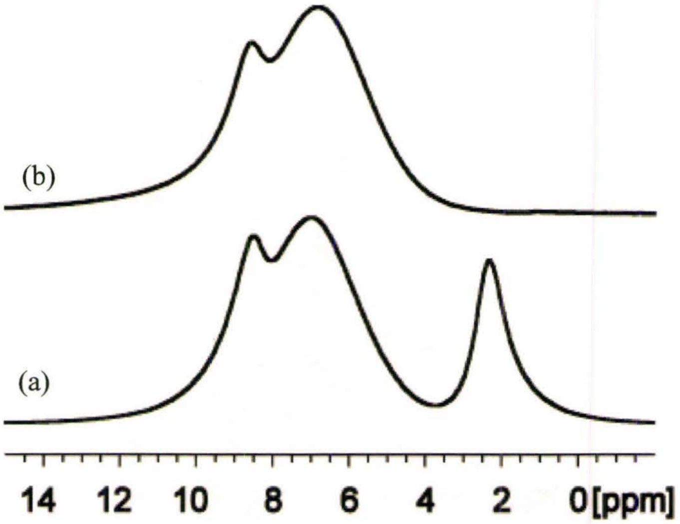

Figure 7-1. ^1H NMR of S-PEEK (DS=72%), dried at 105 °C (a) without being washed by H_2O. (b) washed by H_2O before drying at 105 °C

The ^1H NMR spectra shown in Figure 7-2 provide information about the distribution of H_2O to acid proton values in the membrane. This is non-uniform, as will be discussed below, and contrasts strongly with Nafion [24] which has a uniform distribution.

Table 7-1. Calculated molar ratio of H_2O/-SO_3H for hydrated S-PEEK membranes

Casting Solvent	DMSO	DMSO	DMSO	DMF	DMAc
Degree of Sulfonation	58%	72%	86%	72%	72%
Water content (H_2O/-SO_3H)	12.2±0.3	20.6±0.6	27.4±1.8	13.1±0.3	13.4±0.3

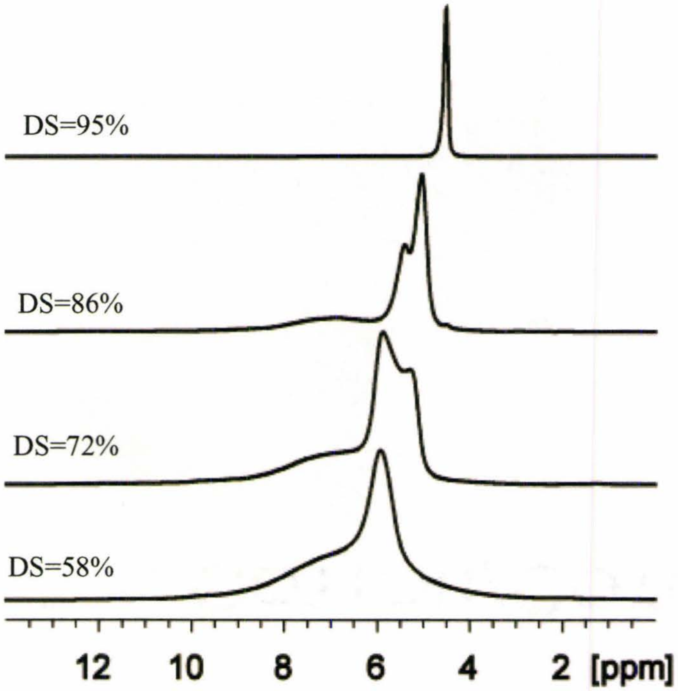

Figure 7-2. ^{1}H NMR of hydrated S-PEEKs with variable DS at ambient temperature. Spectra were scaled to show the same intensity for the strongest peak in each sample.

In general, the fully hydrated S-PEEKs with higher DS show lower chemical shifts for the sulfonic acid protons. This is due to the increased water content with increasing DS. When more water is available for proton exchange with acid protons, the overall proton resonance moves toward the chemical shift of the water proton resonance itself and the exchange process is more rapid which, in general, narrows the resonance peaks. Thus, it is not surprising that the S-PEEK (DS=95%) shows a very sharp peak which is very close to the proton resonance of pure water. The extremely weak relative intensity of the aromatic proton in this sample, unobservable in this figure after the spectrum was scaled, is consistent with a very high water content. A more important difference between the S-PEEKs, observable in Figure 7-2, is that

S-PEEKs (DS=72% and 86%) show multiple acid proton resonances but S-PEEKs (DS=58% and 95%) show only a single acid proton resonance. This indicates that the former have multiple acid proton environments but the latter do not. Therefore, the S-PEEK (DS=58% and DS=95%) materials, considered individually, have similar environments throughout the sample for the $N_{\text{water / acid proton}}$, but the S-PEEK (DS=72% and DS=86%) have multiple environments for the $N_{\text{water / acid proton}}$. Moreover, for these hydrated samples, the observed multiple acid protons, ($\delta \sim 5.9$ ppm and $\delta \sim 5.3$ ppm) do not show any proton exchange in our ^{1}H EXSY NMR experiments (data not shown). The down-field shifted acid protons at $\delta=5.9$ ppm are associated with a relatively smaller number of water molecules than those at $\delta=5.3$ ppm, and the lack of proton exchange between these two sites limits the overall proton mobility of the sample. The high water content of S-PEEKs (DS=72% and DS=86%) are conducive to higher overall proton mobility compared to S-PEEK (DS=58%), but the bulk conductivity differences between them are restricted by the very heterogeneous sulfonic acid proton environments in the DS=72% and DS=86% materials. This is confirmed below by our conductivity data.

Since increased operating temperatures for proton exchange membranes are desirable, information on proton dynamics of S-PEEKs at high temperatures is needed. Variable temperature ^{1}H MAS NMR experiments provide this information. Figure 7-3 shows the ^{1}H NMR spectra of hydrated S-PEEKs with variable DS at 370K. The

S-PEEK (DS=58%) in Figure 7-3 still shows a single sulfonic acid proton resonance at high temperature. But for the hydrated S-PEEKs with higher DS (DS=72% and 86%) the linewidth of the sulfonic acid proton becomes narrower and a new proton resonance appears at ~ 4.3 ppm. This resonance is assigned to free water due to its very high mobility indicated by its sharp peak and also by its low chemical shift.

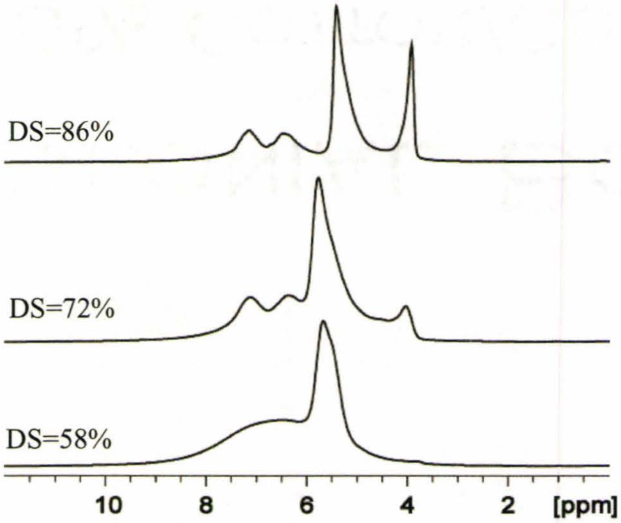

Figure 7-3. ^{1}H NMR of hydrated S-PEEKs with variable DS at 370K

The S-PEEKs (DS=72% and 86%) show two resolved resonances at ~ 7.1 ppm and ~6.4 ppm in Figure 7-3. They are assigned to the aromatic protons. Using the liquid NMR spectrum of S-PEEK [24] as a reference, the aromatic proton resonances at ~ 7.1 ppm are assigned to protons bonding to carbons adjacent to the carbonyl groups of S-PEEK. The resonance at ~ 6.4 ppm is assigned to all the other aromatic protons. This assignment was further confirmed by variable temperature NMR spectra of S-PEEK membranes which were treated with NaOH solutions. The spectra are shown in Figure 7-4. Since there are no acid protons left in the NaOH-treated S-PEEKs, the two resolved proton resonances centered near ~ 7 ppm for S-PEEK (DS=86%) at 370K in Figure 7-4 must be from the aromatic protons. The NaOH-treated S-PEEK (DS=58%) does not show resolved aromatic proton resonances at the same temperature, confirming the relatively higher rigidity of its backbone compared to S-PEEK (DS=86%). The appearance of resolved aromatic proton resonances in Figure 7-3 and Figure 7-4 indicates that the fully hydrated S-PEEKs with higher degrees of sulfonation have more mobile polymer chains and that the interactions between polymer chains must be weaker compared to S-PEEKs with lower degrees of sulfonation. Furthermore, as seen in Figure 7-4, these differences are more evident in NMR spectra obtained at high temperature compared to spectra acquired at room temperature.

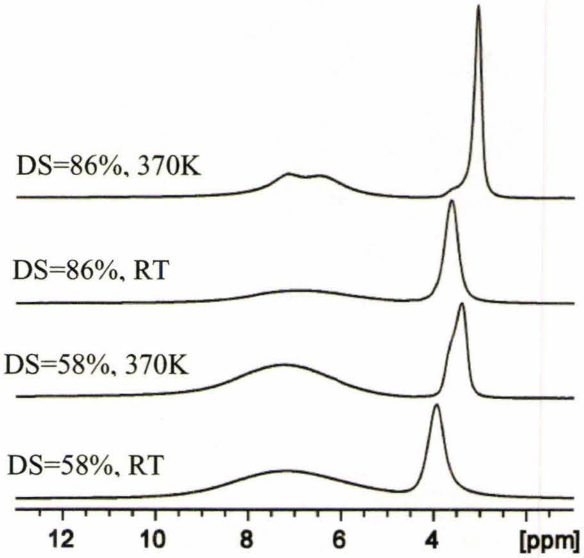

Figure 7-4. ^{1}H NMR of hydrated S-PEEK (DS=58% and 86%) treated by NaOH (aq), then washed until a constant pH was obtained

7.3.2 S-PEEK membranes prepared using DMF and DMAc

Perhaps not surprisingly it has been reported that S-PEEK membranes prepared from different solvents exhibit different proton conductivities. For example, the membrane prepared using DMF shows very low conductivity, compared with those with the same degree of sulfonation but cast from DMAc or DMSO. [28] Solid state NMR studies of these membranes reveal the molecular level details responsible for these differences. Figure 7-5 (a) shows the room temperature spectra of S-PEEK membranes cast from DMF, DMAc, and DMSO. It can be seen that the S-PEEK membranes prepared using DMF and DMAc show sulfonic acid proton resonances narrower than those of the membrane prepared from DMSO. These differences can be correlated with the specific water contents of these membranes. As seen in Table 7-1, the S-PEEK (DS=72%) from DMSO has a much higher $N_{\text{water / acid proton}}$ value than those from DMF and DMAc. Since all these membranes have the same degree of sulfonation, this indicates that casting solvents can change not only the average water content but also the environments of the water molecules and acid protons. Both factors are important for overall proton mobility, and therefore proton conductivity. From the spectra acquired at 370K shown in Figure 7- 5(b), it can be observed that the membranes prepared from DMAc and DMSO display higher backbone mobility, indicating weaker polymer chain interactions, than membranes prepared from DMF since the resolved aromatic proton resonances are not seen in the latter. All solvents have been removed from these S-PEEK membranes. Therefore, the distinct mobility differences of the polymer backbones observed between these membranes indicates that the casting solvents can change the interactions of the polymer chains. However, the differences between membranes cast from DMAc and DMSO are not obvious.

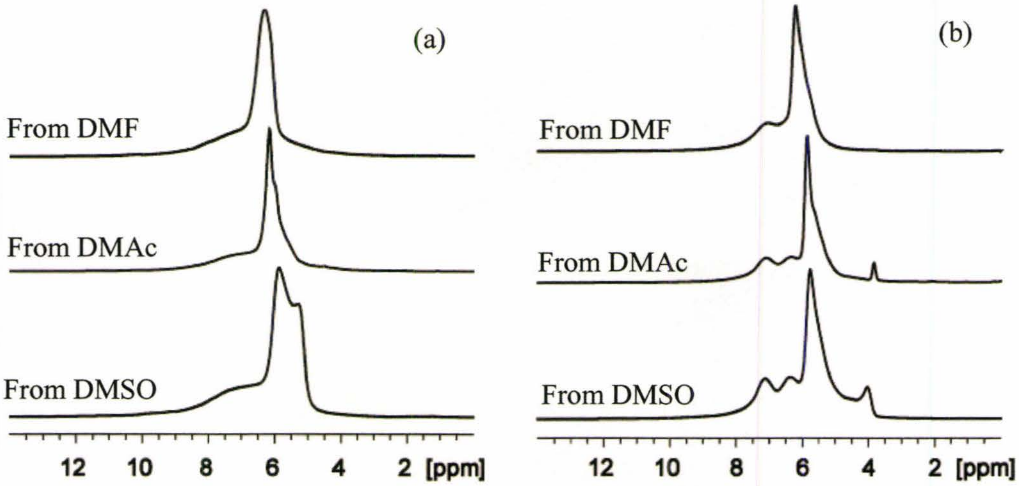

Figure 7-5. ^1H MAS NMR of hydrated S-PEEK (DS=72%) cast from DMF, DMAc and DMSO solvents. Spectra acquired at (a) room temperature (b) 370K

Another distinguishing difference observed for the membrane from DMF is that it does not show any free water even at 370K, but membranes prepared from both DMSO and DMAc do. Since membranes prepared using DMAc and DMF have almost same $N_{\text{water / acid proton}}$, this difference could result from the stronger polymer chain interactions in the membrane from DMF. The correctness of this interpretation is furthered by the observation that in Figure 7-3 and Figure 7-5(b) the appearance of free water is consistently correlated with the presence of well-resolved aromatic protons which implies mobile polymer backbones and weaker interactions between polymer chains.

7.3.3 Proton conductivity of S-PEEKs

Although the solid state ^1H MAS NMR spectra provide useful information regarding the S-PEEK membranes, the proton conductivity data are required for the selection of a useful polymer electrolyte membrane. These data are shown in Figure 7-6 and Figure 7-7. As can be seen in Figure 7-6, the S-PEEKs prepared using DMSO solvent show increased proton conductivity with increasing degree of sulfonation and relative humidity, which is consistent with literature. [15, 29] It is generally accepted that the increased sulfonic acid protons allow higher water content, therefore faster proton motion resulting in higher proton conductivity. Thus, in Figure 7-6 the conductivity of S-PEEK shows a large increase when DS changes from 58% to 68%. Nevertheless, when DS increases from 72% to 86%, the conductivities of S-PEEKs do not show much difference, although a large increment of water content has been observed. This could be due to the same-sample widely varying environments for the $N_{\text{water / acid proton}}$ in these two S-PEEK membranes, as has been discussed. Since the mechanical strength deteriorates with increasing DS, the conductivity data also suggest that S-PEEKs with DS no higher than 72% will be best for PEMFC applications.

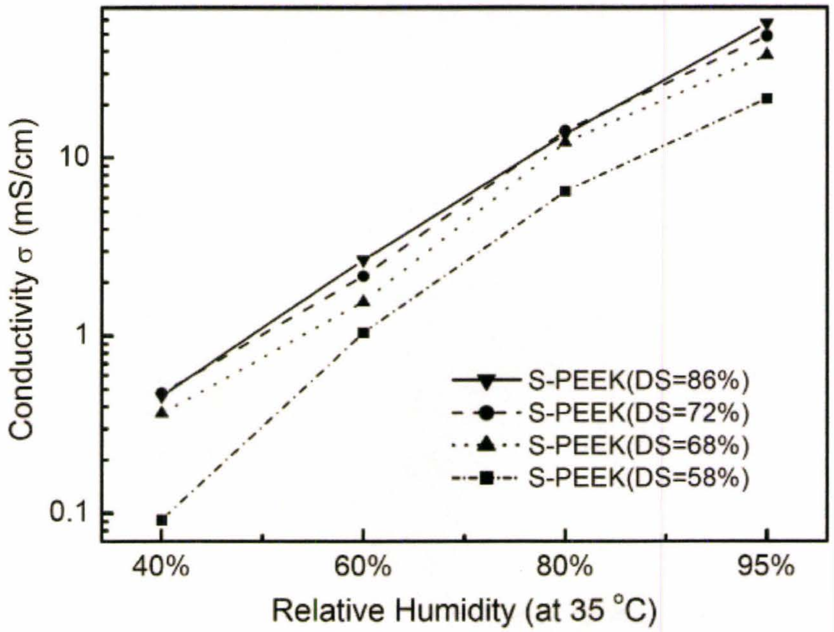

Figure 7-6. Conductivity of S-PEEKs with variable DS cast from DMSO

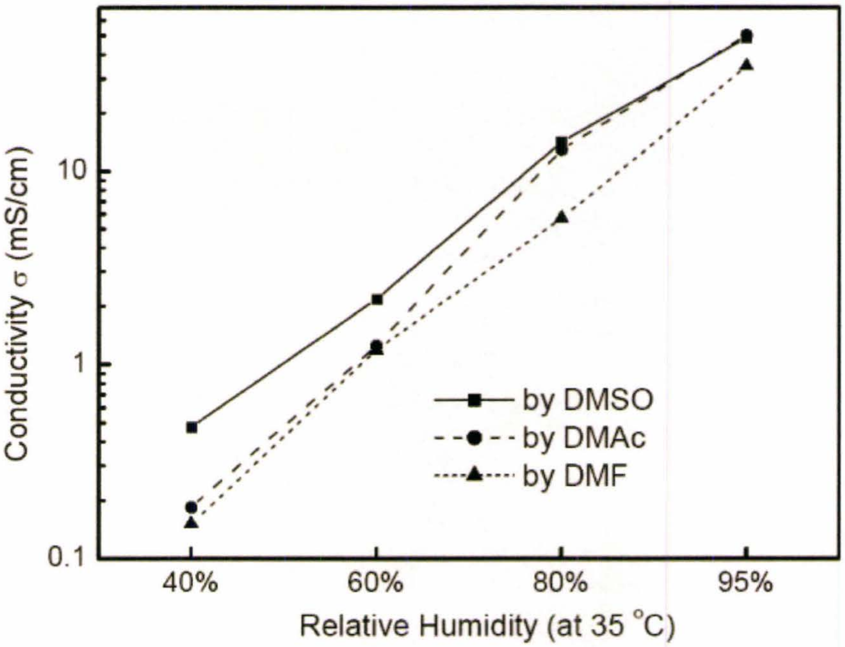

Figure 7-7. Conductivity of S-PEEK (DS=72%) prepared from different solvents

Based on literature and our solid state NMR studies, it is anticipated that the casting solvents used to prepare S-PEEK membranes will play a crucial role in determining macroscopic conductivity. In Figure 7-7, the S-PEEK from DMF shows lower proton conductivity than the S-PEEK membrane with same degree of sulfonation but cast from DMAc. Membranes prepared from DMAc and DMSO show similar conductivity at high relative humidity. Literature indicates that S-PEEKs with the same degree of sulfonation, cast from DMF or DMAc, show one order of magnitude of conductivity difference. [19] This large difference was ascribed by the authors to the hydrogen bond formed between the DMF solvent and the sulfonic acid proton, which results in the lower number of available acid protons for conductivity in the S-PEEK cast from DMF. Nevertheless, the conductivity data in Figure 7-6 and Figure 7-7 were obtained from samples that were washed before measurement and the influence of any residual solvents has been minimized. Thus, the conductivity difference observed in this study can not be attributed to the same reason as cited in the literature.

According to the water content data in Table 7-1, the S-PEEKs prepared from DMF and DMAc are very similar. Both of them have water content much lower than that of S-PEEK by DMSO. The conductivity differences cannot be readily explained by the water contents of the membranes even if all these membranes are in the same polymer family. From our solid state NMR studies, the S-PEEK from

DMF shows stronger polymer chain interactions than S-PEEKs from DMSO and DMAc. This strong interaction contributes to lower proton mobility, and therefore lower proton conductivity. It has been reported that DMF forms hydrogen bonds with sulfonic acid protons during membrane preparation but DMAc does not. [19] Since both solvents were removed from our membranes prior to our conductivity measurements, this could indicate that differences in polymer chain interactions remain, even if the solvent has been eliminated, causing conductivity differences. Therefore, the choice of casting solvent can influence polymer packing and membrane morphology, even after that solvent has been removed. Thus, choosing a solvent with minimal hydrogen bonding character encourages a looser packing of the polymer chains, which is conducive to increased local dynamics and proton transport.

7.4 Conclusions

The fully hydrated S-PEEKs show single or multiple sulfonic acid proton environments, depending on their degree of sulfonation. When the degree of sulfonation is as low as 58% or as high as 95%, the single acid proton environment in the S-PEEKs is relatively uniform throughout the membrane. The low or high water content cause this micromorphology. Multiple acid proton environments exist in the fully hydrated S-PEEK with degrees of sulfonation equal to 72% or 86%, i.e., there is a large variation of $N_{\text{water / acid proton}}$ values throughout an individual membrane. This could be one of the reasons for the small proton conductivity difference between them at high relative humidity. The small conductivity difference between S-PEEKs prepared using DMSO and DMAc could also be attributed to a broad distribution of $N_{\text{water / acid proton}}$ values in the S-PEEK cast from DMSO although it has much higher water content. However, the clear conductivity difference between S-PEEKs cast from DMF and DMAc is due to the distinct mobility differences of their polymer backbones.

7.5 References

[1] K. A. Mauritz, R. B. Moore, *Chem. Rev.,* **2004**, 104, 4535-4585.

[2] G. Alberti, M. Casciola, *Solid State Ionics,* **2001**, 145, 3-16.

[3] M. J. Sumner, W. L. Harrison, R. M. Weyers, Y. S. Kim, J. E. McGrath, J. S. Riffle, A. Brink, M. H. Brink, *J. Mem. Sci.,* **2004**, 239, 199-211.

[4] F. Damay, L. C. Klein, *Solid State Ionics,* **2003**, 162-163, 261-267.

[5] N. Jia, M. C. Lefebvre, J. Halfard, Z. Qi, P. G. Pickup, *Electrochem. Solid-state Lett.*, **2000**, 3, 529-531

[6] H. Wang, B. A. Holmberg, L. Huang, Z. Wang, A. Mitra, J. M. Norbeck, Y. Yan, *J. Mater. Chem.*, **2002**, 12, 834-837.

[7] K. A. Mauritz, J. T. Payne, *J. Membr. Sci.,* **2000**, 168, 39-51.

[8] M. A. Navarra, F. Croce, B. Scrosati, *J. Mater. Chem.*, **2007**, 17, 3210-3215.

[9] P. Costamagna, C. Yang, A. B. Bocarsly, *Electrochim. Acta,* **2002**, 47, 1023-1033.

[10] M. Rikukawa, K. Sanui, *Prog. Polym. Sci.,* **2000**, 25, 1463-1502.

[11] M. A. Hickner, H. Ghassemi, Y. S. Kim, B. R. Einsla, J. E. McGrath, *Chem. Rev.,* **2004**, 104, 4587-4612.

[12] J. Qiao, T. Hamaya, T. Okada, *J. Mater. Chem.*, **2005**, 15, 4414-4423.

[13] K. D. Kreuer, *Solid State Ionics*, **1997**, 97, 1-15.

[14] K. D. Kreuer, *J. Membr. Sci.,* **2001**, 185, 29-39.

[15] S. M. J. Zaidi, S. D. Mikhailenko, *J. Membr. Sci*., **2000**, 173, 17-34

[16] T. Kobayashi, M. Rikukawa, K. Sanui, N. Ogata, *Solid State Ionics,* **1998**, 106, 219-225.

[17] R. Jiang, H. R. Kunz, J. M. Fenton, *J. Power Sources,* **2005**, 150, 120-128.

[18] M. Gil, X. Ji, X. Li, H. Na, J. E. Hampsey, Y. Lu, *J. Membr. Sci.,* **2004**, 234, 75-81.

[19] S. Kaliaguine, S. D. Mikhailenko, K. P. Wang, P. Xing, G. Robertson, M. Guiver, *Catalysis Today,* **2003**, 82, 213-222.

[20] S. M. J. Zaidi, *Electrochim. Acta,* **2005**, 50, 4771-4777.

[21] R. W. Kopitzke, C. A. Linkous, H. R. Anderson, G. L. Nelson, *J. Electrochem. Soc.,* **2000**, 147, 1677-1681.

[22] T. J. Peckham, J. Schmeisser, M. Rodgers, S. Holdcroft, *J. Mater. Chem.*, **2007**, 17, 3255-3268.

[23] P. Xing, G. P. Robertson, M. D. Guiver, S. D. Mikhailenko, K. Wang, S. Kaliaguine, *J. Membr. Sci.,* **2004**, 229, 95-106.

[24] G. Ye, N. Janzen, G. R. Goward, *Macromolecules,* **2006**, 39, 3283-3290.

[25] S. R. Benhabbour, R. P. Chapman, G. Scharfenberger, W. H. Meyer, G. R. Goward, *Chem. Mater.*, **2005**, 17, 1605-1612.

[26] D. Massiot, F. Fayon, M. Capron, I. King, S. LeCalv, B. Alonso, J. Durand, B. Bujoli, Z. Gan, G. Hoatson, *Magn. Reson. Chem.,* **2002**, 40, 70-76.

[27] G. Ye, C. A. Hayden, G. R. Goward, *Macromolecules,* **2007**, 40, 1529-1537.

[28] G. P. Robertson, S. D. Mikhailenko, K. Wang, P. Xing, M. D. Guiver, S. Kaliaguine, *J. Membr. Sci.,* **2003**, 219, 113-121.

[29] D. J. Jones, J. Roziere, *J. Membr. Sci.,* **2001**, 185, 41-58.

Chapter 8

Proton Dynamics of Crosslinked S-PEEK

This chapter has been submitted to J. Phys. Chem. C (2008). The co-authors are C. M. Mills and G. R. Goward. The manuscript was initially prepared by me. Then it was revised by me and G. R. Goward for submission. My contribution to this paper includes the sample preparation, NMR experiments, conductivity measurements, determination of residual degree of sulfonation of crosslinked S-PEEKs, and the understanding of conductivity difference between S-PEEKs and crosslinked S-PEEKs. In this chapter, high-resolution ^{1}H MAS NMR was used to investigate the crosslinked S-PEEKs prepared using ethylene glycol as a crosslinker. It was found that not all crosslinkers in the resulting polymer are fully crosslinked. The residual degrees of sulfonation were determined to be about 13%. Surprisingly, the crosslinked S-PEEK membranes with such a low degree of sulfonation still present good proton conductivity comparable to that of S-PEEK (DS=58%). This is attributed to the exchange between the sulfonic acid proton and the hydroxyl proton of partially crosslinked ethylene glycol, which is observed in ^{1}H EXSY NMR experiments. However, the observed decomposition of the crosslinked S-PEEK in an acidic environment indicates that membranes prepared in this fashion are not appropriate for application in PEM-FCs.

8.1 Introduction

As a typical fluorine free polymer electrolyte, sulfonated PEEK (S-PEEK) was developed to substitute Nafion®, since Nafion has some drawbacks, such as high cost, limited working temperature, and methanol cross over, [1-3]. However, although PEEK has good chemical stability and mechanical properties, [4-7] the sulfonated PEEK with a very high degree of sulfonation (DS), which presents good proton conductivity, often results in deteriorated mechanical strength due to the high water uptake and consequent high swelling of the membrane. One way to improve the mechanical strength of the S-PEEK membrane with a high DS is to crosslink the polymer by linking sulfonic acid groups. [8-10] Obviously, this sacrifices a certain amount of sulfonic acid protons, which ultimately decreases the proton conductivity of the membrane. But if an S-PEEK membrane with a very high DS is chosen for preparing the crosslinked S-PEEK, it was found that the mechanical property and the proton conductivity of the resulting membrane is comparable to those of Nafion. [10, 11]

Although the crosslinked S-PEEK shows desirable mechanical and conductive properties, it is not well characterized. For example, the remaining degree of sulfonation after the crosslinking of S-PEEK, which is very crucial to evaluate the conductivity of the resulting polymer electrolyte, was not reported. Recently, incompletely crosslinking reaction for some of crosslinkers has been reported, [11] which indicates the residual hydroxyl proton of crosslinkers in the treated S-PEEK. To our knowledge, questions like whether these protons are involved in proton conduction and how they participate are not answered. At this point, a solid state NMR study of this proton exchange membrane can provide useful information which allows us to have a better understanding of the conductivity differences between S-PEEKs and crosslinked S-PEEKs on molecular level.

In this chapter, using solid state ^{1}H MAS NMR the crosslinked S-PEEK membranes, which were prepared from S-PEEKs with different degrees of sulfonation, were studied. This allows us to directly probe the proton as the nuclei responsible for conduction. 2D ^{1}H EXchange SpectroscopY (EXSY) NMR is used to study exchange between the sulfonic acid proton and the hydroxyl proton of crosslinker in the hydrated crosslinked S-PEEK. Although both proton exchange and proton spin diffusion can cause cross peaks between proton sites, only the former is temperature dependent, which allows us to distinguish these mechanisms by comparing the intensity of spectra acquired at different temperatures. Homonuclear proton dipolar coupling interactions, which can be recoupled using a double quantum filtering (DQF) sequence, can be used to reveal the relative mobility of protons. The Back-to-Back (BaBa) pulse sequence, [12, 13] was used to recouple the proton dipolar coupling which are removed in a regular single pulse MAS experiment. This technique provides insight into the proton mobilities in the dried crosslinked S-PEEK. Compared with the single pulse MAS spectrum, the BaBa spectrum will only present the rigid protons which have strong dipolar couplings, whereas protons experiencing motionally averaged couplings, typical of rapid dynamics, are removed by the DQ filter. This allows us to distinguish mobile protons from immobile ones. This method is only applied to the dried samples, as the dynamics in hydrated membranes are too rapid to allow for detection of any double quantum filtered resonances. The conductivities of crosslinked S-PEEKs measured by AC impedance spectroscopy are discussed in the context of the NMR results.

8.2 Experimental

8.2.1 Preparation of S-PEEK membranes

Commercial PEEK (Grade 450P, Victrec Company) was dissolved in 98% H_2SO_4 at room temperature. At intervals of tens of hours, samples were taken periodically from the mixture and added to ice water with strong agitation. The residual acid in the polymer precipitates was removed by washing in ice water until constant pH was obtained. For the S-PEEK samples with a very high degree of sulfonation, which is highly swollen in water, the dialysis of S-PEEK was performed. Then, the S-PEEK was dried at 105 ^{o}C to remove water in the polymer. Determination of the degree of sulfonation of S-PEEK was performed by solution state ^{1}H NMR of S-PEEK dissolved in deuterated dimethylsulfoxide (DMSO-d_6). [14] S-PEEK membranes were prepared by dissolving the dried S-PEEK in DMSO solvent and then casting onto glass. After drying, the membranes were washed in distilled water to remove the solvent.

8.2.2 Preparation of crosslinked S-PEEK

The S-PEEKs (DS=86% and 95%) were chosen to prepare the corresponding crosslinked S-PEEK (DS=86% for S-PEEK) and crosslinked S-PEEK (DS=95% for S-PEEK). The procedure is referred to Kaliaguine's work. [10] The dry membrane was dissolved in dimethylacetamide (DMAc) to give a ~9 wt.% S-PEEK solution. The ethylene glycol was then added as a crosslinker. The ratio of crosslinker to sulfonic acid proton of S-PEEK is ~ 7:1. The mixture was agitated for about 1 hour and then cast onto a glass plate. This sample was first dried at room temperature for 3 days and then at 140 °C for 60 hrs. The obtained membranes were washed in water to remove residual solvent and crosslinker since both of them are miscible with water. The obtained membranes did not exhibit any noticeable expansion after being fully hydrated in water, which indicates a certain degree of crosslinking has occured. Some membranes of crosslinked S-PEEK were treated in 1M NaOH $_{(aq)}$ or 1M $H_2SO_{4\,(aq)}$ overnight to study their stability in basic or acidic environment, respectively. Before ^{1}H NMR measurements, excess base or acid in these membranes was removed by washing in water until constant pH was obtained. The back titration of crosslinked

S-PEEKs was performed as follows to determine the equivalent weight (EW) of the crosslinked S-PEEKs. ~0.1g dried sample was added in excess 0.01M NaOH and kept for overnight. The mixture was then titrated with 0.01M HCl to end point. The equivalent weight is calculated as the mass of dried crosslinked S-PEEK per mole of sulfonic acid proton.

8.2.3 ^{1}H NMR

Solid-state ^{1}H NMR experiments were performed on a Bruker AV 500 spectrometer at a ^{1}H Larmor frequency of 500.13 MHz. A 2.5 mm rotor and a 4 mm rotor were used to spin samples at 25 kHz and 14 kHz, respectively. A recycle delay of 3 s was used. The spectra were referenced to adamantane (1.63 ppm for ^{1}H). The spectra were acquired with a 90^o pulse length of 2.5 μs. Variable temperature experiments were performed in the range of 300-370K, with the sample temperature corrected to include heating effect arising from the high-speed MAS. [15] ^{1}H 2D EXSY NMR spectra were recorded by EXSY pulse sequence with mixing time variable from 1 to 150 ms. The rotor synchronized DQF MAS spectra were recorded using the Back-to-Back pulse sequence with τ_{exc} variable from one rotor period τ_r to eight rotor periods $8\tau_r$, and 128 scans. The decomposition of S-PEEK ^{1}H MAS NMR spectra was performed by DMFIT software to determine peak areas of the aromatic proton and the methylene proton of crosslinker. [16]

8.2.4. ^{2}H NMR

The ^{2}H MAS NMR experiments were conducted on a Bruker AV 500 spectrometer at a ^{2}H Larmor frequency of 76.77 MHz. A 4 mm rotor was used to spin samples at 5 kHz. A recycle delay of 3 s was used. The spectra were referenced to D_2O (4.77 ppm for ^{2}H).

8.2.5 Conductivity measurements

The proton conductivity of membrane was measured by AC impedance spectroscopy by a BekkTech four-probe conductivity cell with two platinum foil outer electrodes and two platinum wire inner electrodes. [17] The membrane samples were cut into strips which were 0.3~0.5 cm wide and 2~3 cm long. The thickness of membranes was measured using a micrometer. An AUTOLAB PGSTAT30 impedance analyzer was used for impedance measurements. The instrument was used in potentiostatic mode with an AC potential amplitude of 0.01 V over a frequency range of 10 to 20,000 Hz. The conductivity is calculated using the following equation [18, 19]

$$\sigma = d \;/\; R \cdot l \cdot h \qquad (8\text{-}1)$$

where σ, d, R, l, and h denote the ionic conductivity, distance between the two inner electrodes, the measured resistance of the membrane, the width of the membrane, and the thickness of the membrane, respectively. The samples were equilibrated overnight at 35 °C (the lowest stable temperature) in a humidity chamber (model 9000, VWR) with variable relative humidity and then measured in the chamber. This equilibration time was found to be sufficiently long for the four-probe cell configuration, since the membrane is entirely exposed to the environment in the humidity chamber.

8.3 Results and discussion

8.3.1 Incompletely crosslinked crosslinkers in crosslinked S-PEEK

It is believed that the crosslinking of S-PEEK with a high DS would improve its mechanical strength but retain, in the resulting polymer, good proton conductivity. In this work, crosslinked S-PEEKs based on S-PEEKs (DS=86% and 95%) were prepared using ethylene glycol as a crosslinker. The ^{1}H MAS NMR spectra of the crosslinked S-PEEK prepared from S-PEEK (DS=95%) are shown in Figure 8-1. In Figure 8-1(a), the resonance at ~2.1 ppm is attributed to the methylene protons of ethylene glycol. The resonance at ~5.0 ppm is assigned to the hydroxyl proton of ethylene glycol since it was found that this peak shifts to lower frequency with increasing temperature in Figure 8-1(b), and to higher frequency with decreasing water content in Figure 8-1(c). As the free crosslinker is miscible with water and has been washed out of the membrane, the hydroxyl proton must be from the partially crosslinked ethylene glycol, ie, with one functional group tethered to the sulfonate group as expected, while the other remains unreacted. This suggests that not all crosslinkers are fully crosslinked and the residual hydroxyls of partially crosslinked crosslinkers can help to retain water within the membrane. Therefore, the peak at ~2.1 ppm is comprised of both fully and partially crosslinked ethylene glycol. The other two peaks with weaker intensities at ~7.3 ppm and ~6.7 ppm in Figure 8-1(a) are assigned to the water-associated sulfonic acid proton as they show dependence of chemical shift on temperature as well. The broad resonance ranging from 5 to 9 ppm is attributed to the rigid aromatic protons of the polymer backbone.

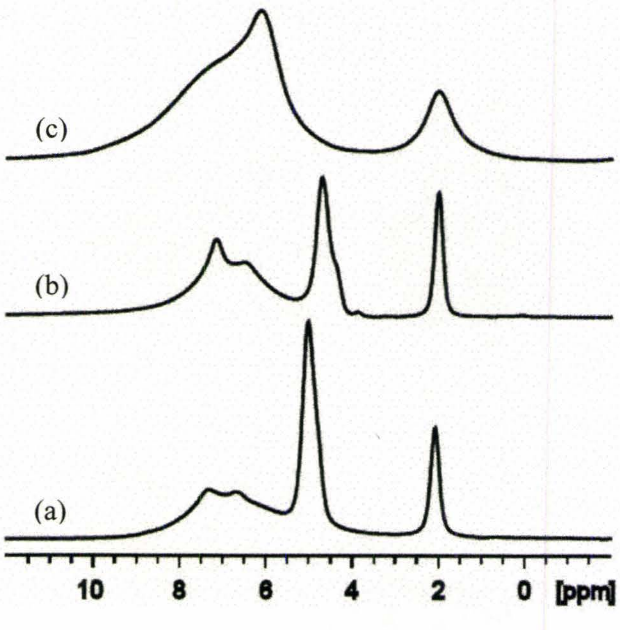

Figure 8-1. ^{1}H MAS NMR of crosslinked S-PEEK prepared from S-PEEK (DS=95%), MAS=25 kHz. (a) hydrated sample at room temperature (b) hydrated sample at 363 K (c) dried sample at room temperature.

The above assignment is proved by the ^2H MAS NMR spectrum of the crosslinked S-PEEK (DS=95% for S-PEEK) which has been treated in D_2O. It was expected that only the sulfonic acid group and the residual hydroxyl group of the crosslinker will undergo hydrogen-deuterium exchange with D_2O to exhibit signal in the ^2H MAS NMR spectrum. From the spectrum shown in Figure 8-2, it can be seen that the strongest resonance is due to the deuterated hydroxyl group of the crosslinker and the two very weak resonances are attributed to the deuterated sulfonic acid group. The large difference in intensity for the hydroxyl group and the sulfonic acid group in this spectrum could indicate a much decreased degree of sulfonation resulting from the incomplete reaction of S-PEEK with ethylene glycol. This is consistent with the following calculated residual degree of sulfonation (RDS).

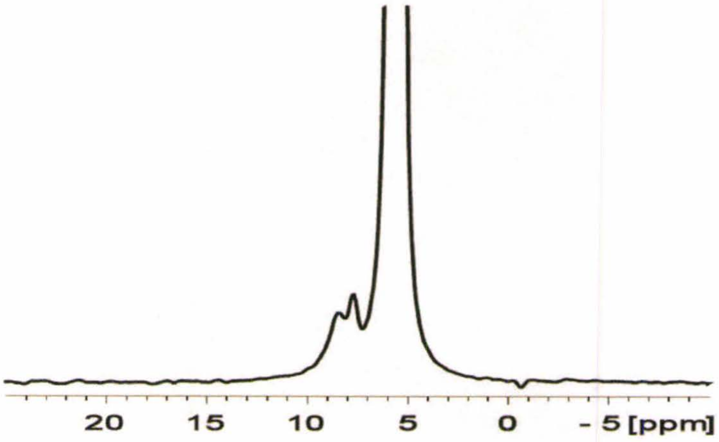

Figure 8-2. ^2H MAS NMR of crosslinked S-PEEK (DS=95%) treated by D_2O, MAS= 5 kHz

8.3.2 Determination of equivalent weight of crosslinked S-PEEKs

Both Figure 8-1 and Figure 8-2 have demonstrated clearly that not all the crosslinkers are fully crosslinked, which makes it difficult to determine the chemical structure of the crosslinked S-PEEK. Moreover, in the above solid-state NMR spectra of the crosslinked S-PEEK, we are unable to tell whether diethylene glycol or/and triethylene glycol are formed and involved as crosslinkers. Using solution state NMR, Kaliaguine reported that these oligomers can be formed and participate in crosslinking reaction. [11] Thus, with including these oligomers as crosslinkers, the chemical structure of crosslinked S-PEEK (DS=95% for S-PEEK) is shown schematically in Figure 8-3.

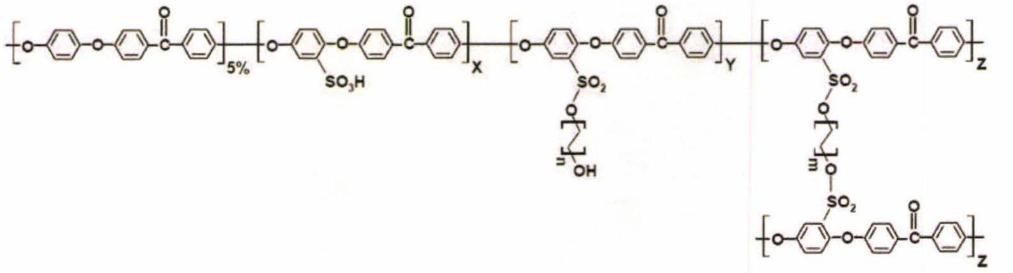

Figure 8-3. Scheme of the crosslinked S-PEEK (DS= 95% for S-PEEK)

Although it is difficult to unambiguously determine the variables in Figure 8-3 because of the residual hydroxyls and the oligomers of ethylene glycol, the equivalent weight of the crosslinked S-PEEKs can be determined straightforwardly by the method of back titration. Since an excess of NaOH is used in this method, it is necessary to know if the crosslinked S-PEEK is stable in this basic environment. Thus, the ^{1}H NMR spectra of NaOH-treated crosslinked S-PEEK were measured. They are shown in Figure 8-4. It can be seen that, as expected, in Figure 8-4(b) the sulfonic acid proton does not exhibit in this spectrum, due to neutralization with NaOH. However, the methylene proton of the crosslinker is not observed in this spectrum. The very sharp peak at ~3.8 ppm is assigned to the water proton or the water-associated hydroxyl proton of ethylene glycol, depending on whether the crosslinker has been removed or the methylene proton resonance overlaps with the hydroxyl proton resonance, respectively. However, once a significant amount of water is removed from the sample by drying, a broad peak at ~3.2 ppm is observed clearly in Figure 8-4(a). Since the hydroxyl proton of the crosslinker generally shifts to higher frequency with decreasing water content, its resonance then overlaps with the broad aromatic proton resonance. Furthermore, due to the decreased mobility of hydroxyl proton with decreasing water content, the hydroxyl proton of the crosslinker is not resolved in this spectrum. Thus, the resonance at ~3.2 ppm is attributed to the methylene proton of the crosslinker. This suggests that the crosslinked S-PEEK did not decompose in the basic environment. Therefore, titrating the NaOH-treated crosslinked S-PEEK can be used to determine its equivalent weight. The determined equivalent weight values are shown in Table 8-1, together with those for S-PEEKs calculated from their degrees of sulfonation. It is clear that the two crosslinked S-PEEKs have very similar equivalent weight, indicating similar ion exchange capacity. Both of them show much higher equivalent weight than S-PEEKs. Therefore, their ion exchange capacity would be much lower than S-PEEKs from which they were prepared.

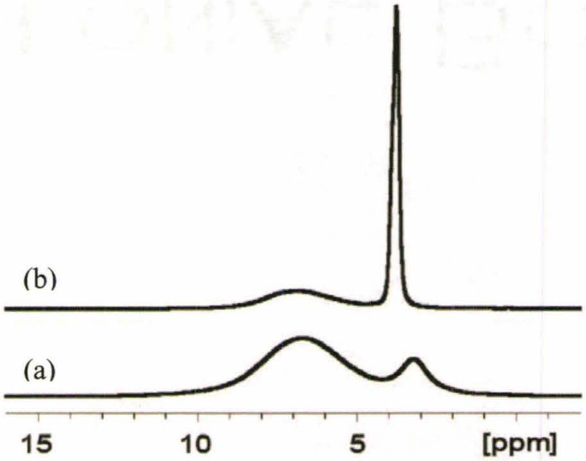

Figure 8-4. ^1H MAS NMR of crosslinked S-PEEK (DS=95% for S-PEEK) treated by NaOH, MAS=25 kHz. (a) dried (b) hydrated

Table 8-1. Equivalent weight (EW) of S-PEEKs and crosslinked S-PEEKs

Samples	S-PEEK (DS=86%)	S-PEEK (DS=95%)	Crosslinked S-PEEK (DS=86%)	Crosslinked S-PEEK (DS=95%)
EW (g/mol)	415	383	3035	3086

8.3.3 Determination of the residual degree of sulfonation of crosslinked S-PEEKs

In order to understand the contribution of the residual hydroxyls to proton conductivity of crosslinked S-PEEK, one has to determine the residual degree of sulfonation (x in Figure 8-3), the degree of crosslinking (z in Figure 8-3), as well as the percentage of units with partially crosslinked crosslinkers (y in Figure 8-3). This makes it necessary to know the ratio of the methylene proton of crosslinker to the aromatic proton of the backbone. This ratio can be calculated from the ^{1}H NMR spectrum of D_2O-treated crosslinked S-PEEK shown in Figure 8-5. Different from the ^{2}H MAS NMR spectrum of D_2O-treated crosslinked S-PEEK shown in Figure 8-2, this spectrum only shows the aromatic proton and the methylene proton of crosslinkers. Thus, the ratio of the two types of protons can be obtained by decomposition of the spectrum. By taking all possible values assigned to m and n in Figure 8-3 (m and n should not be greater than 4. [11]), the RDS, which is the x in Figure 8-3, can be unambiguously determined to be 13.5% ± 0.5% and 13% ± 0.5% for the crosslinked S-PEEK (DS=86% for S-PEEK) and the crosslinked S-PEEK (DS=95% for S-PEEK), respectively. Moreover, it is also found that the RDS is not sensitive to the ratio of the methylene proton of crosslinker to the aromatic proton of the backbone. When the ratio varies from 0.1 to 0.7 (where it is determined to be between 0.3~0.5 from the decomposed spectra of crosslinked S-PEEKs), the difference between the obtained RDS and the previously determined RDS is not greater than 1%. This suggests that the oligomerization of the crosslinker does not significantly influence the residual degree of sulfonation for the crosslinked S-PEEK with determined equivalent weight and ratio of the methylene proton to the aromatic proton. However, the values of y and the z in Figure 3 change with the oligomerization of ethylene glycol. Although they can not be determined, the very strong intensity of hydroxyls in Figure 8-1(a) and Figure 8-2 indirectly indicates that the value of y in Figure 8-3 would not be small.

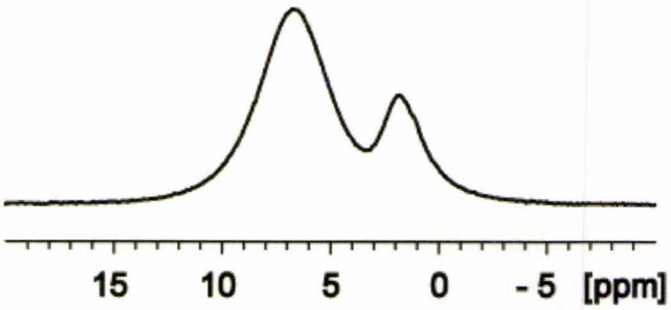

Figure 8-5. ^{1}H MAS NMR of D_2O-treated crosslinked S-PEEK (DS=95% for S-PEEK), MAS=14 kHz. The sample was measured in dried state.

8.3.4 Proton exchange in the hydrated crosslinked S-PEEK

Since the hydroxyl protons of the crosslinker shows relatively stronger signal in Figure 8-1(a), compared with sulfonic acid proton, it would be interesting to know whether this proton can exchange with sulfonic acid proton. Such data aids the determination of the mechanism of proton conductivity of the crosslinked S-PEEK.

This information was achieved from ^{1}H 2D EXSY NMR spectra of the crosslinked S-PEEK (RDS=13%) shown in Figure 8-6. When mixing time is as short as 5 ms in Figure 8-6(a), there is no cross peaks between the hydroxyl proton and the sulfonic acid proton, indicating no proton exchange at this time scale. The weak cross peaks between the acid proton and the methylene proton in Figure 8-6(a) result from proton spin diffusion between them. Nevertheless, when a long mixing time of 150 ms is given, cross peaks between the acid proton and the hydroxyl proton can be seen clearly in Figure 8-6(b). Since spin diffusion between these protons can cause the cross peaks as well, proton exchange between them can not be directly concluded from this spectrum. A ^{1}H 2D EXSY NMR experiment with a short mixing time of 5 ms but at an enhanced temperature of 337K (corrected temperature) has been performed. As spin diffusion is temperature independent, it will not produce cross peaks between these protons in a ^{1}H EXSY spectrum acquired at the enhanced temperature. However, it was found that cross peaks between the acid proton and the hydroxyl proton can be seen clearly at 337K (not shown here). Thus, the cross peaks between the acid proton and the hydroxyl proton in Figure 8-6(b) are due to proton exchange. In addition, proton exchange between sulfonic acid protons in two distinct environments can also be observed at this time scale as shown by the weak but clear cross peaks. From the ^{1}H EXSY experiments, it is implied that the hydroxyl proton of the incompletely crosslinked ethylene glycol contribute to proton conductivity of the crosslinked S-PEEK by exchange with sulfonic acid proton. To our knowledge, such a role of crosslinking groups has not yet been discussed in the literature.

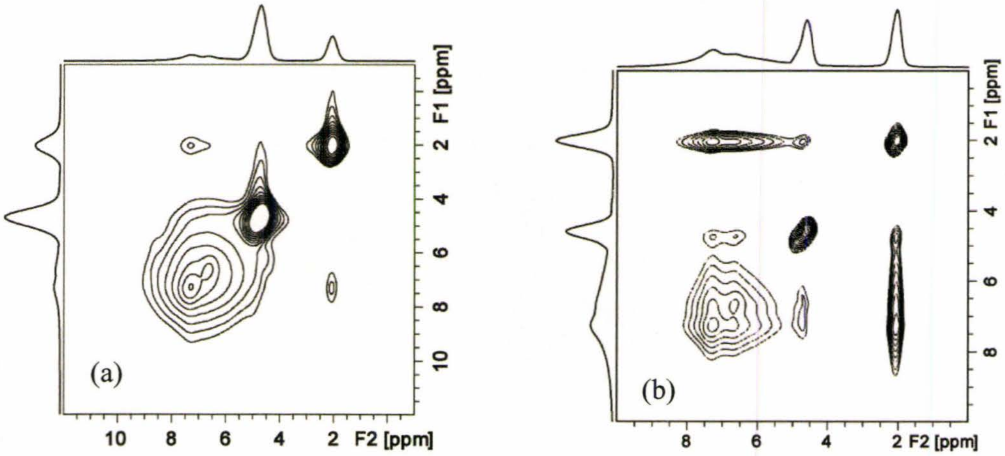

Figure 8-6. ^{1}H EXSY NMR of hydrated crosslinked S-PEEK (RDS=13%), MAS=25 kHz. (a) mixing time = 5ms (b) mixing time = 150ms

8.3.5 Proton mobility in the dried crosslinked S-PEEK

The ^{1}H EXSY spectra have demonstrated high proton mobility in the hydrated sample of crosslinked S-PEEK (RDS=13%). However, as can be seen from the Figure 8-1 (c), the unresolved sulfonic acid proton in the dried sample does not allow investigation of proton mobility by the same EXSY experiments. Alternatively, proton mobility in polymers, particularly in rigid polymers, can be well understood in solid state NMR by using a BaBa pulse sequence through which the mobile protons are filtered in the resulting double quantum filtered (DQF) MAS spectrum. [20, 21] The obtained BaBa spectrum for the dried sample of crosslinked S-PEEK (RDS=13%) is shown in Figure 8-7(b). Compared with the single pulse spectrum shown in Figure 8-7(a), the DQF MAS NMR spectrum does not show observable signal for the hydroxyl proton. This indicates that the hydroxyl proton is still mobile in the dried sample, resulting in a very weak dipolar coupling which can not be detected in this recoupling time. Moreover, even when the recoupling time was extended up to $8\tau_r$, the hydroxyl proton was not observed from the DQF MAS NMR spectrum (not shown here). As the methylene protons of the crosslinking group provide a close-proximity coupling partner, the lack of a DQF signal cannot be attributed to the isolation of the hydroxyl group from other protons. Therefore, the hydroxyl proton in the dried crosslinked S-PEEK must be mobile on the timescale of a rotor period, ie, faster than 40 μs. In addition, it can also be observed that the methylene proton of the crosslinker have very weak intensity in the DQF MAS NMR spectrum, compared with the intensity of the aromatic proton. This is consistent with the observed partially crosslinked crosslinker of which the methylene protons are expected to be more mobile than the aromatic protons of the polymer backbone.

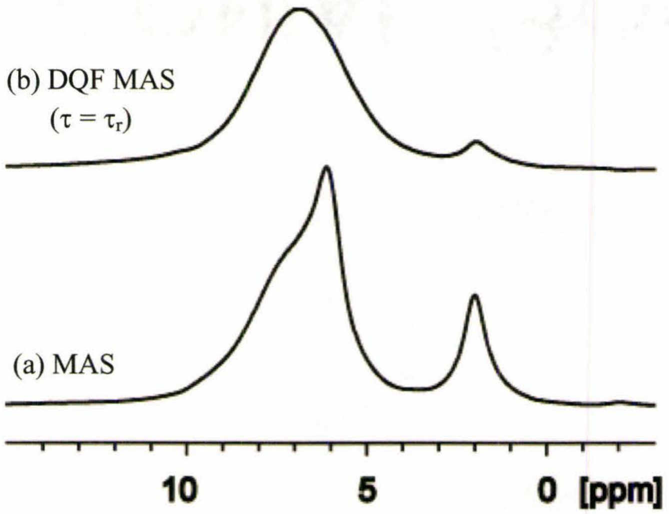

Figure 8-7. ^1H MAS NMR of the crosslinked S-PEEK (RDS=13%), MAS=25 kHz. The Sample was dried before measured.

8.3.6 Proton conductivity of crosslinked S-PEEK

As expected from the ^1H EXSY NMR experiments, the proton conductivities of crosslinked S-PEEKs (RDS=13.5% and 13%) shown in Figure 8-8 are not significantly reduced relative to the parent S-PEEK membranes, due to proton exchange between the sulfonic acid group and the hydroxyl group of the crosslinker, although the residual degree of sulfonation (RDS) of the crosslinked S-PEEKs are only about 13.5% and 13% respectively. The proton conductivity of the crosslinked S-PEEK (RDS=13%) is indeed comparable to that of S-PEEK (DS=58%) at the relative humidity of 95%. Thus, the contribution of hydroxyl proton of the crosslinker to the proton conductivity must be significant. However, due to the much higher pKa of ethylene glycol (pKa=14.22 in H_2O at 25 °C [22]) the hydroxyl proton may not exhibit proton conductivity as high as that observed for the same amount of sulfonic acid protons (pKa=2.8 at 20 °C [23]). The role of the flexible alkyl chain of the crosslinker in increasing the mobility of hydroxyl proton is a variable which is not quantitatively considered, but may improve conductivity in the crosslinked membrane. In addition, despite the similar RDS, the two crosslinked S-PEEK membranes show clear conductivity differences which could be due to the distinct sulfonic acid proton mobility observed in the ^{1}H MAS NMR spectrum (not shown here) and/or different percentage and distribution of polymer units with partially crosslinked crosslinker, which can not be determined yet.

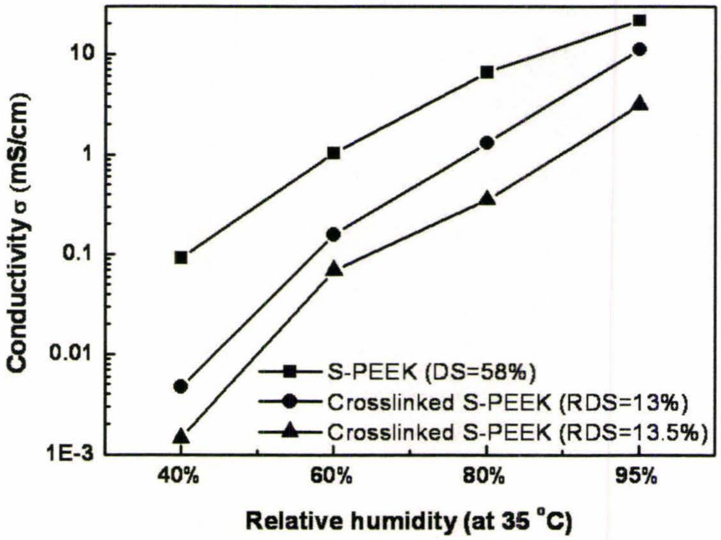

Figure 8-8. Conductivity of S-PEEK (DS=58%), crosslinked S-PEEK (RDS=13.5%, DS=86% for S-PEEK), and crosslinked S-PEEK (RDS=13%, DS=95% for S-PEEK) under variable relative humidity

8.3.7 Decomposition of crosslinked S-PEEK in an acidic environment

The spectra of crosslinked S-PEEK treated by NaOH solution have displayed that the crosslinked S-PEEK does not decompose in a basic environment. It is even more important to investigate the stability of the crosslinked S-PEEK in an acidic environment, since the working environment of proton exchange membrane in fuel cell is acidic. The ^1H MAS NMR spectra of crosslinked S-PEEK which has been treated by 1M H_2SO_4 solution are shown in Figure 8-9. It can be seen that the signal for the methylene proton of ethylene glycol completely disappears from both the dried and the hydrated samples. The several peaks ranging from 4.7 ppm to 6.5 ppm in Figure 9 (a) are attributed to sulfonic acid protons which are associated with different amount of water. The distinct sulfonic acid proton environments in hydrated S-PEEKs with high degrees of sulfonation, for instance DS= 72% and DS=86%, have been observed. [24] However, when the DS is up to 95%, only a single acid proton environment was observed, resulting from a highly swollen membrane. Compared with the S-PEEK (DS=95%), the acid-treated crosslinked S-PEEK (RDS=13%, DS=95% for S-PEEK) shows multiple sulfonic acid proton environments after the crosslinker has been completely removed. This indicates a distinct difference in the structure of the two membranes although they have same initial degree of sulfonation. In Figure 8-9(b), when the acid-treated crosslinked S-PEEK (RDS=13%, DS=95% for

S-PEEK) is dried, the resonance for rigid sulfonic acid proton shifts to higher frequency, resulting in a broad peak at ~8.5 ppm.

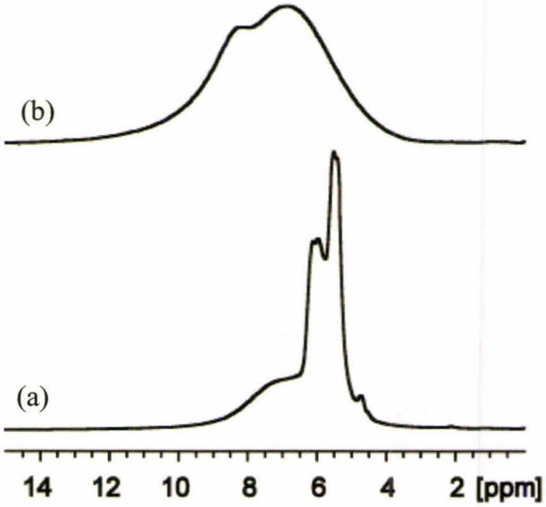

Figure 8-9. ^{1}H NMR of crosslinked S-PEEK (RDS=13%) treated by 1M H_2SO_4, then washed in water until constant pH was obtained, MAS=25 kHz. (a) hydrated sample (b) dried sample

The spectra in Figure 8-9 suggest that both fully and partially crosslinked ethylene glycol units can be eliminated in an acidic solution. This results from the hydrolysis of sulfonate ester which regenerates sulfonic acid and ethylene glycol in the acidic environment. Since the free ethylene glycol is miscible with water, it is then completely removed from the membrane by repeatedly washing in water. Therefore, the decomposition of crosslinked S-PEEK in an acidic environment indicates that the crosslinked S-PEEK would not be feasible in the application of polymer electrolyte membrane fuel cells although it can still present proton conductivity comparable to those of S-PEEKs.

8.4 Conclusions

Not all the ethylene glycol units used in the preparation of crosslinked S-PEEK are fully crosslinked. The equivalent weight of crosslinked S-PEEKs determined by back titration is much higher than those of the S-PEEKs from which they were prepared. The residual degrees of sulfonation of crosslinked S-PEEKs were accurately determined to be 13.5% and 13% for crosslinked S-PEEK (DS=86% for S-PEEK) and crosslinked S-PEEK (DS=95% for S-PEEK), respectively. Although they have such low residual degrees of sulfonation, their conductivities are still comparable to that of S-PEEK (DS=58%). This is due to the contribution from the proton exchange between the sulfonic acid group and the hydroxyl group of crosslinkers. However, the major drawback of the crosslinked S-PEEK is that it decomposes in an acidic environment, implying that it is not applicable in PEMFC.

8.5 References

[1] S. G. Chalk, S. R. Vendateswaran, *Fuel Cell Seminar*, Program and Abstracts, **1996**, p258.

[2] F. Damay, L. C. Klein, *Solid State Ionics*, **2003**, 1-7.

[3] N. Jia, M. C. Lefebvre, J. Halfard, Z. Qi, P. G. Pickup, *Electrochem. Solid-state Lett.*, **2000**, 3, 529-531.

[4] S. M. J. Zaidi, S. D. Mikhailenko, *et al.*, *J. Membr. Sci.*, **2000**, 173, 17-34.

[5] T. Kobayashi, M. Rikukawa, K. Sanui, N. Ogata, *Solid State Ionics*, **1998**, 106, 219.

[6] R. Jiang, H. R. Kunz, J. M. Fenton, *J. Power Sources*, **2005**, 150, 120-128.

[7] M. Gil, X. Ji, X. Li, H. Na, J. E. Hampsey, Y. Lu, *J. Membr. Sci.*, **2004**, 234, 75-81.

[8] S. P. S. Yen, S. R. Narayanan, G. Halper, E. Graham, A. Yavrouian, Polymer material for electrolytic membranes in fuel cells, US Patent 5795496 (**1998**)

[9] S. S. Mao, S. J. Hamrock, D. A. Ylitalo, Crosslinked ion conducitive membranes, US Patent 6090895 (**2000**)

[10] S. D. Mikhailenko, K. Wang, S. Kaliaguine, P. Xing, G. P. Robertson, M. D. Guiver, *J. Membr. Sci.*, **2004**, 233, 93-99.

[11] S.D. Mikhailenko, G. P. Robertson, M. D. Guiver, S. Kaliaguine, *J. Membr. Sci.*, **2006**, 285, 306-316.

[12] M. Feike, D. E. Demco, R. Graf, J. Gottwald, S. Hafner, H. W. Spiess, *J. Magn. Reson. A.* , **1996**, 122, 214-221.

[13] I. Schnell, H. W. Spiess, *J. Magn. Reson.*, **2001**, 151, 153-227.

[14] G. Ye, N. Janzen, G. R. Goward, *Macromolecules*, **2006**, 39, 3283-3290.

[15] S. R. Benhabbour, R. P. Chapman, G. Scharfenberger, W. H. Meyer, G. R. Goward, *Chem. Mater.*, **2005**, *17*,1605-1612.

[16] D. Massiot, F. Fayon, M. Capron, I. King, S. LeCalv, B. Alonso, J. Durand, B. Bujoli, Z. Gan, G. Hoatson, *Magn. Reson. Chem.,* **2002**, 40, 70-76.

[17] G. Ye, C. A. Hayden, G. R. Goward, *Macromolecules*, **2007**, 40, 1529-1537.

[18] J. J. Sumner, S. E. Creager, J. J. Ma, D. D. DesMarteau, *J. Electrochem. Soc.*, **1998**, 145, 107-110.

[19] Y. Sone, P. Ekdunge, D. Simonsson, *J. Electrochem. Soc.*, **1996**, 143, 1254-1259.

[20] M. McCormick, R. N. Smith, R. Graf, C. J. Barrett, L. Reven, H. W. Spiess, *Macromolecules*, **2003**, 3616-3625.

[21] C. G. Densmore, P. G. Rasmussen, G. R. Goward, *Macromolecules*, **2005**, 38, 416-421.

[22] J. A. Dean, *Lange's Handbook of Chemistry*, fifteenth edition, section 8, page 47.

[23] R. W. Kopitzke, C. A. Linkous, H. R. Anderson, G. L. Nelson, *J. Electrochem. Soc.*, **2000**, 147, 1677-1681.

[24] G. Ye, C.M. Mills, G.R. Goward, *J. Membr. Sci.*, **2008,** 319, 238-243.

Chapter 9

Summary and Outlook

Solid state NMR is used in this thesis as a powerful tool to investigate proton dynamics within PEMs, including Nafion®, Nafion/SiO_2 composites, Nafion/ZrP composites, S-PEEKs and crosslinked S-PEEKs. Combining proton conductivity data obtained using impedance spectroscopy, with the NMR data gives deeper understanding of the molecular-level proton dynamics in these materials. Such data is critical to the selection of good PEMs and the development of new PEMs. The insights gained in this research are as follows.

The proton mobility of these materials is dependent on both the temperature and the water content. High proton mobility can be observed by NMR in samples with high water content at high temperatures. The activation energy for proton transport in these materials generally increases with decrease in hydration level. These findings are consistent with established conductivity data. Beyond these bulk properties, the solid-state NMR provides further insight, on the basis of the spectral resolution together with several multi-pulse sequence studies. Although both Nafion and S-PEEKs show dependence of proton mobility on water content, Nafion shows proton dynamics quite different from that of S-PEEK at low hydration level when humidification changes (see Chapter 3), due to their structural differences. This implies an important consideration for the development of PEMs. Namely, the PEM should have flexible polymer backbones as well as side chains with appropriate length, which allow close proximity between acid protons. This facilitates proton transport between acid groups even at low hydration levels. This feature may allow for improved performance of PEMs, since the PEM maintain acceptable proton conductivity under the industrial target of hotter, drier conditions.

For Nafion/SiO_2 composites, the preparation of the composites can cause large difference in their proton diffusion coefficients and proton conductivities in dried states. A high concentration of TEOS usually causes incomplete hydrolysis of TEOS in the resulting Nafion/SiO_2 composites if the time for treating Nafion in the TEOS solution is too long. Moreover, the silica particle size is much larger in the composites prepared from the high concentration of TEOS, due to the high degree of condensation between surface hydroxyl groups of silica. Both the existence of residual ethyl groups from incompletely hydrolyzed TEOS and the condensation of hydroxyls negatively impact the proton diffusion of the composites. It should be pointed out that although the high loading of dopants is usually pursued in order to have a greater extent of modification to the polymer, the similar high degree of condensation of hydroxyls could take place easily, which should be avoided in the preparation of Nafion/SiO_2 composites. This also suggests that a better way to control for smaller silica particle size is to allow the hydrolysis of TEOS to occur in the swollen water channels of hydrated Nafion, rather than hydrolyzing TEOS in the Nafion solution in which a high degree of condensation of hydroxyls will be expected. It has been found that the best Nafion/SiO_2 composite can be obtained using a low concentration of TEOS in methanol solution. This composite displays much higher diffusion coefficient than pure Nafion in the dried state. Therefore, Nafion/SiO_2 composites synthesized using these optimized procedures hold promise for being used as proton exchange membranes working at an elevated temperature and reduced relative humidity.

The solid state NMR results in Chapter 5 present a good understanding of conductivity differences between α-ZrP, anhydrous α-ZrP and amorphous ZrP. The proton exchange between acid group and residual water contributes to the highest proton conductivity of amorphous ZrP. The stronger dipolar coupling between acid protons in the anhydrous α-ZrP results in its lowest proton conductivity. These results imply that amorphous ZrP is the best choice of dopant in Nafion. More importantly, the studies of interaction between ZrP and the acid proton of sulfuric acid show important findings that the strong acid not only protonates the phosphoric acid group, but also catalyzes the condensation of phosphoric acid group, leading to the formation of pyrophosphate at much lower temperature. The observation of the interaction between ZrP and the strong acid is crucial for a complete understanding of interaction between ZrP and the Nafion in the subsequent chapter.

For the Nafion/ZrP composites, all hydrated composites show lower activation energies for proton transport, in contrast to reduced proton conductivity, compared with unmodified Nafion. Although the composite is designed to work at high working temperature, both the conversion of monohydrogen phosphate into pyrophosphate and the protonation of monohydrogen phosphate have been observed after the composite was dried at 160 °C. This indicates that the composite is not stable under such conditions. More importantly, the subsequent hydration of the dried composite shows much reduced proton conductivity even if the pyrophosphate has converted back to monohydrogen phosphate by hydrolysis. Furthermore, the following drying of the composite did not cause the conversion of monohydrogen phosphate into pyrophosphate and the protonation of monohydrogen phosphate. These observations clearly indicates a dramatic change of interaction between Nafion and ZrP. Since the change during the fist drying-rehydration process is not reversible and causes reduced proton conductivity, it should be avoided for the purpose of practical application. This indicates that a very dry environment is still a major challenge for using the Nafion/ZrP composite in fuel cells at a high temperature. A compromise between the very low humidification and the high working temperature is to take a relatively lower temperature, for example ~ 110 °C. At such a temperature, the conversion of monohydrogen phosphate into pyrophosphate is minimized, since the acid proton is still associated with water, and therefore does not catalyze the conversion. These data highlight the importance of temperature and humidity cycling studies of PEMs.

In the fully hydrated S-PEEKs, sulfonic acid proton environments change with the degree of sulfonation. When the degree of sulfonation is 58% or 95%, the S-PEEK has uniform acid proton environment, which is due to low or high water content, respectively. When the degree of sulfonation changes from 58% to 95%, the water content of S-PEEK increases from low to high, leading to multiple acid proton environments in the polymer. This indicates a large variation of $N_{\text{water / acid proton}}$ values through an individual membrane, which explains well the small conductivity difference between S-PEEK (DS=72%) and S-PEEK (DS=86%). The understanding of the conductivity differences among the S-PEEKs samples suggests that it is very important for PEMs to have evenly distributed water molecules per acid proton although high water content is critical to maintain high proton conductivity. In a sample with unevenly distributed water molecules, the acid protons associated with fewer water molecules could create a bottle neck of long range proton transport. In addition, S-PEEKs with same degree of sulfonation but cast from different solvents (DMSO, DMF and DMAc), present distinct proton conductivities, which was explained by the different mobility of their polymer backbones. This clearly shows the importance of choosing the appropriate casting solvents to allow looser packing of polymer chains and thereby, increased local dynamics and proton transport.

In the crosslinked S-PEEK, it was found that not all the additive ethylene glycol molecules create complete crosslinks. The residual degree of sulfonation was determined to be only ~ 13%. With such a low degree of sulfonation, the crosslinked S-PEEK nevertheless presents very good conductivity which is comparable with that of S-PEEK (DS=58%). This impressive conductivity of crosslinked S-PEEK was attributed to the fast proton exchange between the residual hydroxyls from the crosslinker molecules and the sulfonic acid groups from the S-PEEK. Since the hydroxyl of the crosslinker has much higher pKa compared with sulfonic acid group (see Chapter 8), this suggests that functional groups with low acidity can still significantly contribute to proton transport in the proton exchange membrane through proton exchange with acid groups. Therefore, in the development of new PEMs, some functional groups with low acidity but having ability to exchange proton with acid groups should be considered as well. However, in this research although the crosslinked S-PEEK presents acceptable conductivity and improved mechanical strength, it decomposes in an acidic environment. Since in the actual fuel cell the proton exchange membrane will be highly acidic, the crosslinked S-PEEK will degrade with time once the fuel cell with this polymer is operated. Therefore, the crosslinked S-PEEK prepared by this method is not feasible for practical application.

As summarized above, in this thesis the studies of these materials have focused primarily on the proton dynamics at relatively low temperatures (below 100 °C). Multi-nuclear NMR studies at high temperatures, such as 100~160 °C are the obvious next step in this research program, as manufacturers target "hot and dry" conditions for enhanced fuel cell performance and reliability. It has been reported that Nafion composites show higher conductivity than unmodified Nafion in this increased temperature range. Thus, studies of proton dynamics of these materials in this elevated temperature range would provide useful information for understanding and optimizing the improved performance of various Nafion composites.

In conclusion, solid state NMR studies provide valuable insight into the molecular level dynamic and chemical processes which govern ion transport in polymer electrolyte membranes. Considerations of PEM performance and durability under temperature and humidity cycling, as well as exposure to the electrochemical fuel cell processes will be necessary as automotive manufacturers seek to bring fuel cells into competition as green vehicles of the future.